Characterization and Control of Cyclic Variability in a Gasoline/Natural Gas Dual-Injection
Spark Ignition Engine

by

Daniel A Stang

A thesis submitted in partial fulfillment of the requirements for the degree of

Master of Science

Department of Mechanical Engineering
University of Alberta

Abstract

Reducing the cyclic variability of a gasoline/natural gas dual injection spark ignition engine using minimum variance control is the subject of this thesis. Cylinder pressure is used to calculate four combustion metrics, the standard deviation of which is used as an indicator of cyclic variability. Spark timing, fuel type, and engine speed are varied to characterize the cyclic variability of the engine. Location of peak pressure is found to be the best combustion metric for use as feedback in a closed loop controller. Using the location of peak pressure as an engine output and spark timing as an engine input, system identification is used to develop input-output models. Using the model, a minimum variance controller is developed which is able to reduce the cyclic variability by 1.4% by changing the spark timing in response to the measured location of peak pressure. A detuned minimum variance tracking controller is designed to produce maximum power in changing operating conditions by using 16 crank angle degrees after top dead center as the location of peak pressure set-point. The detuned minimum variance controller is able to track and maintain the set-point under constant operating conditions and as disturbances such as, changing fuel type, addition of internal exhaust gas recirculation, and changing coolant temperature, are introduced into the system. The detuned minimum variance controller rejects these disturbances when experimentally tested and maintains optimal engine operating conditions.

ACKNOWLEDGEMENTS

TABLE OF CONTENTS

List of Tables

LIST OF FIGURES

Nomenclature

Acronyms

ATDC — After Top Dead Center

BTDC — Before Top Dead Center

CAD — Crank Angle Degree

CA50 — Crank Angle of 50% mass burned

DTC — Diagnostic Trouble Code

EGR — Exhaust Gas Recirculation

EGT — Exhaust Gas Temperature

ECU — Engine Control Unit

iEGR — Internal Exhaust Gas Recirculation

IMEP — Indicated Mean Effective Pressure

MAB — MicroAutoBox

MVC — Minimum Variance Controller

RBS — Random Binary Sequence

RP — RapidPro

RPM — Revolutions Per Minute

SI — Spark Ignition

TDC — Top Dead Center

Symbols

$^\circ$ — Crank Angle Degree

θ_{Pmax} — Location of Peak Cylinder Pressure

γ — Ratio of Specific Heats

G_{RBS} — RBS Input Gain

k — Time Delay

CHAPTER 1

INTRODUCTION

1.1 Motivation

Worldwide, fuel economy standards are demanding increasing levels of engine efficiency [An and Sauer, 2004]. The EPA has set standards that will bring the average fuel economy of passenger vehicles operating in the United States to 54.5 miles per gallon by 2025 [EPA, 2012]. A method to increase the fuel efficiency of spark ignition engines is to use closed loop controllers to ensure that the engine is always operating at peak efficiency despite constantly changing operating conditions. A main issue with this approach is that cyclic variability, which is an inherent problem in spark ignition engines [Finney et al., 2015], is exacerbated by the inputs of closed loop controllers. If cyclic variability could be completely eliminated, power output would increase 10% with the same amount of fuel consumption [Ozdor et al., 1996]. However studies have found that the cyclic variability cannot be eliminated but only minimized [Dai et al., 2000]. Thus to increase the fuel efficiency of spark ignition engines, a balance must be struck between the amount of cyclic variability and the ability to operate a closed loop controller to maintain optimal engine operating conditions.

1.2 Problem Statement

The objective of this study is to experimentally characterize the cyclic variability of a General Motors production 4 cylinder engine and to examine the potential of using minimum variance control to reduce the amount of cyclic variability produced in a spark ignition engine. The minimum variance control is tested and its ability to reject disturbances and track a reference point is evaluated.

1.3 Thesis Outline

This thesis is organized into 6 chapters. Chapter 2 gives background information on cyclic variability by examining previous research to characterize and control it. Chapter 3 details the experimental setup of the research engine. Using a production General Motors engine to do research is typically difficult due to the proprietary nature of the engine control systems so significant effort was required to make the engine capable of research. However, now that the ability to do a wide range of research topics is available, it is important to document the setup so future researches will have the required documentation of the numerous experimental systems. Chapter 4 characterizes the effects of spark timing, fuel, and engine speed on cyclic variability. The results of system identification and development of a model based minimum variance controller is described in Chapter 5. The minimum variance controller is operated in constant engine conditions to test its effect on cyclic variability. Then disturbances are introduced to test the controllers ability to track a reference combustion metric. Chapter 6 presents the conclusion of this study and outlines areas for possible future research.

1.4 Contributions

The major contributions of this study are:

- Creating a flexible gasoline direct injection research engine with natural gas port injection using a production 4 cylinder engine. The engine, along with the required controllers, sensors, and measurement systems/software will be an excellent facility for future research projects.

- Characterizing the cyclic variability of the engine.

- Developing a minimum variance controller which is capable of tracking a reference with minimal increase to the cyclic variability and is able to reject disturbances to the engines operating conditions.

CHAPTER 2

BACKGROUND

2.1 Spark Ignition Overview

In a spark ignition (SI) engine the combustion of the fuel and air mixture is initiated by the electric discharge of a spark plug. The flame kernel caused by the spark discharge grows and develops into a turbulent flame front which consumes the bulk of the mixture before extinguishing [Chanchaona, 1990]. Ideally under constant operating conditions, the entire combustion from flame kernel to flame extinguishing will be identical from one cycle to the next. However engine observations done from 1921 to the present have found variations in the combustion from cycle to cycle [Clerk, 1921; Finney et al., 2015].

Figure 2.1 shows cylinder pressure for 10 consecutive cycles for the engine used in this study. For this figure, all control inputs such as spark timing and all engine operating conditions such as engine coolant temperature, are kept constant. As seen in the figure, the pressure traces are very similar until ignition, after which the pressure traces vary. This cycle to cycle variation is defined in this study as cyclic variability. Despite cyclic variability, the spark ignition timing is determined only for the average cycle at a set operating condition. This causes slower combusting cycles, which could benefit from a more advanced spark timing, to burn incompletely [Chanchaona, 1990].

If the cyclic variability could be controlled so that every cycle performed as well as the best cycle at a set operating condition, an increase in engine efficiency would be expected [Chanchaona, 1990].
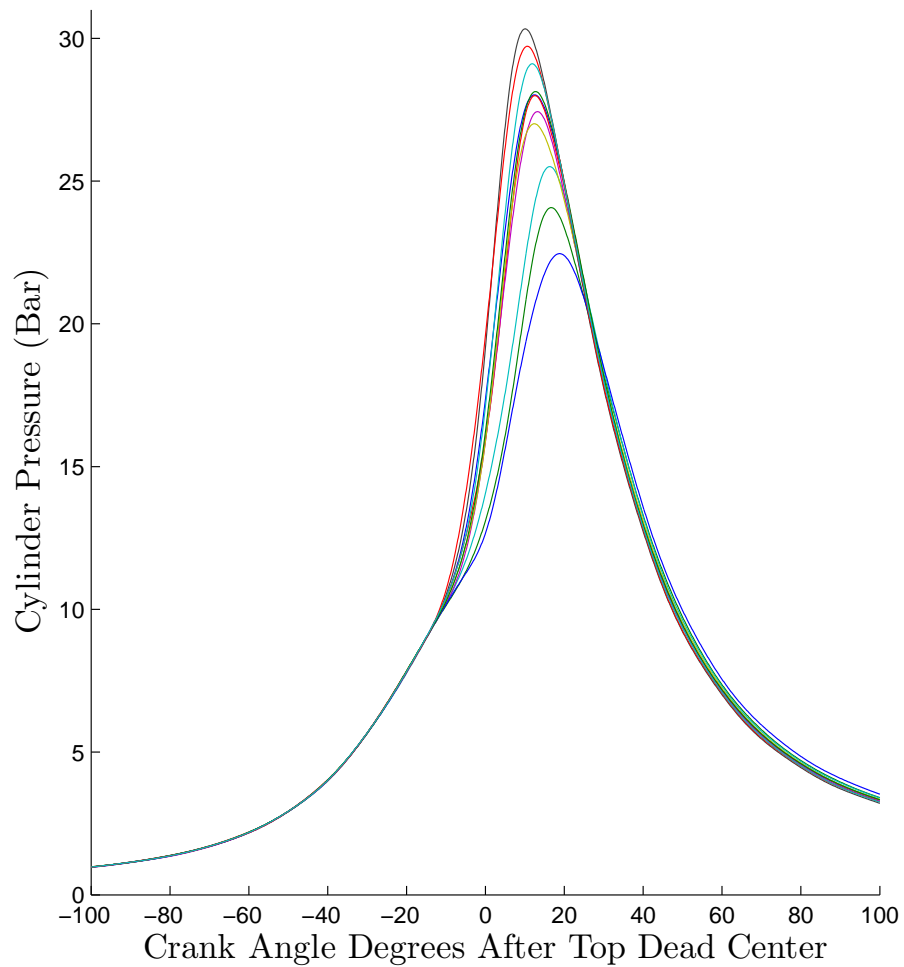
Figure 2.1: Example of Cylinder Pressure for 10 Consecutive Cycles of Natural Gas, 62 Nm of Torque at 1250 RPM

2.2 Cyclic Variability Combustion Metrics

Cyclic variability can be studied in the lab using several different instruments which produce different combustion metrics. For example, laser beams and ionization probes

can measure full flame velocity, flame formation, and flame propagation [Swords et al., 1982; Petrovic, 1982] or cylinder pressure sensors can measure cylinder pressure at top dead center and location of peak cylinder pressure [Li et al., 2009; Zhu et al., 2003]. Regardless of the instrument or combustion metrics used, the standard deviation or variance of the selected combustion metric is defined as the amount of cyclic variability.

For this study, the four selected combustion metrics, shown in Table 2.1, are all calculated from the engines cylinder pressure.

Table 2.1: Combustion Metrics used in this Study

Combustion Metric	Symbol	Units
Peak cylinder pressure location	θ_{Pmax}	Crank Angle Degrees
Peak cylinder pressure	Pmax	Bar
Crank Angle of 50% Mass Fraction Burned	CA50	Crank Angle Degrees
Indicated Mean Effective Pressure	IMEP	Bar

Peak cylinder pressure location (θ_{Pmax}) is the location in crank angle degrees (CAD) where the peak pressure is measured by the cylinder pressure sensor. This value is typically located after top dead center [Triantos et al., 2003]. Peak cylinder pressure (Pmax) is the absolute value of cylinder pressure that is measured by the cylinder pressure sensor. Crank angle of 50% mass fraction burned (CA50) is the location in CAD where 50% of the mass of fuel has been burned. For this study, CA50 is calculated this heat release method [Heywood, 1988]:

$$\delta Q_{netR} = \frac{\gamma}{\gamma - 1} p \mathrm{d}V + \frac{1}{\gamma - 1} V \mathrm{d}p$$

where δQ_{netR} is the net heat released by combustion, p is the cylinder pressure, and V is the volume of the combustion chamber and the ratio of specific heats, γ, is 1.4.

The mass fraction burned, MFB_θ, is the cumulative heat released at crank angle θ, divided by the total heat released:

$$\text{MFB}_\theta = \frac{\sum_{CAD=0}^{CAD=\theta} \delta Q_{netR}}{\sum_{CAD=0}^{CAD=720} \delta Q_{netR}}$$

The crank angle, where the mass burned fraction is 0.5 (50%), is defined as CA50. This CA50 calculation assumes that there is no heat transfer between the the combustion and the cylinder walls, and that there is no losses do to cylinder blow-by [Heywood, 1988].

Indicated mean effective pressure measures the engines power output by integrating the cylinder pressure with respect to volume over the entire engine cycle and then dividing by the displacement volume [Heywood, 1988]:

$$\text{IMEP} = \frac{\int p \mathrm{d}V}{V_d}$$

where V_d is the displacement volume of the engine.

The combustion metrics θ_{Pmax}, Pmax, and CA50 are used in this study to allow comparison to closed loop controllers for cyclic variability in the literature as will be discussed in section 2.4. IMEP is also selected because it has been used as a metric for cyclic variability in a number of papers including Chanchaona [1990] and Zhang et al. [2013].

2.3 Characterization

A characterization of combustion metrics θ_{Pmax}, Pmax, and IMEP, by Chanchaona [1990] found that Pmax and IMEP are best suited for measuring cyclic variation as they account for the entire release of combustion. However, Pmax was only recommended for spark timing producing maximum brake torque.

Cyclic variability has been characterized in a natural gas engine by Reyes et al. [2015]. This paper studied the effect of fuel/air equivalence ratio and engine speed on cyclic variability. The results of the paper showed that the standard deviation of the combustion metric CA50, increased as the engines speed was increased from 1000 RPM to 1750 RPM. This result is replicated experimentally in section 4.4.

The effect of engine operating parameters on cyclic variability and the correlation between the combustion metrics θ_{Pmax}, Pmax, and IMEP in a natural gas spark ignition engine is studied in Zhang et al. [2013]. They found that the average value and standard deviation of IMEP varies non-linearly with spark timing which is experimentally replicated and described in chapter 4. Thus to optimize spark timing for maximum IMEP, a non-linear control scheme is needed. However, results in chapter 4 show that θ_{Pmax} varies linearly with spark timing and has a consistent value (θ_{Pmax} =16 crank angle degrees after top dead center) which produces maximum IMEP at all the operating conditions used in this study. Using θ_{Pmax} as a control input, a linear control scheme can be used to optimize spark timing for maximum IMEP.

2.4 Control of Cyclic Variability

To characterize the main results of the literature on control of cyclic variability in SI engines 5 published papers will be used. These papers, with the controller output (u) and plant output (y) are listed in Table 2.2. For these papers, the plant output is

also used as the combustion metric for cyclic variability. In the table, the maximum acceleration of location of mass fraction burned is $MAMFB_\theta$, and P_{TDC} is the cylinder pressure at top dead center (TDC).

Table 2.2: Summary of Controllers used for Cyclic Variability in SI Engines.

Author	u	y
Daw [2002]	Fuel	Crankshaft Acceleration
Zhu et al. [2003]	Spark Timing	θ_{Pmax}
	Spark Timing	CA50
	Spark Timing	$MAMFB_\theta$
Triantos et al. [2003]	Spark Timing	θ_{Pmax}
Li et al. [2009]	Spark Timing	4 cycle average of P_{TDC}
Kaleli et al. [2015]	Spark Timing	Pmax

Controlling the cyclic variations present at low engine speeds of 200-1000 rpm in a lean fueled spark ignition engine is studied by Daw [2002]. The controller input is crankshaft acceleration and the controller output is fuel injection pulse width. The engine was run at the lean fueling limit and the variation in RPM was a sinusoidal movement of rpm between 200 and 1000 rpm. The period of the oscillations is approximately 60 cycles. A partial misfire which increases the fuel to air ratio in the residual gas for the next burn is main factor attributed to higher cyclic variations. Feedback control is used to reduce the cyclic variations.

Zhu et al. [2003] focused mainly on closed-loop control on a cylinder pressure combustion metric. Closed loop control on a combustion metric resulted in reduced variance of that metric. A PI controller is used which has similar attributes to minimum variance control with detuned tracking that will be tested later in this study. The combustion metrics used for closed loop control are θ_{Pmax}, CA50, and $MAMFB_\theta$. The papers method is duplicated in simulation and a similar minimum variance con-

trol test is performed to try and replicate the results.

Triantos et al. [2003] used minimum variance control to reduce the variance of θ_{Pmax}. This minimum variance controller was developed using system identification. They use a similar minimum variance controller that is used in this study. One main difference is that they reported a time delay of 2 between the input of spark timing and the output of θ_{Pmax} while a time delay of 1 is found in this study. This results in a different model structure in this study. They used a $\theta_{\text{Pmax}} = 16$ crank angle degrees after top dead center as the controller reference to get maximum IMEP, and defined cyclic variability as the standard deviation of θ_{Pmax}. A decrease in cyclic variability (standard deviation of θ_{Pmax}) of 3% was reported when using an minimum variance controller. When using a minimum variance tracking controller, a decrease in cyclic variability of 0.5% was reported despite simulation results predicting a cyclic variability increase of 3.7% when using the tracking controller. The results of this paper are tested in simulation and experimentally with a similar minimum variance controller in Chapter 5.

Li et al. [2009] used a minimum variance controller to reduce the variance of a 4 cycle moving average of P_{TDC}. A decrease in cyclic variability (standard deviation of P_{TDC}) by 20% was reported when using a minimum variance controller. Validation of their results is attempted in section 2.5.

Kaleli et al. [2015] used a minimum variance controller to reduce the variation of Pmax. A decrease in cyclic variability (defined as standard deviation of Pmax) of 7.9% is reported when using a minimum variance controller. It will be shown that the modeling results, shown in Figure 6(a), cannot be replicated when following the system identification procedures outlined in Ljung [1987]. The system identification results presented in this study in section 5.1 are not compatible with the results presented in Kaleli et al. [2015].

2.5   Analysis of Li et al. [2009] and Tesing on GM GDI Engine

A paper by Li et al. [2009] proposed a system of controlling and reducing cyclic variations in a gasoline SI engine. This control system used a four cycle moving average of the pressure at TDC as its input and spark timing as its output. The paper reported a 20-40% reduction in cyclic variability using its controller.

The system identification model used in the paper is an ARX model. The design of a minimum variance controller follows the same methodology used in this study in section 5.2.1.

The experimental design to test for a reduction in cyclic variability was done by operating the controller for roughly 100 cycles, running a baseline spark for another 100 cycles, then turning the controller back on. The difference between the baseline and the average of the two controller variances was then used to calculate the percentage change in cyclic variability.

A replication of the results of the paper is attempted with minor modifications to the experimental design. The number of cycles to calculate a standard deviation was increased from 100 to 1,000 and the number of switches between baseline and controller was increased from 2 to 6. For this replication Pmax will be used instead of P_{TDC} so that the results can be compared to further work done in this study. The correlation between Pmax and P_{TDC} can be seen in Figure C.1. P_{TDC} has no benefit over the other combustion metrics in terms of modeling cyclic variability in as shown in Table D.2.

The paper also uses a saturation value of $\pm 2°$ on the controllers spark output. Figures 9 and 11 in Li et al. [2009] show that the controller spends a majority of its time at one of the limits of this saturation. This is contrary to minimum variance control theory as it nullifies the system identification values if the control values are always being saturated to a maximum or minimum value.

The results in Figure 2.2 were gathered by using the same controller setup and the same system identification model as Li et al. [2009]. Each data point is the standard deviation of 1,000 cycles of data. The ARX model used in the paper is shown below. From the figure it can be seen that the controller reduces the variability of a four cycle moving average of Pmax.

$$A(z) = 1 - 0.88587z^{-1} + 0.16736z^{-2}$$

$$B(z) = 0.13226z^{-1}$$
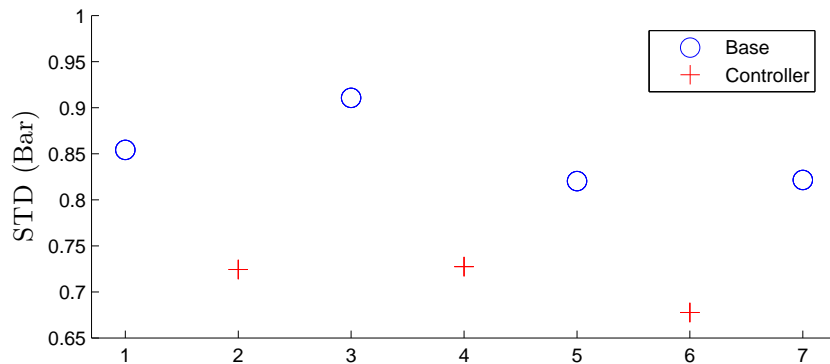
Figure 2.2: Pmax 4 Moving Average, Standard Deviation

Figure 2.3 shows the same controller setup but with a system identification model done for the engine used in this study. The ARX model values can be seen below. Comparing the ARX model from the paper to the values seen below, there is very little difference in the models even with the different engines and different combustion metric. The figure shows that there is almost no difference in the amount of reduction of variability. Since the models are so close and a saturation exists on the output, it is likely that these different values would yield no difference in effective control output.

$$A(z) = 1 - 0.8366z^{-1} + 0.1364z^{-2}$$

$$B(z) = 0.1787z^{-1}$$
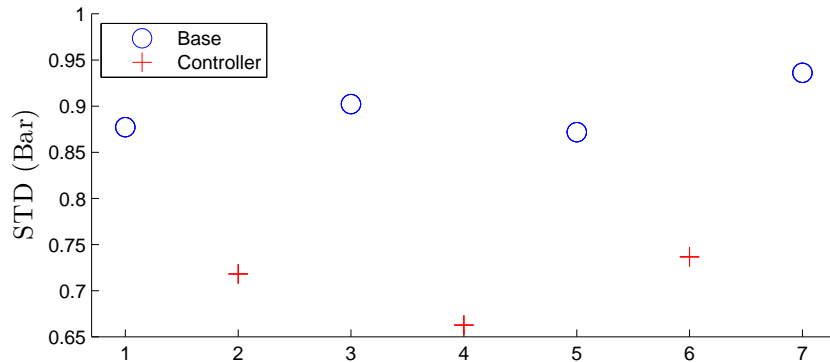
Figure 2.3: Pmax 4 Moving Average, Standard Deviation

Figure 2.4 shows the standard deviation, for all combustion metrics used in this study, taken from the same test as Figure 2.2. As seen in the figure, even though the standard deviation of the four cycle moving average decreased, the standard deviation on individual cycle combustion metrics greatly increased. The same results can be seen for the model developed specifically for this tests in Figure 2.5.

These results can be expected as filtering a system identification input has to be done with extreme care. If the filtering is done incorrectly, the system identification will tend to identify the dynamics of the filter, over the actual signal.

2.6   Summary

Four combustion metrics, θ_{Pmax}, Pmax, CA50, and IMEP are chosen based on previous research of characterization and control of cyclic variability. These combustion metrics are all measured by in cylinder pressure sensors. The control of cyclic vari-
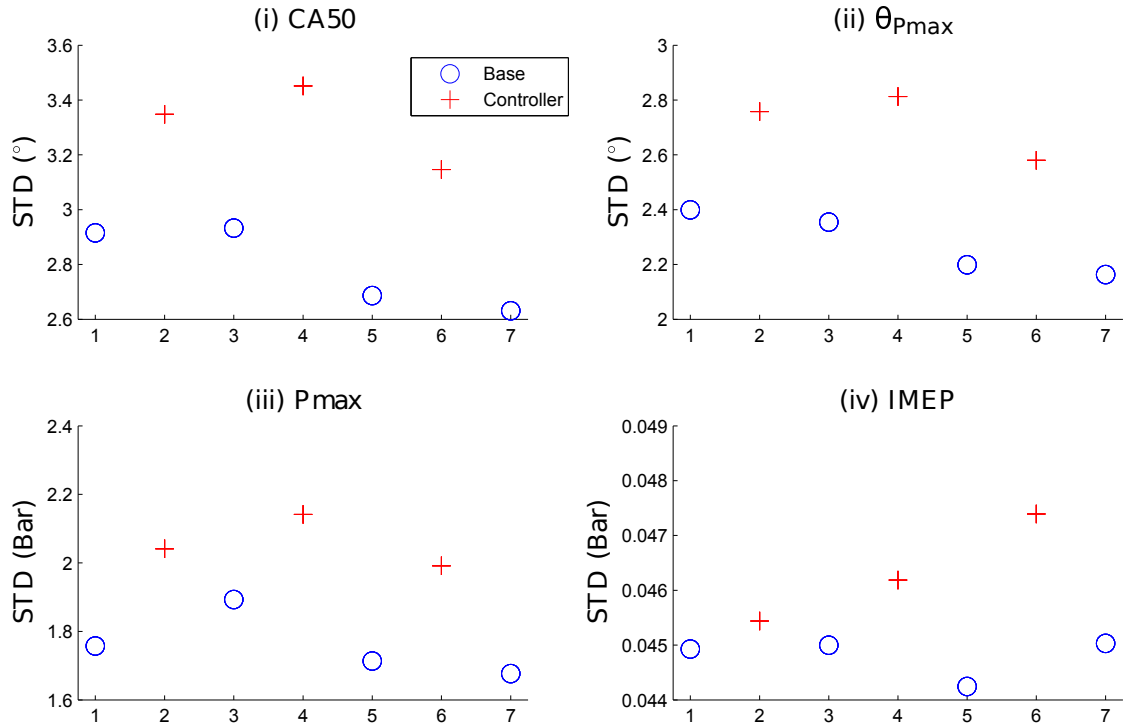
Figure 2.4: Standard Deviation of All Parameters

ability literature reviewed in this chapter reported between 0.5% to 20% decreases in cyclic variability when operating the controllers. The results of Li et al. [2009] which reported a 20% decrease in cyclic variability, were unable to replicated on the engine used in this study. The controller proposed by this study increased the cyclic variability of all four combustion metrics that are tested. Kaleli et al. [2015] reported a 7.9% decrease in cyclic variability, but the modeling results presented in this paper are unable to be replicated.
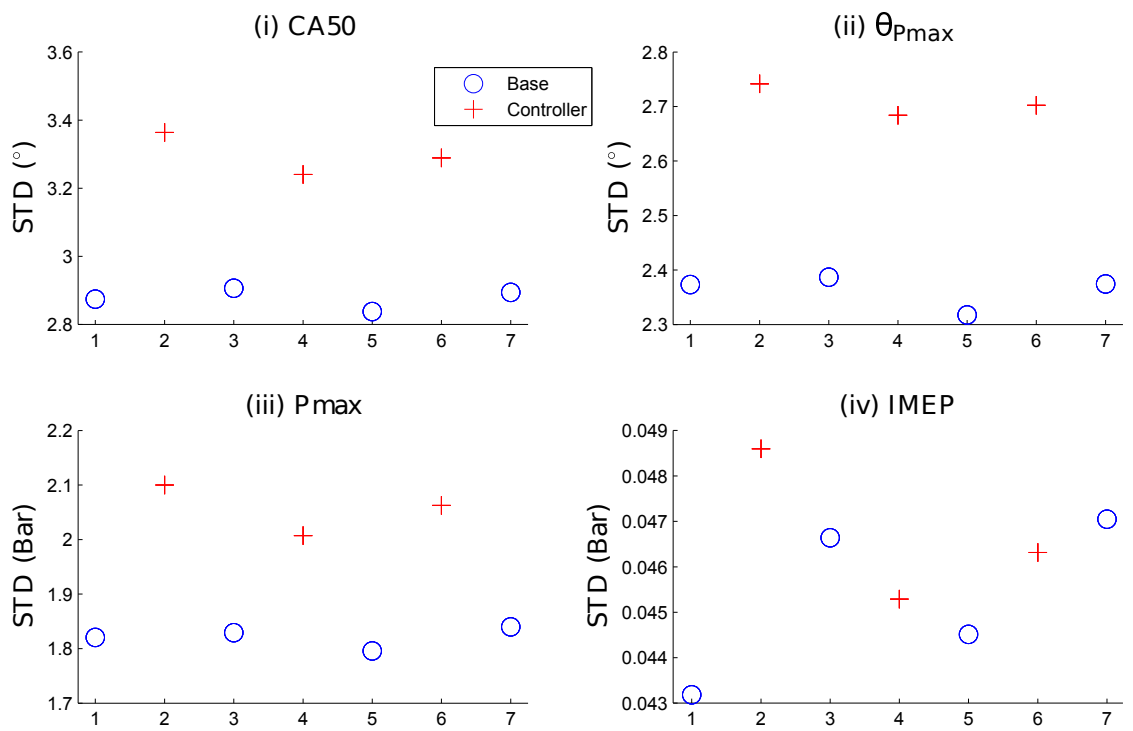
Figure 2.5: Standard Deviation of All Parameters

CHAPTER 3

EXPERIMENTAL SETUP

The experimental setup is an important part of this work as a modern test facility has been developed which will be useful for future research in the areas of natural gas combustion, gasoline direct injection, and engine controls. An overall schematic of the experimental setup is shown in Figure 3.1 with more detailed schematics of each system in the following sections. A picture of the engine, which all the systems are connected to, is shown in Figure 3.2.
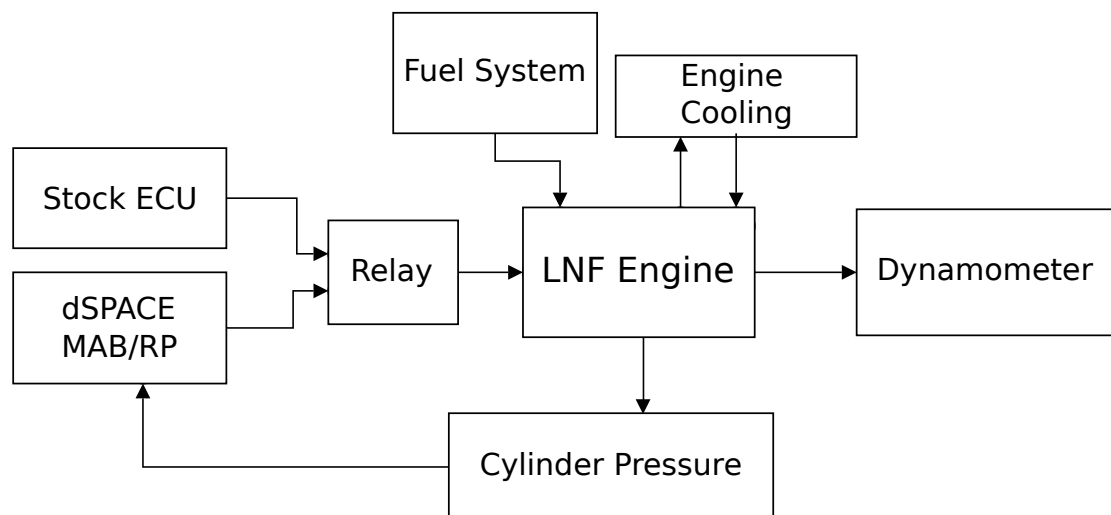
Figure 3.1: Overall Experimental Setup Schematic
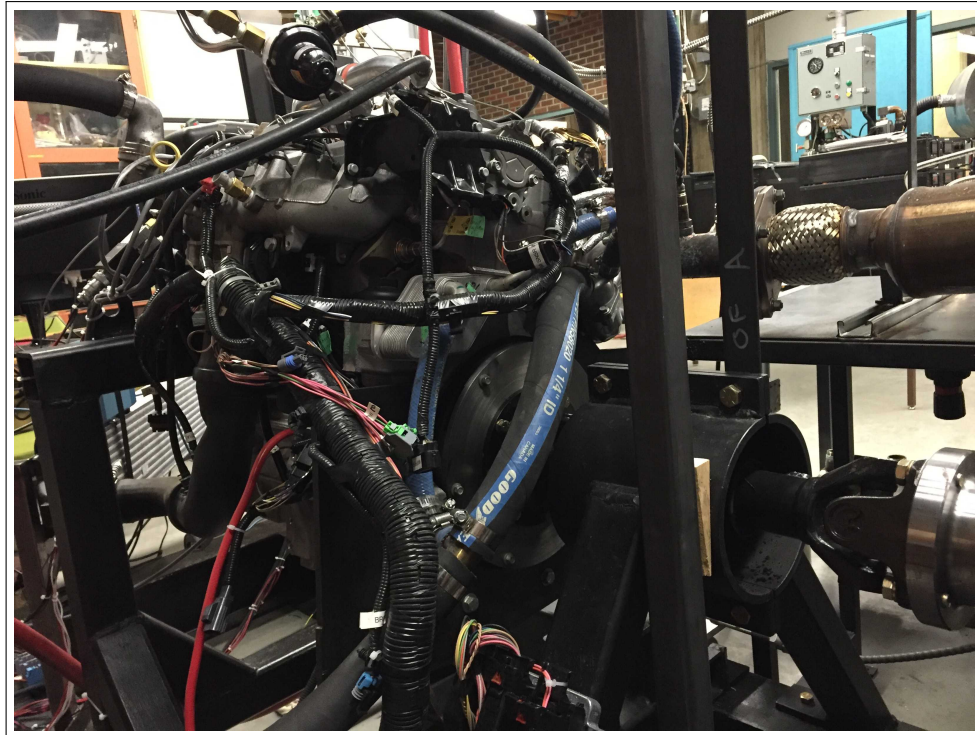
Figure 3.2: 2.0 L General Motors Ecotec II LNF Engine

3.1 LNF Engine

The engine block used in this report is a 2.0 L General Motors Ecotec generation II LNF engine with engine specifications listed in Table 3.1. This engine is equipped with dual camshaft variable valve timing phasers, cam powered high pressure fuel pump for direct injection fuel, and a twin scroll turbocharger. The engine control is a stock controller which can be overridden as will be discussed in section 3.8. A major addition to the stock engine is a port fuel injection rail, equipped with Bosch NGI-2 injectors, mounted on the intake manifold. NGI-2 injectors are capable of running both gas fuels such as natural gas and liquid fuels such as gasoline or biofuels. The injectors are mounted on the intake manifold very close to the valves as seen in Figure 3.3.

Table 3.1: LNF Engine Block Specifications

Bore	86 mm
Stroke	86 mm
Displacement	2.0 L
Compression Ratio	9.2:1
Valves Per Cylinder	4
Max Valve Lift	10.3 mm

3.2 Fueling System

The direct injection fuel system has a low pressure component consisting of a Walbro GSL 391 inline fuel pump and an Aeromotive 13129 EFI fuel pressure regulator which supplies the fuel at 60 psi to a high pressure system. The stock high pressure system is capable of pressures up to 15 MPa. The high pressure fuel pump regulates fuel rail pressure through a closed loop controller. For all experimental tests performed in this study, the fuel rail pressure will be regulated at 2 MPa. If the direct injection pulse width is rapidly increased, particularly at low speeds, the pump output can lag behind for a number of cycles as the stock controller was not designed to deal with the rapid step changes in injection pulse width that are done in this study.

There is also a duplicate low pressure fuel system, which was built for future liquid biofuel research but not used in this study, that can supply fuel to the port injectors for liquid fuel port injection when the port injection is not natural gas. The natural gas is regulated from the line pressure of 2,000 psi to 100 psi by an IMPCO Technologies HPR-3600 high pressure regulator. The IMPCO HPR-3600 is heated from the engine coolant loop to prevent freezing of the natural gas lines by the pressure drop. A schematic of the entire fuel system is shown in Figure 3.4.
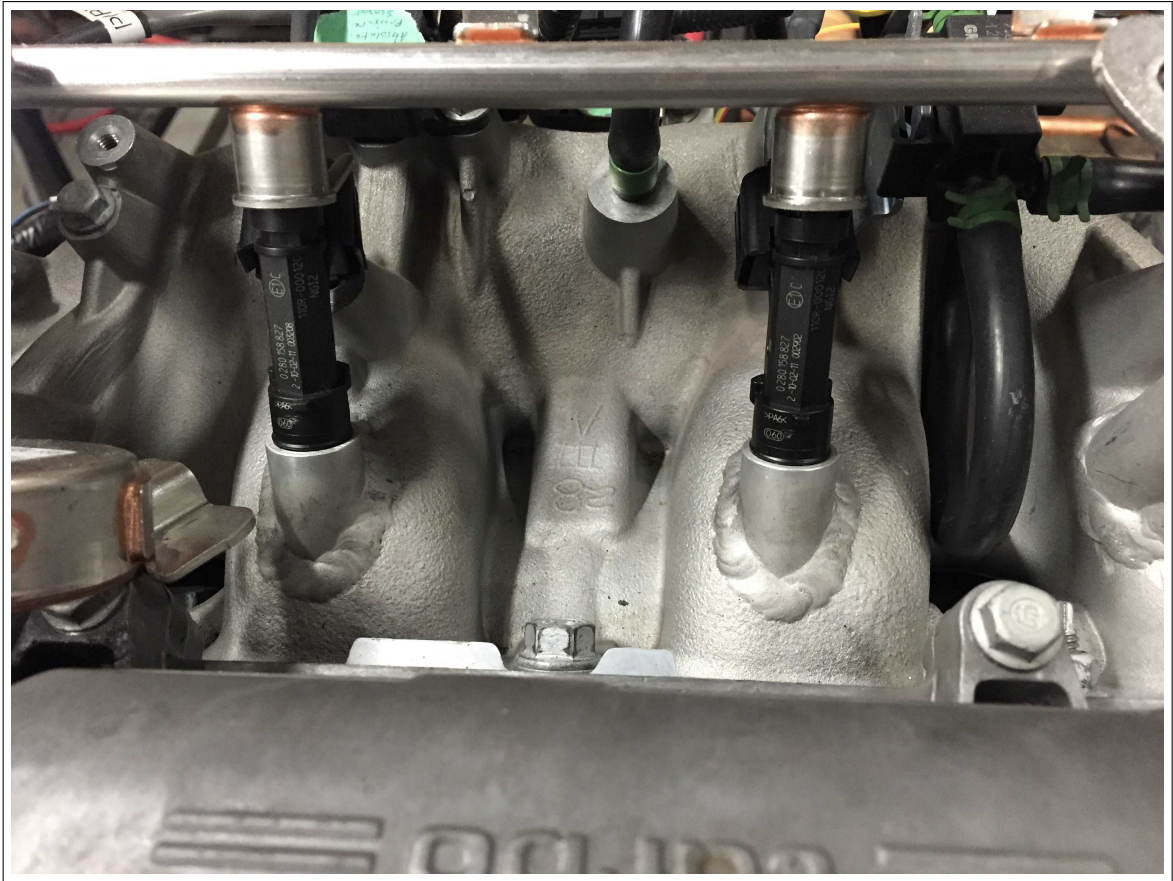
Figure 3.3: NGI-2 Port Injectors

3.3   Engine Dynamometer

The engine output is connected to a Dyne Systems 1014W passive dynamometer by a Machine Service MSI-41RE ISO-TEC vibration dampening rubber isolated driveshaft, as shown in Figure 3.5. The dynamometer is over designed to handle the speed and load ranges covered in this study as seen from the specification sheet in Figure 3.6. The Dynamometer speed is set by using the Dyne Systems panel shown in Figure 3.7.
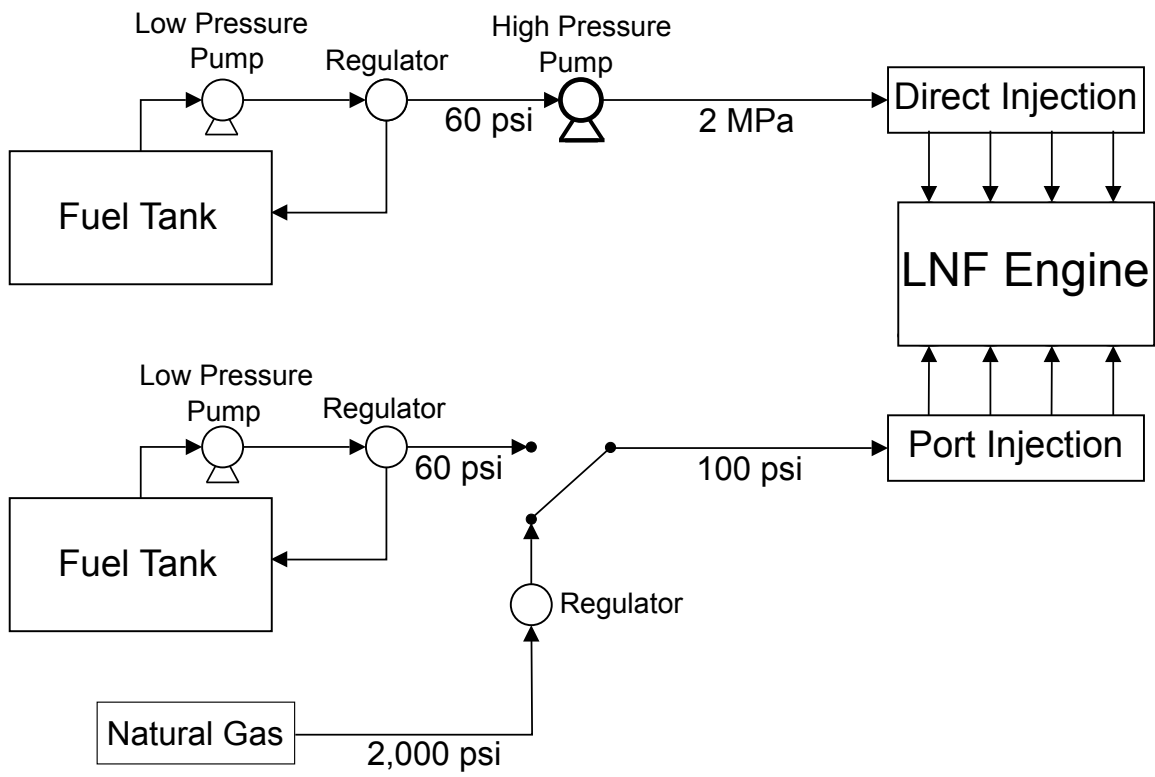
Figure 3.4: Fuel System Schematic
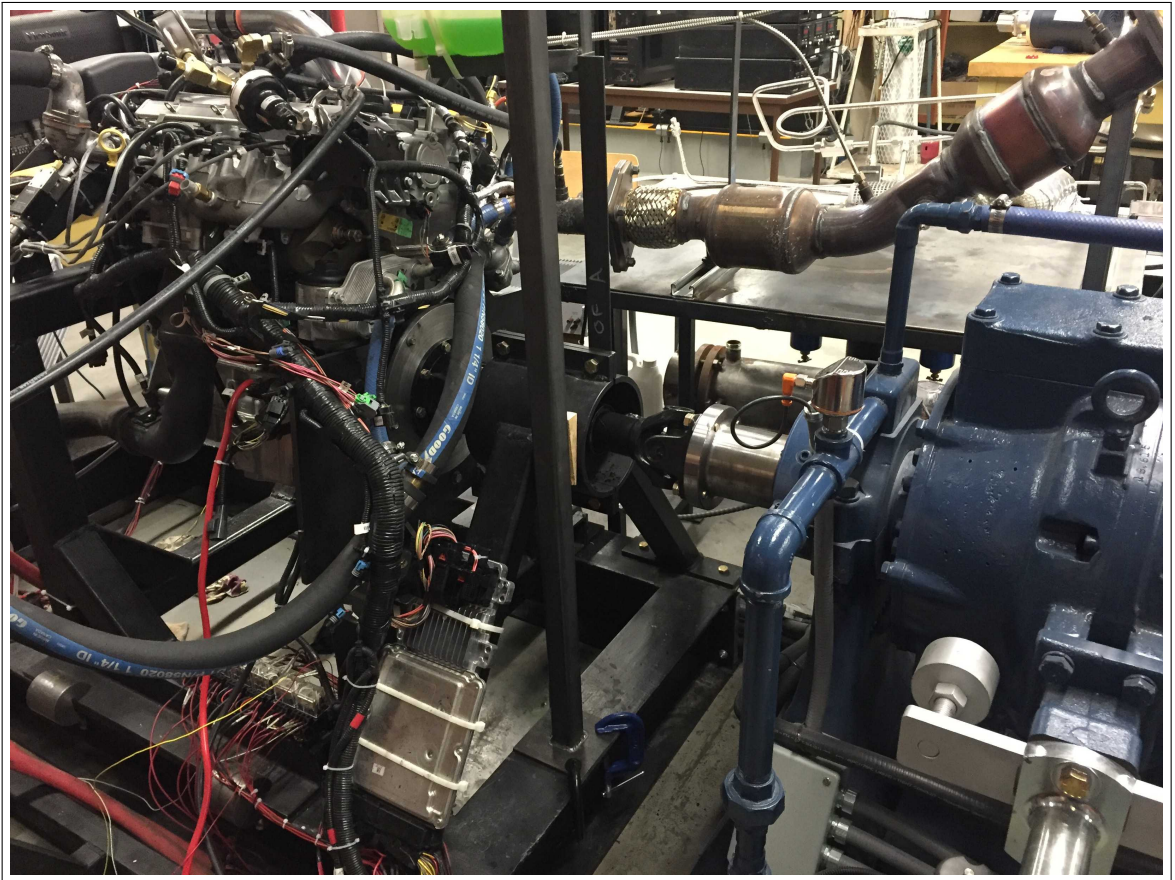
Figure 3.5: Dyne Systems Dynamometer Connected to LNF Engine
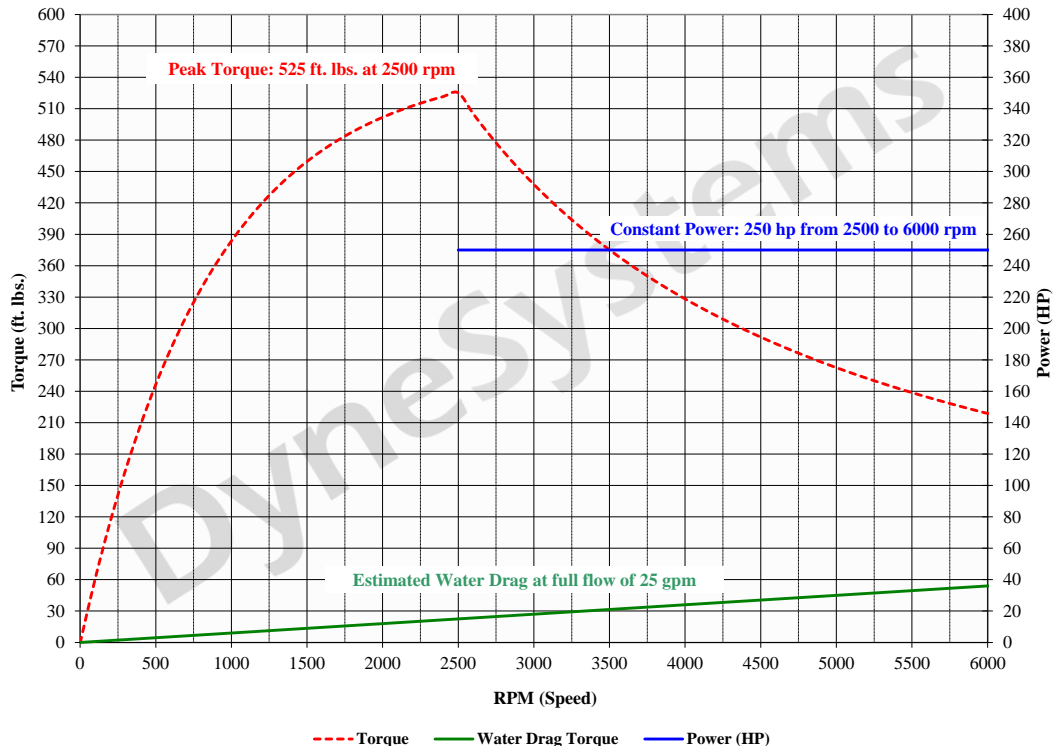
Figure 3.6: Dyne Systems Eddy Current Dynamometer Model 1014W

Figure 3.7: Dyne Systems Panel

3.4   Engine Cooling

The engine coolant is run through a CB100-24L flat plate heat exchanger where it is cooled by domestic cold water. The CB100-24L is designed to cool 90 gallons per minute of engine coolant from 90 °C to 75 °C using 25 gallons per minute of 20 °C water. The pressure drop across the heat exchanger is 5.1 psi at 90 gallons per minute. The LNF engine thermostat has been removed from its original position into a holder on the hot intake of the heat exchanger. The standard position of the thermostat on the inlet of the engine coolant was not suitable for lab use. This is because it is very difficult to get the inlet water temperature high enough to open the thermostat. A pressure relief valve, set to open at 15 psi, is mounted down stream of the thermostat. The engine coolant temperature is regulated around 90 °C. A schematic of the overall cooling system is shown in Figure 3.8. Pictures of the flat plate heat exchanger and pressure relief valve are shown in Figure 3.9
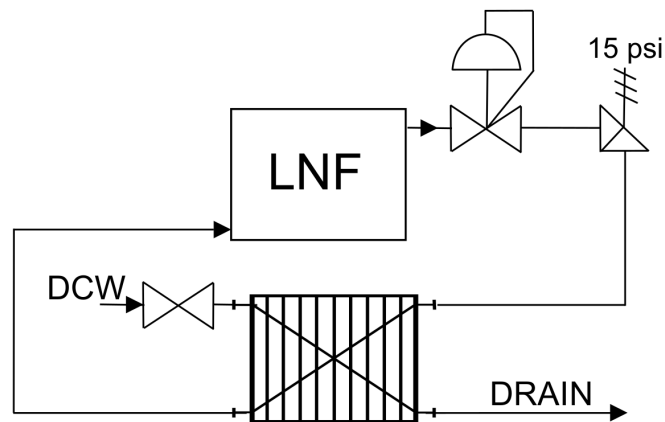
Figure 3.8: Engine Coolant Loop Schematic, LNF is 2.0 L Ecotec Engine, DCW is Domestic Cold Water.

Figure 3.9: Flat Plate Heat Exchanger and Pressure Relief Valve.

3.5   Engine Controller Relay

The engine is partially controlled by either the stock engine control unit (ECU) or a
dSPACE MicroAutoBox II 1511/1512 with RapidPro 1601 power electronics system
to drive spark and fuel injection. The dSPACE system as a whole will be referred to
as the dSPACE controller and the individual hardware pieces of the MicroAutoBox
II 1511/1512 and RapidPro 1601 will further be referred to as MicroAutoBox (MAB)
and RapidPro (RP). The engine has a 60 tooth encoder with a 2 tooth gap to find the
engines current crank angle. A 4 pulse signal from both camshafts, which rotate once

per engine cycle, are used to know the current engine stroke. These signals, along with a spark signal from cylinder 1, can be seen in Figure 3.10. The cam signals move with the camshafts so that the engine controller can control and monitor their positions. The engines crank and cam signals wires are split so that the MicroAutoBox and the stock controller can simultaneously measure these engine timing signals.
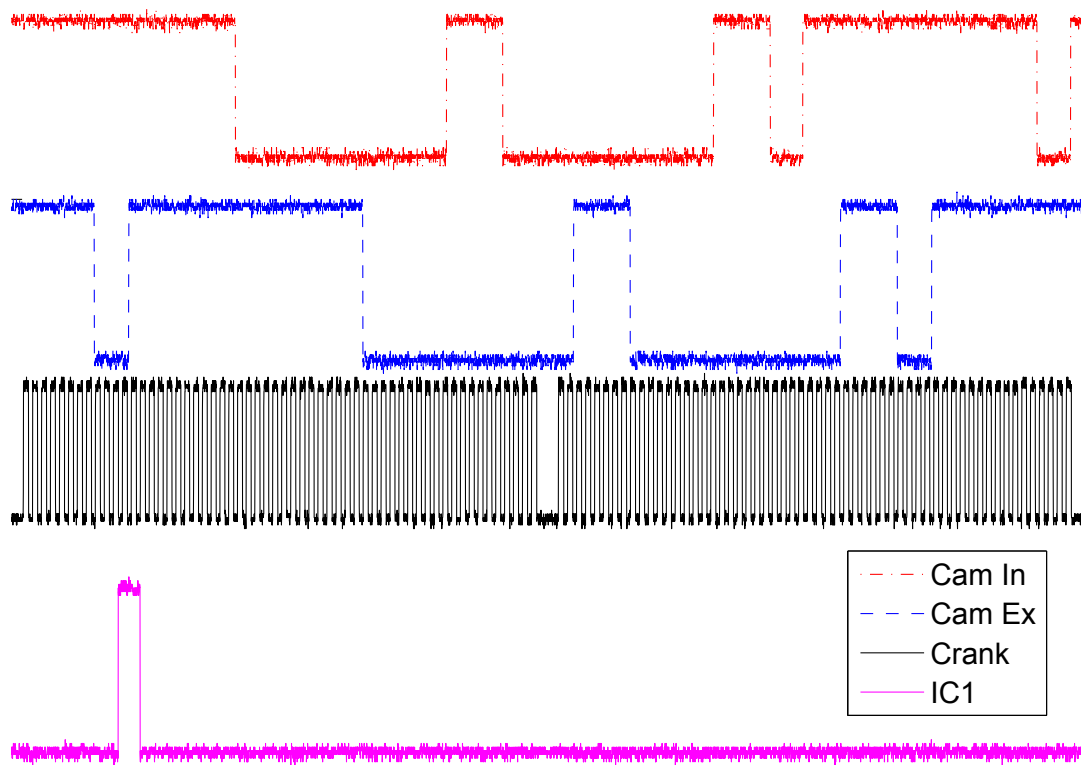
Figure 3.10: Cam Intake (Cam In), Cam Exhaust (Cam Ex), Crank, and Spark Ignition for Cylinder 1 (IC1)

The wired connection to the direct injection and spark ignition systems are switched using a set of electrical relays which changes the connection of these systems between the two controllers as shown in Figure 3.11. The dSPACE controller has greater flexibility compared to the stock controller as the dSPACE controller can vary injection

timing, duration, and number of fuel pulses as the engine is running. The port injectors are controlled by low side drivers on the dSPACE controller. The port injectors are not part of the relay system since the stock controller is built for direct injection and isn't capable of controlling them and so a separate dSPACE controller is used.
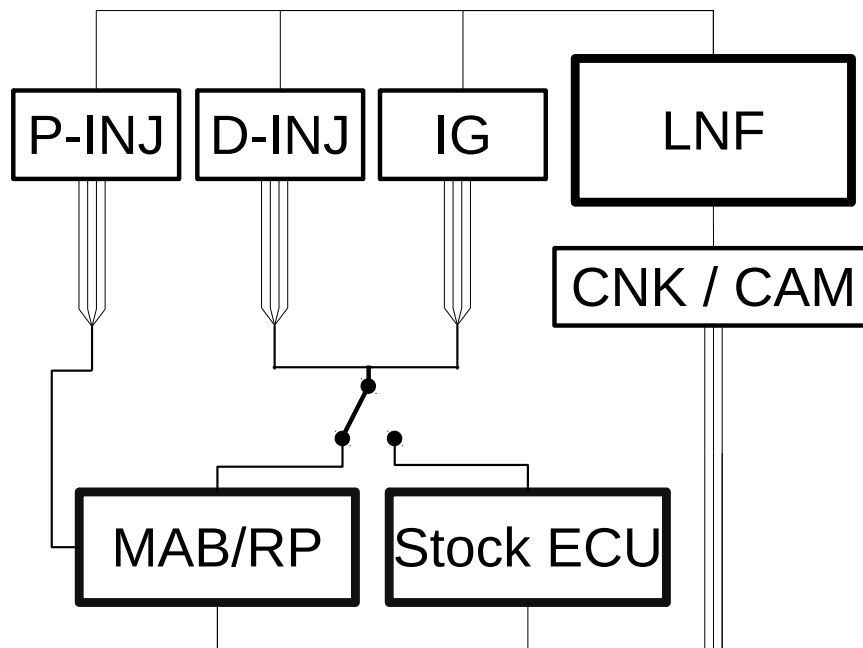
Figure 3.11: Engine Controller Wiring where dSPACE MicroAutoBox and RapidPro system is denoted MAB/RP, the 2.0 L General Motors Ecotec generation II LNF engine is denoted LNF, Port Injection is P-INJ, Direct Injection is D-INJ, and Spark Ignition is IG, and Crank and Cam Signals are CNK/CAM.

When the engine is switched to the dSPACE controller, the stock ECU direct injection wires are connected to a set of dummy injectors to prevent tripping diagnostic trouble codes (DTC) of the stock controller. Leaving the stock controller direct injection wires open results in the high pressure fuel pump shutting down as a fail safe. The dummy injectors are simply a resistor connected to a double coiled wire. The resistor provides similar resistance to the injectors while the double coiled wire provides a similar inductance. Both the resistor and the inductance wire are needed

to avoid triggering the engines fail safe mode. The inductance required was not near the inductance of the actual injectors. The inductance on the coiled wire is 43.9 μH and the resistor is 3 Ω. Although the dummy resistance of $3\,\Omega$ is close to the direct injectors (General Motoros Part Number 1263611) resistance of $10\,\Omega$, the dummy inductance of 43.9 μH is not close to the inductance of the injectors of thousands of μH but it is sufficient to avoid triggering the fail safe. The method used to measure the inductance of dummy injectors was not capable of precisely measuring such a large inductance. The stock ECU spark wires are left open when the dSPACE controller is used which triggers a DTC code but no further action from the controller is taken.
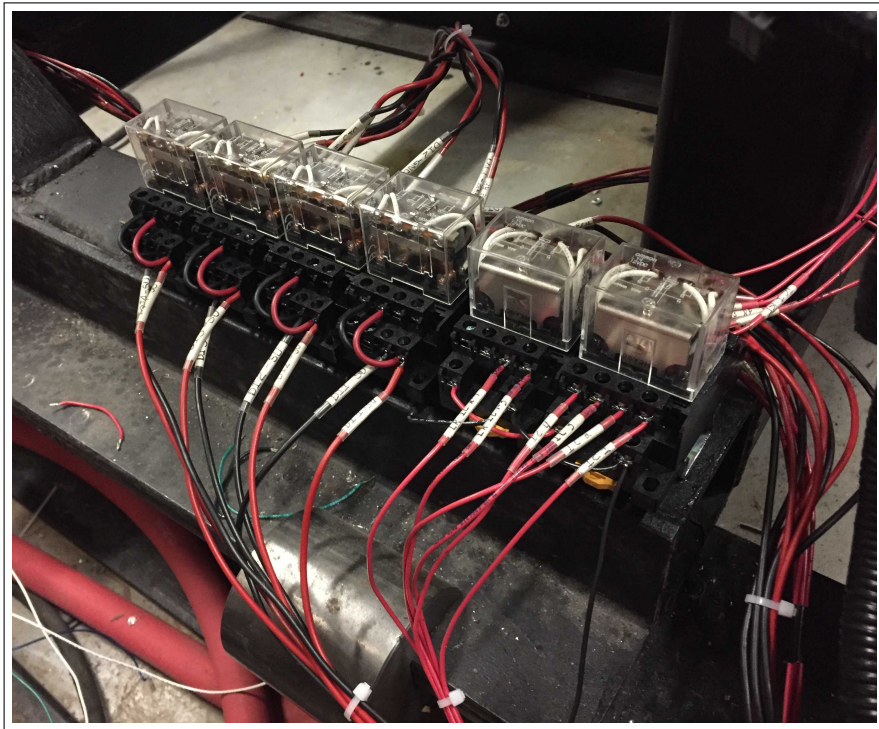
Figure 3.12: Relays for Switching Controllers

The cam phasers can also be controlled by either the stock controller or the dSPACE controller by changing which system has a physical connection to the phasers. However, this system is not controlled by electrical relays but rather by manually swapping connectors attached to the phasers. The cam phasers can only work to

increase the valve overlap, which means the intake valve timing can only be advanced and the exhaust valve can only be retarded. Both valves have a maximum phasing of 50 crank angle degrees (CAD) and further details of how the dSPACE controller manipulates the cam phasers will be discussed in section 3.8.1.

3.6   Sensors

The engine is equipped with a variety sensors that are sampled at a low speed (1 to 10 hz). These are listed in Table 3.2. In the table exhaust gas temperature is shortened to EGT, and engine speed is defined in revolutions per minute (RPM). For this study the unit symbol for degree ° will always reference crank angle degrees unless stated otherwise. The sensors sampled at 10 hz are recorded by VCM scanner, which reads the outputs connected to the stock ECU through a on-board diagnostics II cable. The VCM scanner interface is shown in Figure 3.13. The sensors sampled at 1 hz are recorded by LabVIEW, the interface to which is shown in Figure 3.14.

3.7   Cylinder Pressure

3.7.1   Charge Amplifiers

The engines cylinder pressure is measured with Kistler 6125C11U20 sensors capable measuring pressures up to 300 bar. The sensor for cylinder one is connected to a Kistler 5010B 1 channel charge amplifier. Cylinders 2, 3, and 4's Kistler 6125C11U20 sensors are connected to a MTS 1108 4 channel charge amplifier. Two separate charge amplifiers are used because only one Kistler charge amplifier is available. The Kistler charge amplifier has greatly reduced noise in the signal compared to the MTS 1108 which is attributed to ground loop noise as the MTS 1108 is physically removed from the setup as it is part of the adjacent engine test cell. The MTS 1108 however is a 4 channel amplifier where as the Kistler can only amplify a single sensor.

Table 3.2: Low Speed Sensors

Sensor Measurement	Measurement Range	Resolution	Sample Rate
Accelerator Position	0-100 %	1	10 hz
Barometric Pressure	0-240 kPa	1	10 hz
Boost Sensor	0-320 kPa	1	10 hz
Dyno Power	0-250 hp	1	1 hz
Dyno RPM	0-6000 RPM	1	1 hz
Dyno Torque	0-712 Nm	1	1 hz
Engine Coolant Temp	1-125 °C	1	10 hz
Engine Oil Temp	0-110 °C	1	10 hz
Engine Speed	0-6300 RPM	1	10 hz
Exhaust Cam Angle	0-50 °	0.1	10 hz
EGT after first Catalyst	0-500 °C	0.1	1 hz
EGT after second Catalyst	0-500 °C	0.1	1 hz
EGT after Turbo	0-500 °C	0.1	1 hz
Fuel Rail Pressure	0-20 MPa	0.1	10 hz
Intake Air temp	0-50 °C	1	10 hz
Intake Cam Angle	0-50 °	0.1	10 hz
Manifold Air Pressure	0-240 kPa	1	10 hz
Mass Air Flow	0-100 g/sec	0.05	10 hz
Throttle Position	0-100 %	1	10 hz
WB Lambda	0.5-1.5 λ	0.05	10 hz

The MTS 1108 is suitable for cylinders 2, 3, and 4, because the data for those cylinders is only used for offline calculation where complex non-casual filters can be used to reduce the noise. Figure 3.15 shows both the unfiltered signal directly from the MTS system and the offline filtered data. It can be seen that the noise in the signal is easily filtered out using a 4th order low pass zero phase Butterworth filter that filters both forward and backward in time.

Figure 3.16 shows the unfiltered and filtered data from the Kistler charge amplifier with the same voltage scale as in Figure 3.15. Comparing the two figures it can be seen that noise amplitude for cylinder 1 peak is approximately 20 times smaller than cylinder 3 at peak pressure. When the intake valve opens there is considerable noise in the pressure signal for cylinder 1, as shown in Figure 3.17, which is not important for online calculations and is easily filtered offline.

Figure 3.13: VCM Scanner

Figure 3.14: LabVIEW Interface

The MTS 1108 charge amplifier is connected to a MTS CAS 2816/2840. The MTS CAS then outputs all the cylinder pressures as 0-5 V analog output which is then

routed into the same NI which records the Kistler charge amplifier output as shown in Figure 3.19.
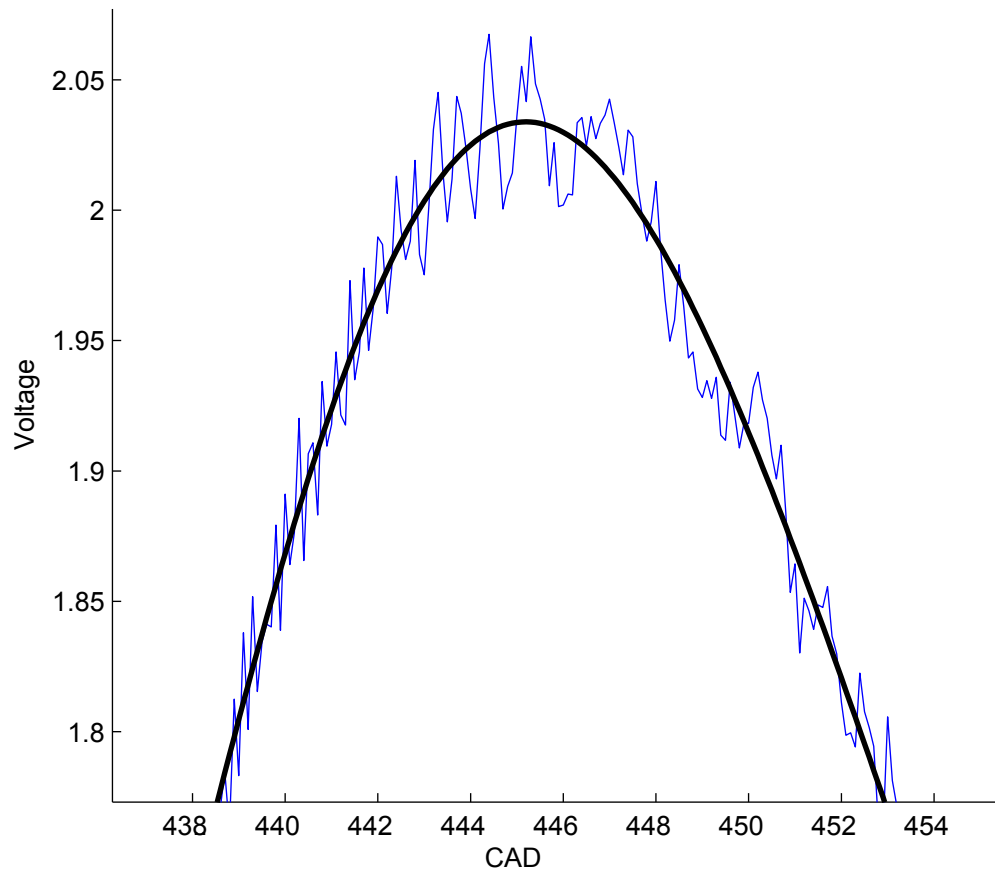
Figure 3.15: Cylinder 3 Peak with Filter

3.7.2 Data Acquisition Timing

The analog output for all cylinders pressure is recorded by an NI PCIe-6351 data acquisition card. A BEI 3600 encoder (model XH25D-F1-SS-3600-ABZC-28V/V-SM18) is mounted to the engines crankshaft pulley. The encoder's A signal produces 3600 pulses per revolution. This encoder signal is sent to the NI card and triggers the sampling of the cylinder pressure from the charge amplifier 3600 times per revolution.
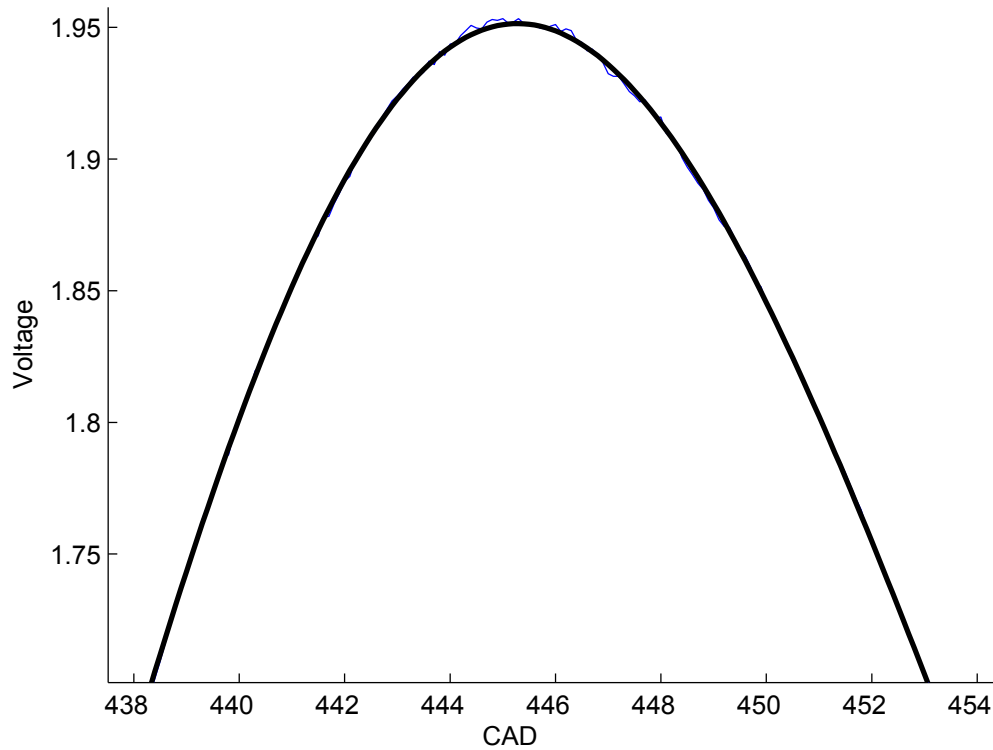
Figure 3.16: Cylinder 1 Peak with Filter

The result is the cylinder pressure data is sampled every tenth (0.1) of a CAD.

The Z signal from the encoder is a pulse that is the same width as the A signal but occurs once per revolution. Since a complete engine cycle is 720°, the Z signal cannot be used to trigger the NI card data acquisition at a constant crank angle. To get a 720° trigger signal, the Z signal is combined with a signal sent by the dSPACE MicroAutoBox controller, which sends out a high digital signal between the crank angles of 350° and 440°. This signal and the encoder Z are both sent to a NAND hardware gate (chip DM5400). Two NAND gates on the chip are combined to produce a logical AND. With the encoder Z signal occurring at 371.8° (which is 428.2° before top dead center (BTDC) of cylinder 1) the output from this AND gate provides the NI card with a once per cycle trigger it can use to start recording an engine (720°)
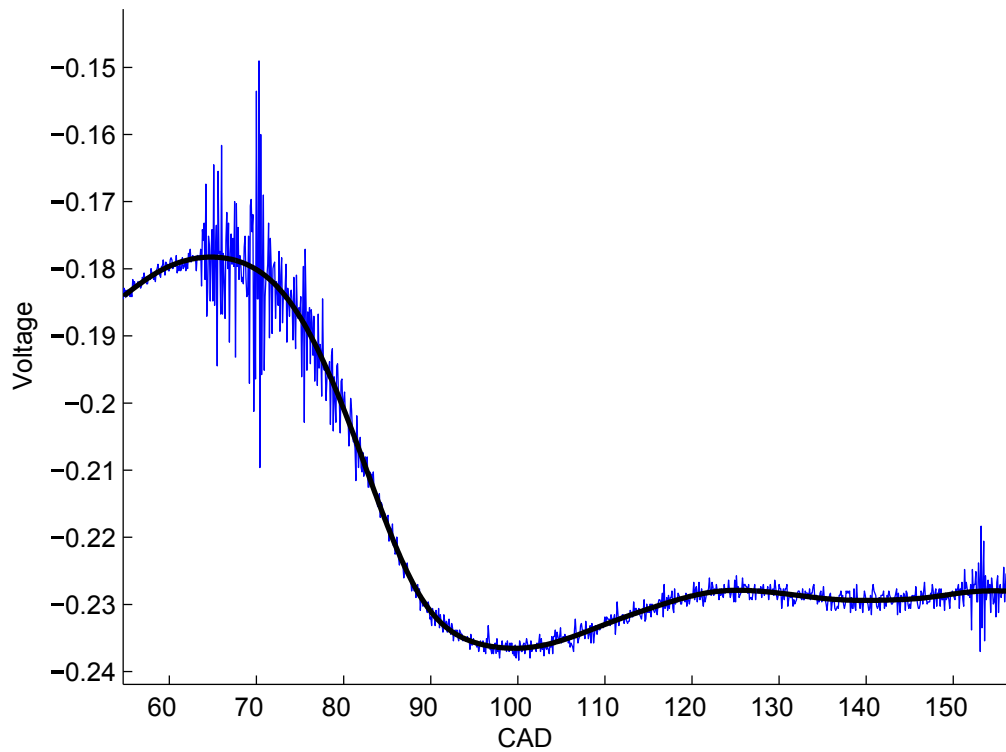
Figure 3.17: Cylinder 1 Intake Valve openning

cycle or 7200 cylinder pressure samples.

3.7.3 Cylinder Pressure Pegging

A Validyne P305A absolute pressure sensor, with a 0-20 psi diaphragm, is mounted on the intake manifold close to cylinder 1. Since the Kistler cylinder pressure sensors used in this study only measure pressure differential, there is substantial drift in the absolute pressure value over time [Audet, 2008]. To correct for the drift, the pressure measured by the Validyne is sent to the NI card where it is used to give an absolute reference to the cylinder pressure every engine cycle.

Just before the intake valve closes on the intake stroke, the pressure in the manifold and the cylinder are assumed equal. The absolute manifold pressure measured by the

Validyne is used to "peg" the cylinder pressure to the same value every engine cycle. Cylinder 1 is pegged at the point corresponding to just before intake valve closing for that cylinder. Cylinders 2, 3, and 4 are all pegged to the same pressure as Cylinder 1. Figure 3.18 shows manifold air pressure (MAP) for one complete engine cycle with the locations corresponding to just before intake valve closes. For the case of 1250 RPM and 62 Nm running natural gas, the maximum difference between the values of all 4 cylinders at their respective pegging location is 0.35 kPa.
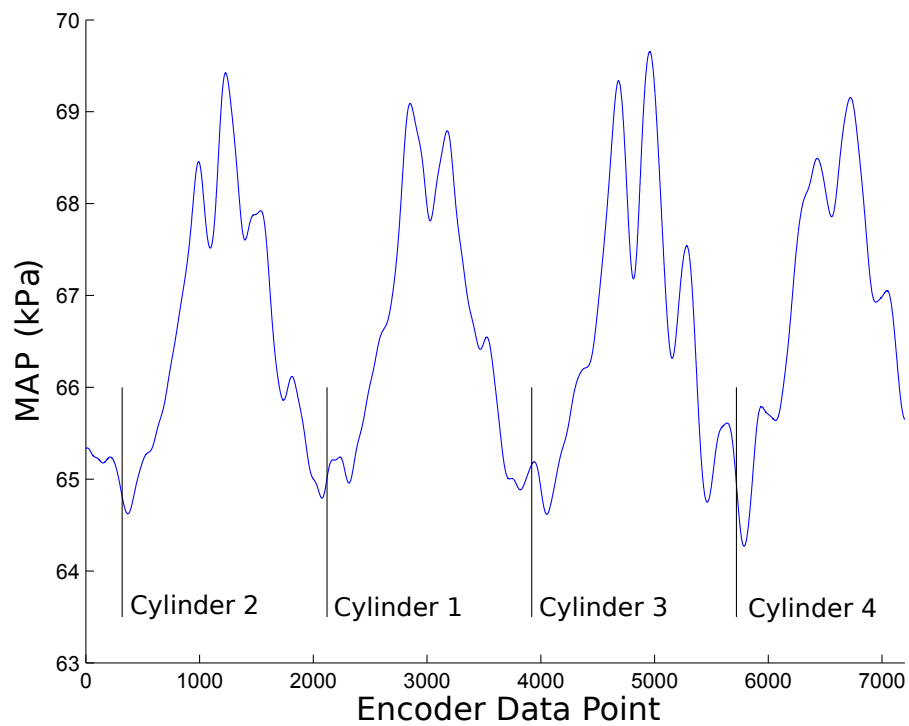
Figure 3.18: MAP for One Engine Cycle.

3.7.4 Control Output Parameter

To control the combustion of the subsequent cycle the cylinder pressure trace of cylinder 1 is analyzed on the NI card computer and depending on the control type a combustion metric, such as peak pressure location, is calculated. This calculated

value is then sent to the dSPACE controller to be used in a closed loop controller such as a minimum variance controller. An analog output on the NI card connected to an analog input on the MicroAutoBox, is used to send this value. The NI card starts the cylinder pressure recording 428.2° BTDC of cylinder 1 and continues for 720°. Then the NI card pegs the cylinder 1 pressure; calculates the combustion metric; and outputs the results as an analog signal to the MicroAutoBox. The calculation time is between 30-45 CAD at 1750 RPM. To keep this calculation time at a minimum, the pressure trace of cylinder 1 is not filtered. The affect of not filtering will be discussed in section 3.8.8.

A schematic of the entire cylinder pressure setup is shown in Figure 3.19.
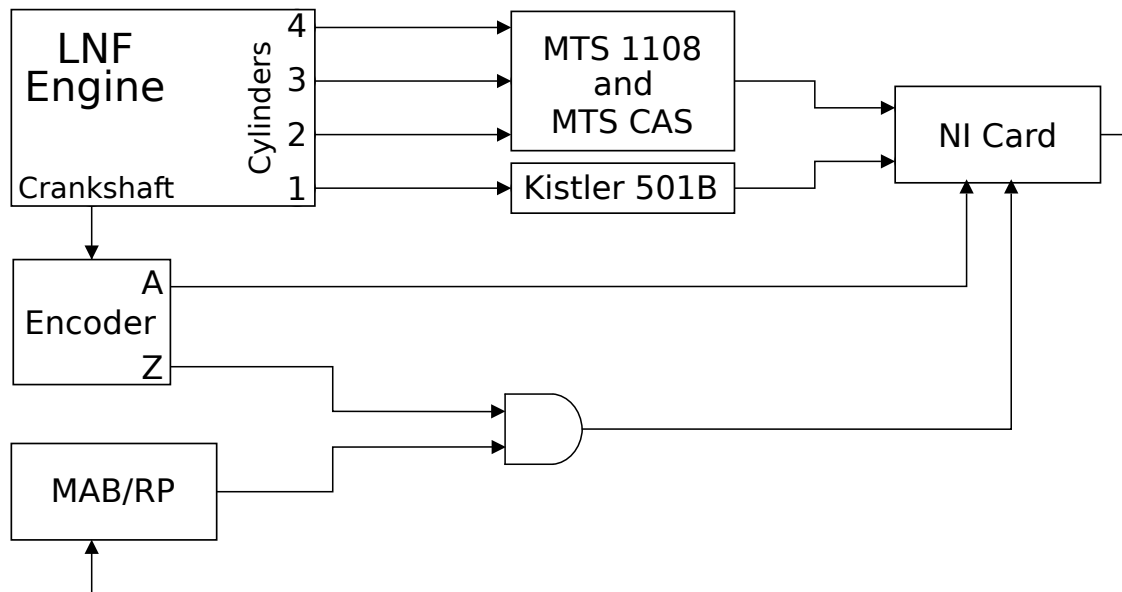
Figure 3.19: Cylinder Pressure System Schematic

3.8 dSPACE Controller

3.8.1 dSPACE Hardware and Software Overview

The system referred to as the dSPACE controller is a set of two separate pieces of hardware, the MicroAutoBox (MAB) and the RapidPro (RP), which are connected by a low voltage differential signalling cable. Pictures of the MAB and RP can be seen in Figures 3.20 and 3.21. The MAB runs the system model while the RapidPro is the power electronics that drives the various engine components.

The control algorithm running in the dSPACE controller is specified using a Matlab Simulink block diagram model, shown in Figure A.1. Simulink allows for reading the inputs of the system and visually programming (using block diagrams) of what the specified outputs should do. Special blocks provided by dSPACE for Simulink allows reading and writing on the hardware I/O such as displaying the engine speed measured from the crank sensor. The reading and writing between the hardware is done through an Ethernet cable connected to the computer and the MAB. An example of the model that drives the port injectors by defining the start angle and duration of injection is shown in Figure 3.22. After the Simulink model is loaded onto the dSPACE controller, the dSPACE program ControlDesk allows the changing of engine inputs, such as start angle and duration of the port injectors, through the interface shown in Figure A.2.

The hardware modules installed for the RP used in this study, along with a brief description, are listed in Table 3.3.

3.8.2 Hardware Interrupts

The dSPACE hardware is capable of individual cylinder interrupts. This means that there is a single main task running at all times and each cylinder being controlled is interrupted separately at a specific crank angle. The updating of a cylinder control

Table 3.3: MAB Installed Modules (* Indicates modules not used in this study.)

Module Name	Description
DS1634	Lambda Sensor Input*
DS1637	Crankshaft/Camshaft Sensor Input
DS1638	8 Channel Thermocouple Input*
DS1647	8 Channel Digital Out
DS1661	2 Channel Universal Driver*
DS1662	6 Channel Low Side Driver
DS1663	6 Channel High Side Driver*
DS1664	Direct Injection Driver

Figure 3.20: MicroAutoBox

Figure 3.21: RapidPro

input such as spark or fuel pulse width only happens during the interrupt. For each cylinder interrupt all of the code within its block is calculated and the new values for both spark and fuel are sent to the RapidPro module that actually generates the signals. If the MAB sends updated spark or fuel information after the the RP has generated spark or fuel signals, a double spark or injection, or a missed spark or injection can occur. For example, if the system is set to spark at 50° BTDC and the interrupt for the same cylinder is set to 30° BTDC, then the interrupt and the sending of updated information to the module is happening after the the start of the spark signal. If the spark value is then changed to 10° BTDC, the controller will produce a double spark. This is because the first spark at 50° BTDC will happen and then the interrupt and the new spark timing will be sent to the spark module

at 30° BTDC. Then at 10° BTDC the system will spark again as this is the new value. If the spark value is now changed from 10° BTDC to 50° BTDC, no spark will happen.

For this reason the interrupt angle for an individual cylinder must be set before the earliest possible starting point for either spark or fuel injection. This can become an issue when operating a closed loop controller as discussed further in section 3.8.7.

The Simulink model is designed with the engine components broken into 8 virtual cylinders. Virtual cylinders 1 through 4 control the spark timing and the direct injectors for the actual cylinders 1 through 4, while virtual cylinders 5 through 8 control the port injectors for the actual cylinders 1 through 4. Even though Simulink is able to handle having a single virtual cylinder with both port injectors, direct injectors, and spark, this is not done because of the complexity of the interrupt timing for closed loop control that will discussed in section 3.8.7. The interrupt setup for virtual cylinders 5 through 8 is shown in Figure 3.22. The left side of the figure shows the port injection duration and timing common for all 4 cylinders. These common values are then modified inside each cylinder so that each cylinder can run on individual values if needed.

The amount of crank angle degrees the interrupt is before the top dead center (TDC) of the cylinder is shown in Table 3.4. TDC is given in reference to the first falling edge after the 2 tooth gap on the crank encoder and $\Delta°$ signifies the number of degrees between the interrupt and the cylinder TDC.

3.8.3 Spark Control

The General Motors Ecotec LNF engine comes standard with a coil on plug ignition system. The stock ECU controls the spark timing by sending a digital signal to the ignition coils. The digital signal rising edge begins the charging of the ignition coil. The digital falling edge is the signal that fires the spark. The amount of time it takes
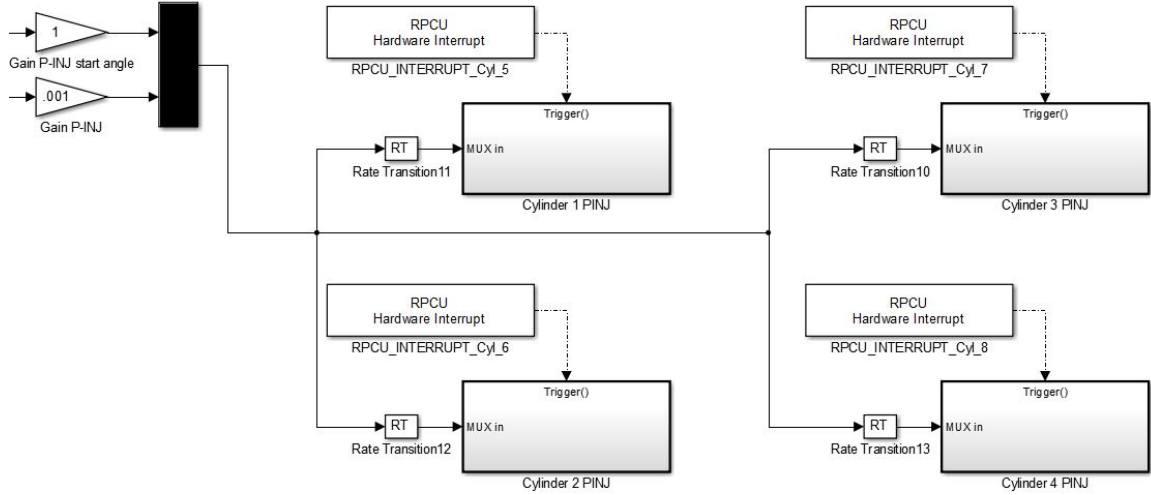
Figure 3.22: dSPACE Interrupt Simulink Blocks

Table 3.4: Simulink Interrupt Settings (Negative Indicates Previous Cycle)

Virutal Cylinder	Actual Cylinder	Cylinder TDC °	Interrupt °	Δ°
1	1	80	-240	320
2	2	620	190	430
3	3	260	-170	430
4	4	440	10	430
5	1	80	-360	440
6	2	620	180	440
7	3	260	-180	440
8	4	440	0	440

to charge the ignition coil is approximately 3 ms.

To control the spark with the dSPACE controller, the wires for each cylinder that lead to the ignition coil have been placed into the relays described in section 3.5. The wires from the relay are connected to the RapidPro DS1647 module described in Table 3.3. The Simulink model allows for setting both the start angle (rising edge) and the end angle (falling edge) of the spark signal in °BTDC. This is sufficient for setting the end angle since the actual firing of the spark (which occurs with a digital falling edge) is always determined in °BTDC. The start angle of the spark however, must always be 3 ms before the end angle to account for the charging of the ignition coil.

Since Simulink can only specify the start and end angle in CAD, the 3 ms ignition coil charging time must be converted to CAD which is dependent on the engines speed.

The calculation for ignition start angle is: shown in the equation below.

$$\theta_{\text{start}} = \theta_{\text{end}} + \frac{n}{60} \cdot 360\,° \cdot 0.003\,s$$

where θ_{start} is the start angle, θ_{end} is the end angle, and n is the engine speed in RPM. For this study, spark timing is always referencing the actual firing of the spark plug which is set by the end angle. When the engine is operating at a fixed RPM, the engine dyno holds the RPM within ±1 RPM so this calculation is switched off and a steady state value for that RPM is added to the falling edge angle. This helps restrict the number of engine input variables that are changing.

3.8.4   Port Injector Control

Port Injectors are controlled by low side power drivers that are pulled to ground. The high side of the port injectors is always connected to the battery of power supply that is powering the injectors. To open the port injectors the low side of the system, that is connected to RP DS1662 module described in Table 3.3, is switched to ground allowing the flow of current.

Initially there is a large current draw from the system in order to open the injectors. Once the injectors are open the current draw reduced to a steady current value called the hold current. The time from low side driver grounding to the start of the hold current is called the opening time. Due to the physical construction of the injectors there is a minimum time the injectors must be activated for before fuel will flow through the injectors. For the Bosch NGI-2 port injectors used here the opening time is 1.4 ms at the supplied voltage of 13.5 V. The dSPACE controller sets both the start angle for port injection and the open duration using the pulse width.

3.8.5 Direct Injector Control

The stock ECU can be switched (see Figure 3.11) to the engines direct injectors with 4 pairs of wires for each of the 4 direct injectors. These 4 wire pairs are connected to two high side drivers and 4 low side drivers. Cylinders 1 and 4 share one of the high side drivers and cylinders 2 and 3 share the second. If cylinder 4's direct injector wires are attached to an oscilloscope while cylinder 1 was injection, the normal voltage spike would be seen in cylinder 4. However if a resistor is attached so that the current flowing through the wires could be measured, there would be almost no current flow. This is because the low side driver for cylinder 4 would be open if cylinder 1 was injecting.

The RapidPro module DS1664 described in Table 3.3 uses the same high side driver and low side driver configuration as the stock ECU. A current control system alternates the current between upper and lower limits to open the injector and to hold the injector open. The opening current upper and lower limits are 11 A and 9 A and the hold current upper and lower limits are 3 A and 2 A. These values were determined by measuring the open and hold current the stock ECU uses to operate the direct injectors.

3.8.6 Cam Phaser Control

The intake and exhaust cam phasers are are connected to the Rapid Pro DS1662 module described in Table 3.3. The cam phasers operate on a pulse width modulated signal. Two proportional-integral-derivative controllers operate both cam phasers with the control input being the amount of cam phasing measured by each cam signal, shown in Figure 3.10, and the control output being the duty cycle % of the pulse width modulated signal. The Simulink block diagram and PID gains for cam phasing control were supplied by Professor Mahdi Shahbakhti of Michigan Tech University, and can

be seen in Figures A.3 and A.3.

3.8.7   Closed Loop Control

As discussed in section 3.7.4 a selected combustion metric from the analysis of the cylinder pressure of cylinder 1 is sent from the NI card and read into the MicroAuto-Box as the closed loop feedback signal.

The control algorithm is generated from a Simulink block diagram that is compiled, downloaded and run on the MicroAutoBox at a fixed sample rate $T_s = 0.5$ ms. To reduce noise of the analog signal between the NI card and the MAB, a 10 point moving average filter on the analog input is used. The 10 point filtering algorithm takes 0.05 s which is 25 CAD at 1750 RPM. This means that the MicroAutoBox has calculated the combustion metric roughly 350 ° BTDC of cylinder 1 which is 30 ° before the cylinder 1 interrupt shown in Table 3.4. This 30 ° is used as a safey factor since the combustion metric calculation time can vary slightly. The entire closed loop control timing, including the information discussed in section 3.7.4, is shown in Figure 3.23.

3.8.8   Control Signal Sources of Error

The cylinder pressure trace data used in the real time closed loop controller cannot be filtered as discussed in section 3.7.4. This causes the combustion metrics that are calculated from filtered data and unfiltered data to differ slightly.

For example, a comparison of 40 cycles of θ_{Pmax} calculated from offline filtered data and the θ_{Pmax} value recorded online in the dSPACE controller is shown in Figure 3.24. Using the θ_{Pmax} values recorded on the dSPACE controller includes not only the error in the unfiltered data being analyzed but also the error from transmitting the analog signal between the NI card and the MAB. Assuming that the offline filtered data yields the exact θ_{Pmax}, a bias error of -0.23 ° after top dead center (ATDC) is found in the

online input when comparing 1,000 cycles of both data sets. The error has a standard deviation of .18°. The 95% confidence interval for a single measurement would be ± 0.35°. This error would propagate through the minimum variance controller used in section 5.3.4 and yield a spark timing confidence interval of ± 0.035°.

3.9 Summary

A 4 cylinder General Motors direct injection engine is modified into a modern engine test facility. The facility is able to compare a production vehicle controller to a flexible dSPACE controller capable of changing engine inputs, such as spark timing or fuel, during engine operation. Port injectors are added to the engine so that dual fuel injection strategies can be tested. The port injectors are also capable of running either liquid fuels, such as gasoline or biofuels, or gaseous fuels, such as natural gas. The measurement of the engines in cylinder pressure every 0.1 crank angle degrees for all 4 cylinders allows for detailed offline analysis of the engine operation. Online feedback of a single combustion metric into the dSPACE controller allows for use of closed loop controllers using the in cylinder pressure measurements as feedback.
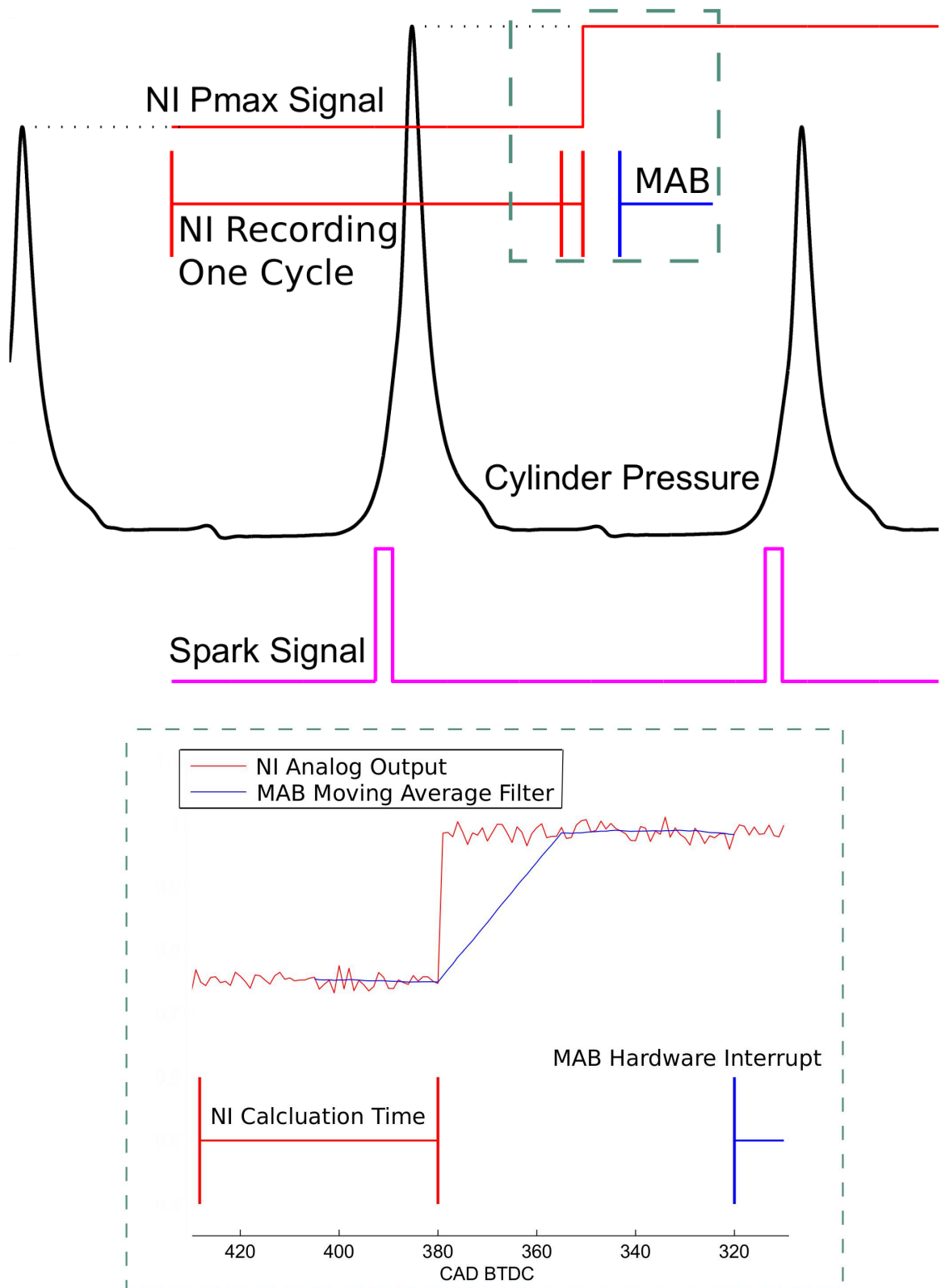
Figure 3.23: Input-Output Data Timing
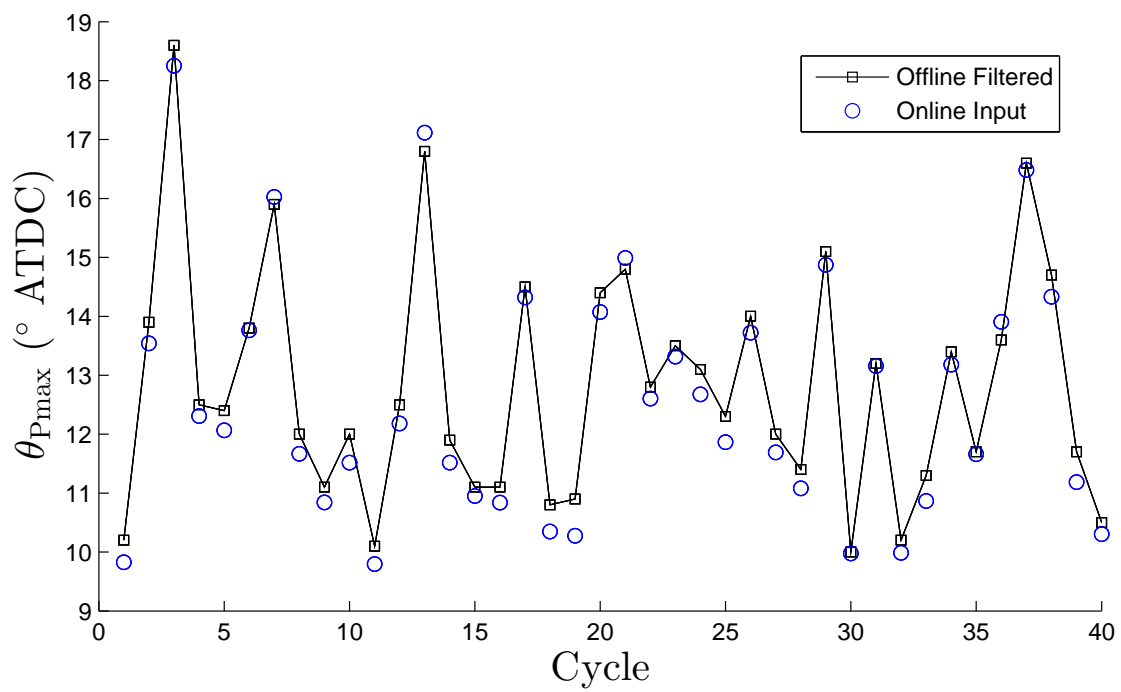
Figure 3.24: Difference Between θ_{Pmax} received in online input and θ_{Pmax} calculated using offline filtering.

CHAPTER 4

CHARACTERIZING CYCLIC VARIABILITY

4.1   Test Conditions

For this study, all of the experiments performed will either be a steady state test, system identification test, or transient test. Engine inputs, variables, and outputs are defined in Figure 4.1. For the steady state tests, the engine inputs are constant and the engine variables are kept within the bounds specified in Table B.1. These tests are primarily used to characterize the engine and provide baseline data for comparison to the closed loop control data. System identification tests are performed at steady state except for the plant input. The plant input is used to excite the system so the paired input output data can be used to develop system identification models [Ljung, 1987]. In this study, transient tests will have a single engine input that varies during the test. These tests are used to test the implemented controllers ability to reject the transient disturbances.

To check the response of the system at several conditions, four test conditions, listed in Table 4.1, are chosen. The letters beside each condition will subsequently be used to refer to the particular condition. For all tests some slight variation in the engine variables can't be avoided. All engine inputs and variables for each test condition, along with the maximum variation, are listed in Table B.1.
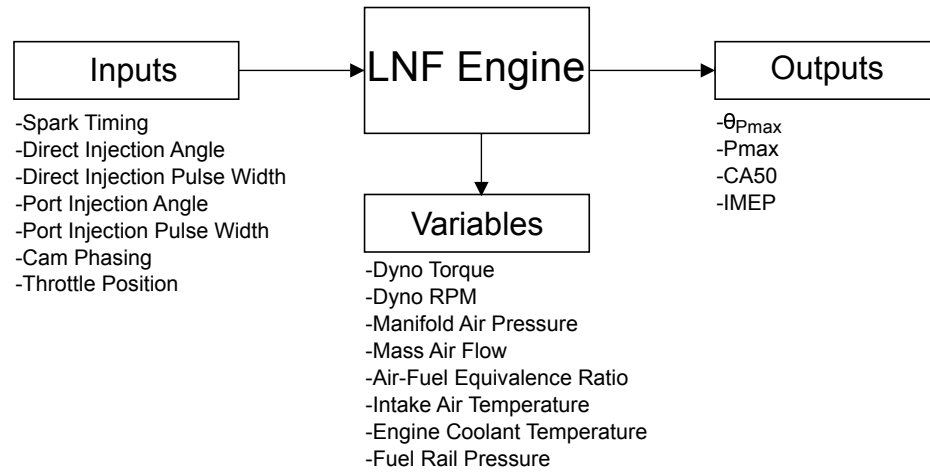
Figure 4.1: Engine Inputs, Variables, and Outputs

Table 4.1: Test Conditions

(A) 1250 RPM, Natural Gas, 4 Bar BMEP.

(B) 1750 RPM, Natural Gas, 4 Bar BMEP.

(C) 1250 RPM, Gasoline, 4 Bar BMEP.

(D) 1750 RPM, Gasoline, 4 Bar BMEP.

4.2   Effect of Spark Timing on Cyclic Variability

Each figure data point in this section and sections 4.3 and 4.4 is calculated from 1,000 engine cycles of cylinder pressure data for each of the four cylinders. The four combustion metrics (CA50, θ_{Pmax}, Pmax, and IMEP) are calculated for each of the 1,000 cycles for each cylinder. The average value and standard deviation (STD) of the 1,000 cycles for each individual cylinder are then calculated. Next, the average values and standard deviations of all the cylinders are averaged together to produce one average value and one standard deviation for each of the 4 combustion metrics at each spark timing. The standard deviations are combined together using the pooled variance method [Killeen, 2005]. For the average values, the 95% confidence interval

(CI) of the sampled mean is calculated using the standard error calculation:

$$95\% \text{ CI} = \overline{x} \pm \frac{s}{\sqrt{n}} \cdot 1.96$$

where $\overline{x}$ is the sample mean, s is the sample standard deviation, and n is the number of samples. The confidence interval is represented on average value figures as the error bars.

For test condition (C) in Table 4.1, the spark timing is varied from 16-28 ° BTDC. Then the four combustion metrics (CA50, θ_{Pmax}, Pmax, and IMEP) average value at each spark timing is calculated as shown in Figure 4.2. IMEP has a maximum value at a spark timing of 20 ° BTDC. At this point of maximum IMEP, $\theta_{\text{Pmax}} = 16$ ° ATDC. Using $\theta_{\text{Pmax}} = 16$ ° ATDC to set spark timing is found to produce maximum IMEP [Heywood, 1988]. Zhu et al. [2003] and Triantos et al. [2003] both used $\theta_{\text{Pmax}} = 16$ ° ATDC as the reference for maximum IMEP control.

The standard deviation of each combustion metric is defined as its cyclic variability. With increasing spark advance (spark timing is in ° BTDC so a larger value indicates advance), all four values of cyclic variability increases as shown in Figure 4.3. Pmax and θ_{Pmax} seem to have the largest drop when comparing the standard deviation at the least advanced spark (16 ° BTDC) to the standard deviation at the most advanced spark (28 ° BTDC). CA50 combustion metric also seems to have more variation in its standard deviation than the other combustion metrics. IMEP appears to hit a minimum standard deviation at the maximum spark advance. Previous research that measured the coefficient of variation of Pmax and IMEP with respect to spark timing, found the same linear relation with Pmax, and non-linearity of IMEP presented in this study [Stone, 2012].

Figure 4.2: Combustion Metrics Average Value and Error bars representing Standard Error for spark sweep at Test Condition (C) in Table 4.1

Figure 4.3: Combustion Metrics Cyclic Variability (Standard Deviation) as a function of Spark Sweep for Test Condition (C) in Table 4.1

4.3 Effect of Fuel on Cyclic Variability

To look at the effect of fuel type on cyclic variability, the same spark sweep as in section 4.2 (from 16-28° BTDC) is performed using natural gas instead of gasoline. The test conditions for gasoline and natural gas are conditions (C) and (A) in Table 4.1. Both fuels follow the same trend of an IMEP plateau to a maximum value then decreasing as shown in Figure 4.4. However, all four combustion metrics are shifted approximately 2° later (less advance) for natural compared to gasoline.
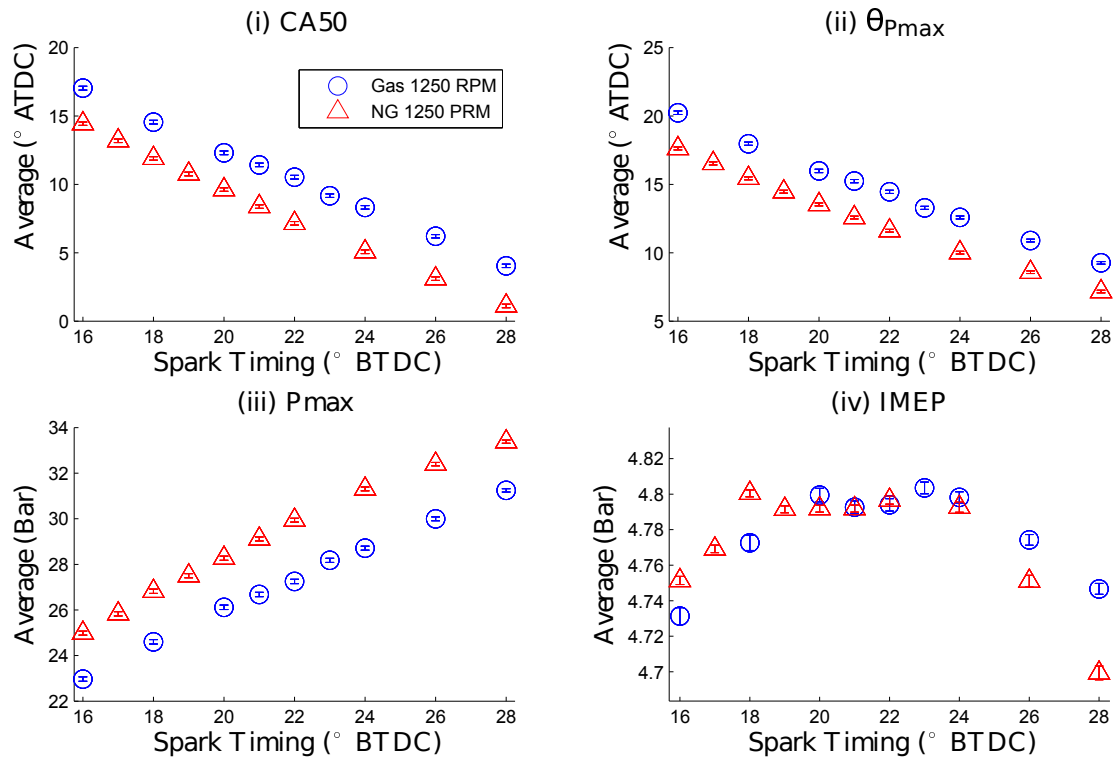
Figure 4.4: Combustion Metrics Average Value and Error bars representing Standard Error for Spark Sweep at Test Condition (C) and (A) in Table 4.1

By plotting all of the combustion metrics with respect to θ_{Pmax} as opposed to spark timing, this offset is removed as shown in Figure 4.5. It appears that the averaged combustion metrics show similar trends when plotted with respect to θ_{Pmax} for these two fuels. Although both fuels obtain peak IMEP at approximately the

same θ_{Pmax}, natural gas combustion has a longer plateau section and begins dropping off later than gasoline does. Based on the data presented using a different fuel will only change the spark timing needed to obtain a θ_{Pmax}, but not the θ_{Pmax} needed to obtain peak IMEP as suggested in the literature [Heywood, 1988].
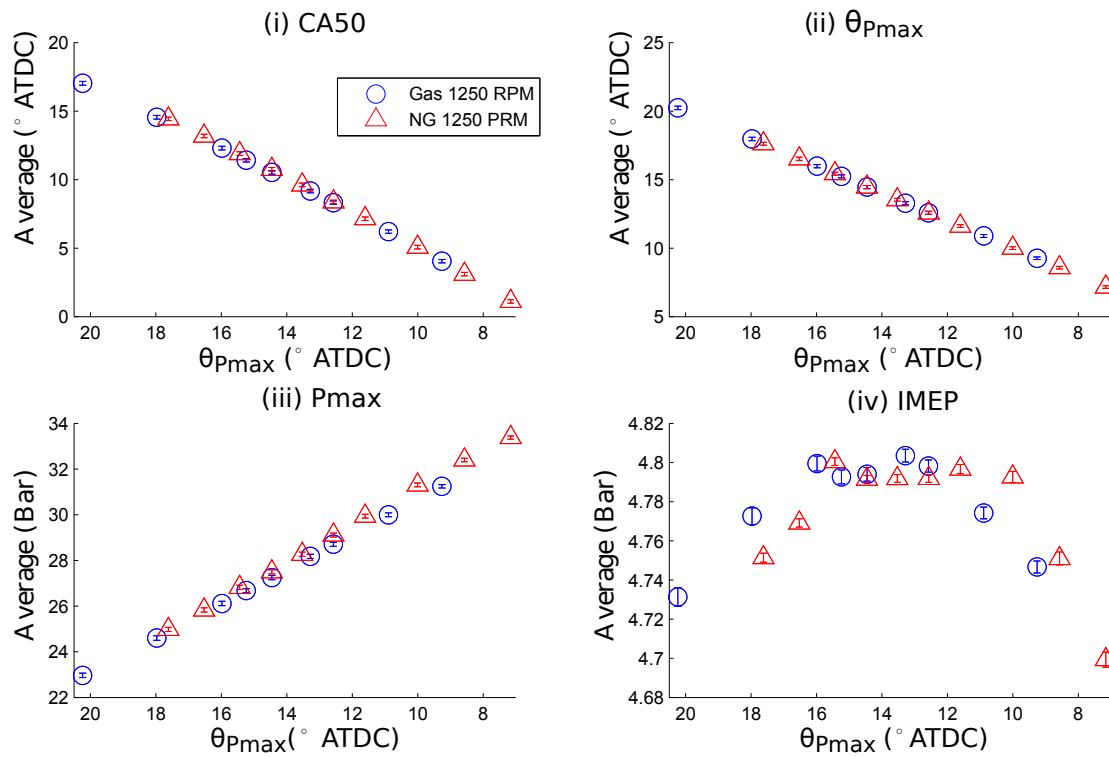
Figure 4.5: Combustion Metrics Average Value and Error bars representing Standard Error for Changing θ_{Pmax} at Test Condition (C) and (A) in Table 4.1

The amount of cyclic variability in both natural gas and gasoline with respect to θ_{Pmax} is shown in Figure 4.6. As seen in the figure, θ_{Pmax} and CA50 seem to have a larger cyclic variability for gasoline compared to natural gas. This indicates that although a set θ_{Pmax} for either fuel will yield the same average CA50, the variability of the combustion metric will change based on the fuel. The Pmax variability seems to be identical for both fuels with respect to θ_{Pmax}. The IMEP cyclic variability for natural gas seems to decrease, level off, and then increase. The IMEP cyclic variability

for gasoline seems to follow the same trend except it has an offset both in terms of the amount of cyclic variability, and the location of the plateau. The offset in amount of cyclic variability indicates that at the same operating conditions gasoline will have a larger variability of IMEP than natural gas does.

Figure 4.6: Combustion Metrics Cyclic Variability (Standard Deviation) for Changing θ_{Pmax} at base points (C) and (A) in Table 4.1

4.4 Effect of RPM on Cyclic Variability

The spark sweep for natural gas at test condition (A) is repeated at 1750 RPM for test condition (B) (defined in Table 4.1) to test the effect of engine speed. The 1,000 cycle average values for the 4 combustion metrics for both natural gas operating conditions are shown in Figure 4.7. A spark timing offset of $2°$ (1750 RPM requires $2°$ of extra spark advance to output same value as 1250 RPM) appears to be only difference between the average combustion metric values for the two test conditions. The difference in peak IMEP is attributed to the torque resolution ($\pm$ 1 NM = $\pm$ 0.063 Bar) of the dynamometer which prevented the engine operator from knowing that the exact same load point had not been reached. The Y axis for the IMEP plot in Figure 4.7 subplot (iv) means that difference between the two operating conditions is quite small in terms of engine torque.

Figure 4.8 shows the standard deviation of the combustion metrics plotted as a function of θ_{Pmax} as opposed to spark timing. Even when plotted based on θ_{Pmax} values, the 1750 RPM condition has a higher variability (standard deviation) for CA50, θ_{Pmax}, and Pmax. The cyclic variability of IMEP seems to be similar for both engine speeds for the same θ_{Pmax} values.

4.5 Summary

Four combustion metrics, θ_{Pmax}, Pmax, CA50, and IMEP are calculated for two fuels and at two different engine speeds for several spark timings. The effects of changing spark timing, fuel type, and engine speed have on cyclic variability is examined. For the conditions tested, advancing spark timing reduces the standard deviation of all combustion metrics except for IMEP, which varies non linearly with spark timing. At a given θ_{Pmax} value, gasoline produces a higher standard deviation for all combustion metrics except for Pmax. Increasing engine speed is found to increase
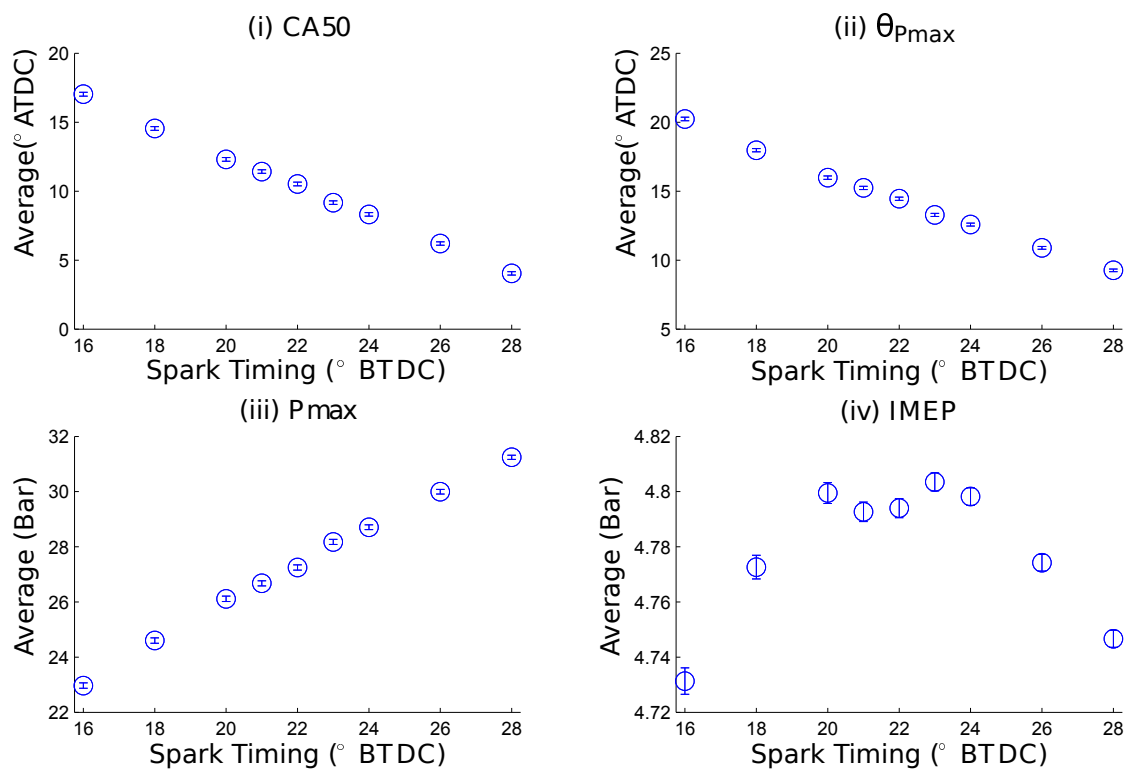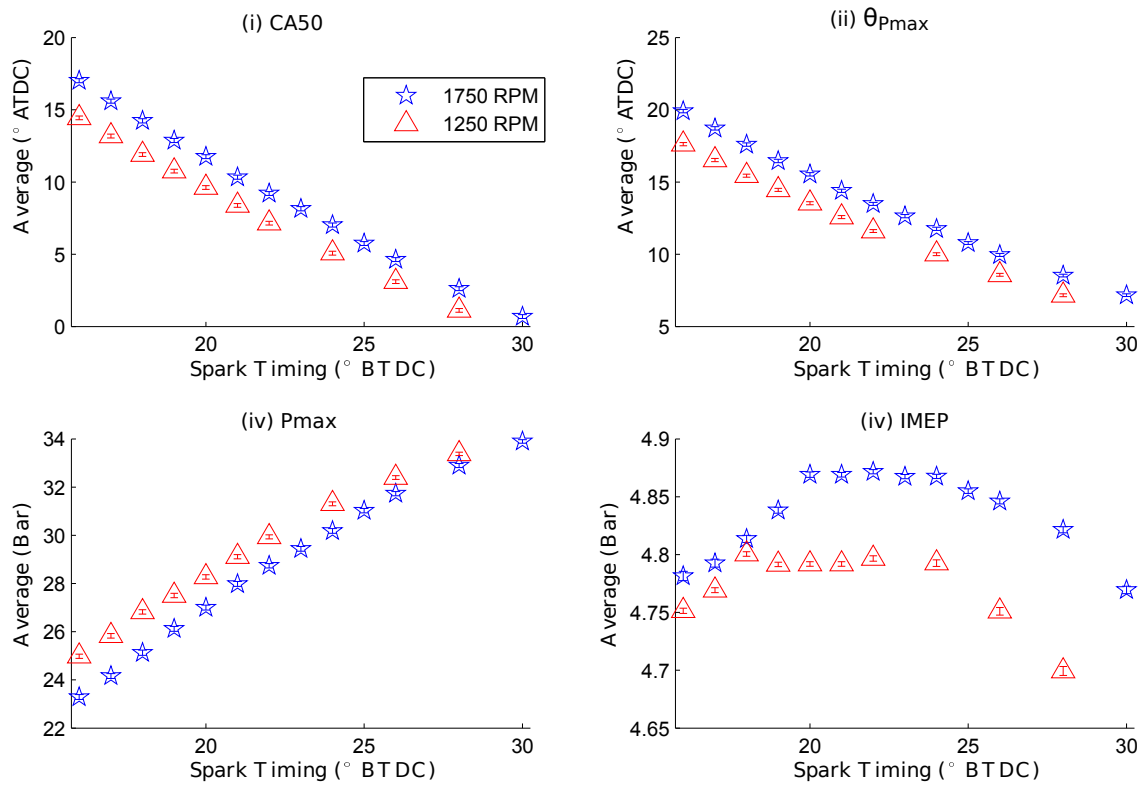
Figure 4.7: Combustion Metrics Average Value and Error bars representing Standard Error for Spark Sweep at Test Conditions (A) and (B) in Table 4.1
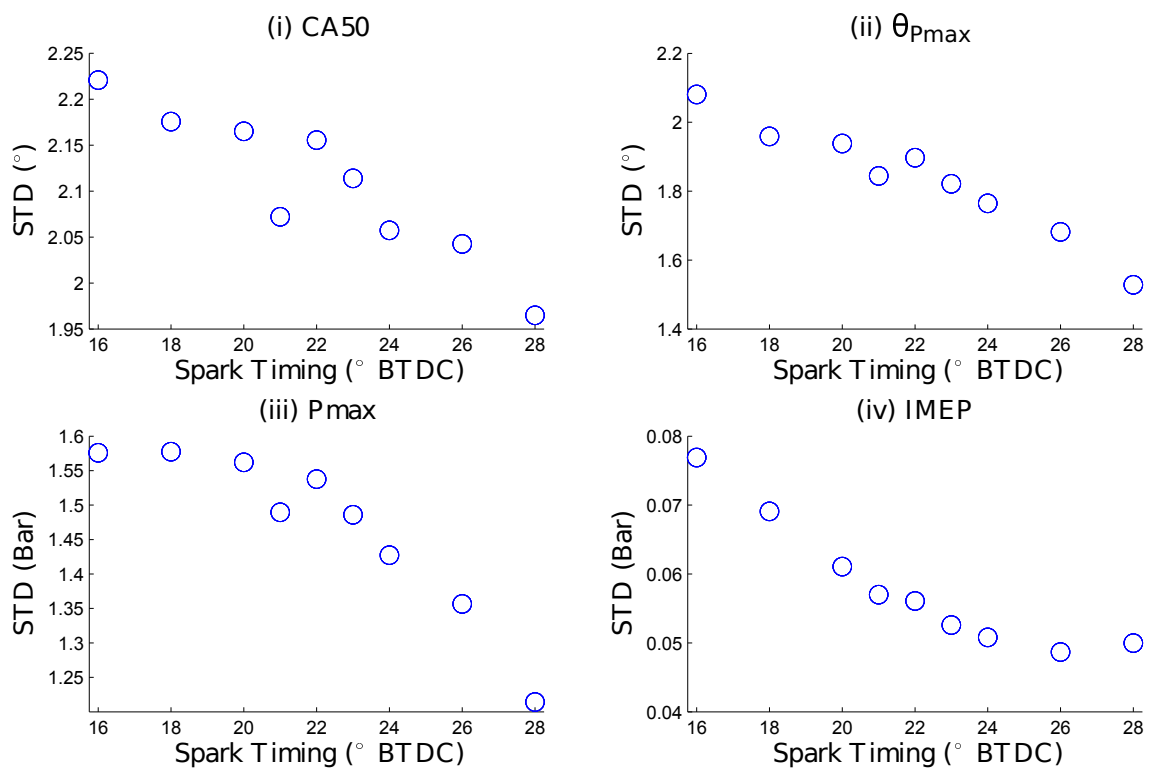
the standard deviation of all combustion metrics except for IMEP. As spark timing is advanced IMEP increases until it peaks, drops slightly for $\approx 4\,^\circ$ of spark advance then peaks again before dropping as shown in Figure 4.2. This first peak corresponding to $\theta_{\mathrm{Pmax}} = 16\,^\circ$ ATDC is confirmed by previous researching using $\theta_{\mathrm{Pmax}} = 16\,^\circ$ ATDC as a reference for a spark timing controller to achieve maximum IMEP.
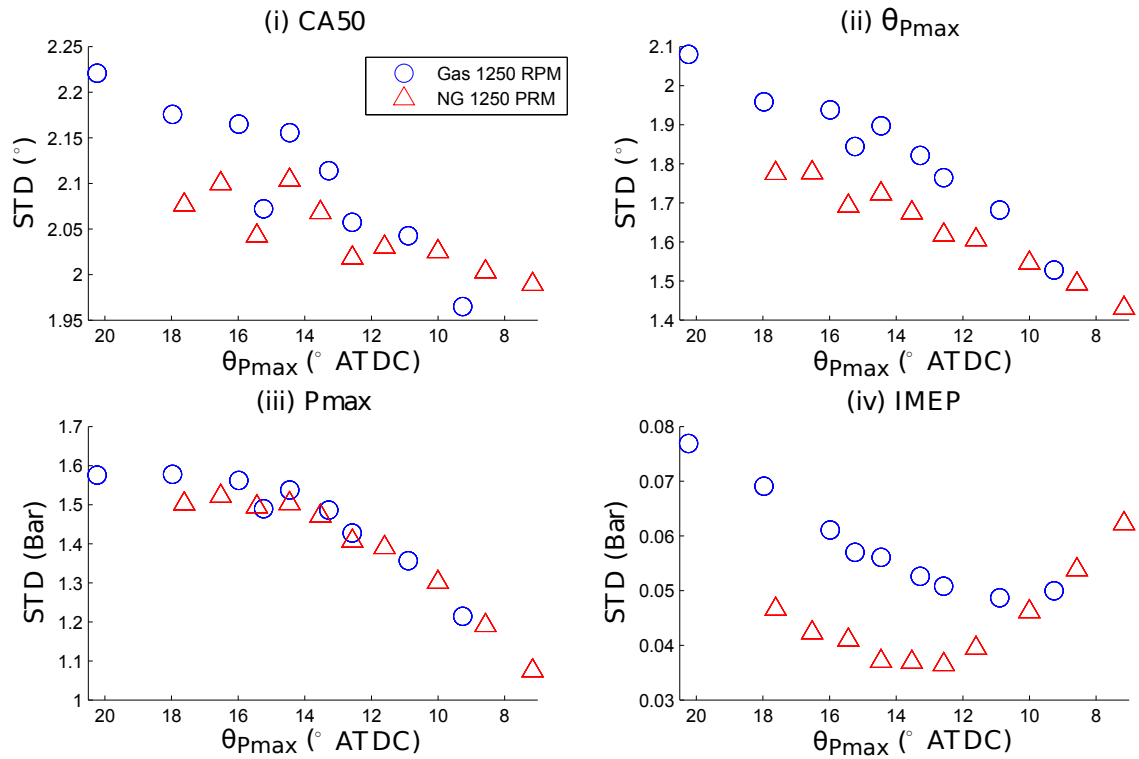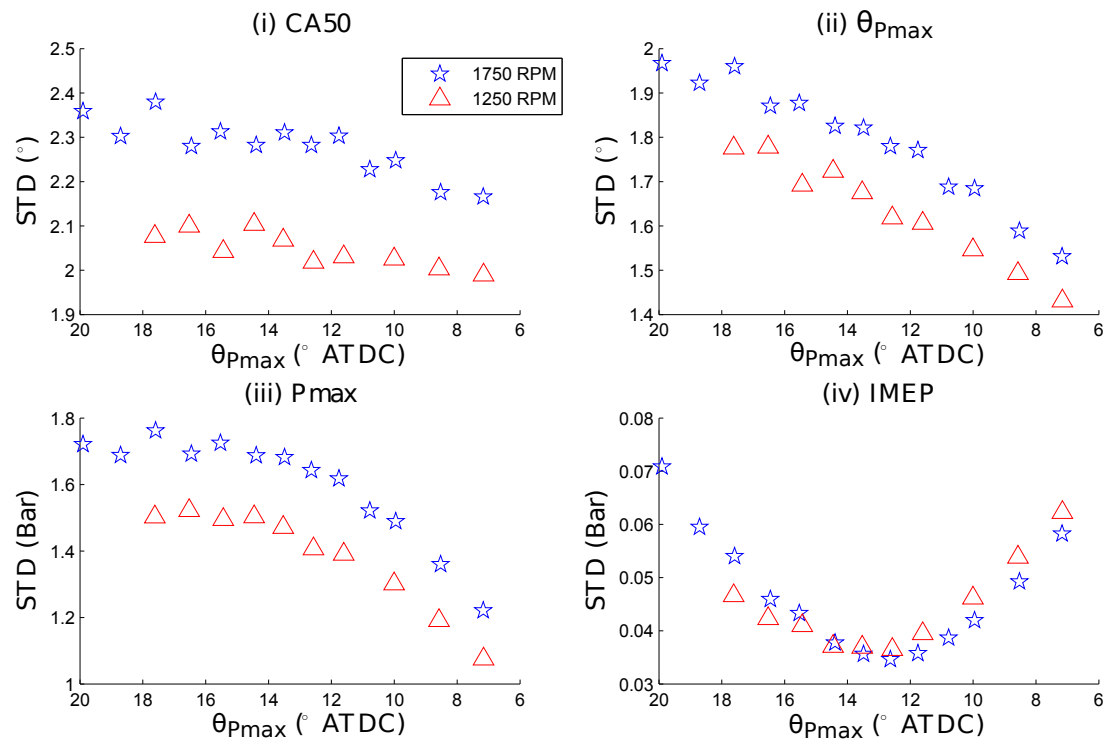
Figure 4.8: Combustion Metrics Cyclic Variability (Standard Deviation) for Changing θ_{Pmax} at base points (A) and (B) in Table 4.1

CHAPTER 5

MINIMUM VARIANCE CONTROL

5.1 System Identification

Minimum variance control is a model based control method where at each time step a control signal is applied which minimizes the variance of the output of a system [Wellstead and Zarrop, 1991]. This section will outline the use of system identification to build the model to be used in the minimum variance controller. System identification is the building of mathematical models of a dynamical system based on observed data from the system [Ljung, 1987]. Prior knowledge of the physical system is used for experimental design and to validate that the model is accurate, but is not required for model development [Ljung, 1987].

The purpose of this section is not to find exact system identification values for use in future tests, but to find general system identification trends in relation to different test conditions and combustion metrics. The first subsection covers the experimental setup for data collection, data timing, and experiment length. The following subsection details the design of the input signal to be used for the test. The third subsection presents the full results of the system identification analysis. The final subsection discusses the results of the analysis and confirms that the results match the physical understanding of the system.

5.1.1   Experimental Design

The system identification tests are performed at each of the test conditions detailed in section 4.1. The engine input for all tests is the spark timing and the measured outputs are: the crank angle at which 50% of the mass of fuel has burned (CA50), peak cylinder pressure (Pmax), peak cylinder pressure location (θ_{Pmax}), and indicated mean effective pressure (IMEP). These measured engine outputs are referred to as combustion metrics for the remainder of the study. During the tests all other engine inputs are constant and the engine variables, defined in Figure 4.1, are held within the ranges specified in Table B.1. System identification can handle multiple input and multiple output systems, but for this study a single input single output system is being identified [Ljung, 1987]. This means that only one of the 4 combustion metrics is used in system identification at a time. While for these tests specifically the 4 combustion metrics are calculated offline using the recorded cylinder pressure data, when the controller is actually implemented the method described in section 3.7.4 allowing the online feedback for a single combustion metric will be used. This system is not used for these tests so that all 4 combustion metrics at the same test condition can be compared using the exact same cylinder pressure data.

Prior knowledge of the system is used both for experimental design and to validate the developed model [Ljung, 1987]. This paragraph will outline the prior knowledge of the system that the model must validate. When spark timing is advanced, θ_{Pmax} and CA50 are advanced, and the absolute value of Pmax is increased for all test conditions as shown in chapter 4. It can be estimated that for every degree of spark change, both θ_{Pmax} and CA50 move approximately a degree, and Pmax changes roughly 1 Bar, for test conditions (A) and (B) based on the information in Figure 4.7. At test condition (C) θ_{Pmax}, CA50, and Pmax are all affected by a change in spark timing less than they are at test condition (A) as shown in Figure 4.4. The developed models

effect of spark timing on those 3 combustion metrics must follow the same trend to be validated. IMEP varies non-linearly with spark angle for all test conditions. The developed models must match this information to be validated.

The timing of the input and output data collection is shown in Figure 3.23. As detailed in section 3.8.7 the current spark input and previous cycles output are recorded together. This means that an input will effect the next recorded output. For example in continuous time, $u(t)$ signifies input and $y(t)$ the output, spark timing of $u(t)$ will effect $y(t+1)$. In discrete, time spark timing of $u(z^{-k})$ will affect $y(z)$ where k is the time delay of the system. Based on input-output timing information, a time delay (k) of 1 cycle is used. Zhu et al. [2003] and Kaleli et al. [2015] also get a $k = 1$ with the use of spark timing as an input. Triantos et al. [2003] reported a time delay of 2 however, no reason for this is suggested in the paper. Finding the exact time delay will be found by the system identification analysis. However a rough estimate of time delay is needed for input design and is chosen to be 1.

5.1.2 Input Design

System identification requires an excitation of the selected input in order to determine a model for the measured output[Ljung, 1987]. The bandwidth and gain of the input signal must be designed properly to achieve this excitation. A theoretically ideal input bandwidth is white noise since it has equal energies at all frequencies to persistently excite all frequencies of the process [Huang et al., 2013]. Since real processes have a limited bandwidth, a limited bandwidth input is sufficient. In fact, picking too wide of a frequency range can excite dynamics of the system which are not of interest for identification [Huang et al., 2013]. A correctly designed input gain is essential to create acceptable signal to noise ratios in the frequency bandwidth of the system to obtain for low variance parameters with system identification.

A random binary sequence (RBS) is a signal that alternates between two defined

levels within a specified bandwidth range [Huang et al., 2013]. For this study, the two RBS levels are defined as 1 and -1 as shown in Figure 5.1. The input gain (G_{RBS}) is defined as a value by which both RBS levels are multiplied by. This multiplied value is then added to the engines current operating spark timing and sent to the engine. A G_{RBS} value of 4 would mean the engines current spark timing would change by $\pm 4°$.
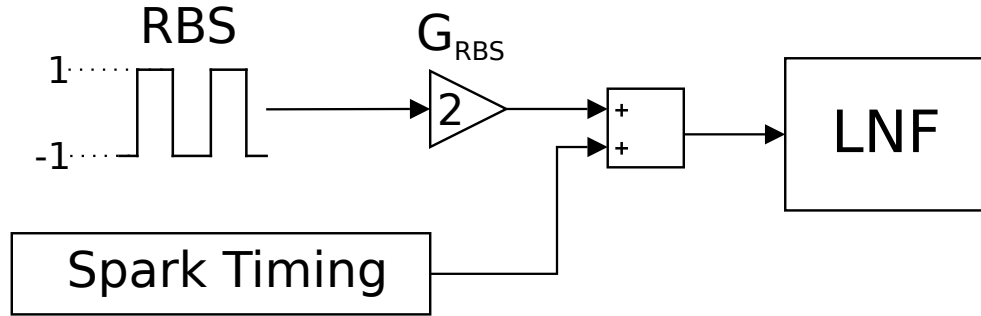
Figure 5.1: RBS and Gain G_{RBS}, LNF signifies 2.0L Ecotec Engine

The bandwidth that should be used for the input is defined by equation 5.1 where T_s is the sampling time, and τ is the time constant of the system [Huang et al., 2013]. Using this the minimum gap (corresponding to the maximum bandwidth) between change in RBS inputs should be 1 cycle. In section 5.1.1 the overall test cycle length was increased two orders of magnitude. Following the work done in previous research, this minimum gap was increased an order of magnitude to roughly 10 cycles [Li et al., 2009; Kaleli et al., 2015].

$$0 \leq \omega_{max} \leq \frac{3\,T_s}{\pi\tau} \tag{5.1}$$

Previously performed system identification tests using spark timing as an input by Li et al. [2009] and Kaleli et al. [2015] used $G_{RBS} = 2$. Since linear system identification is performed, G_{RBS} should be based on the controller operating region without getting into the non-linear sections or unstable sections of spark timing.

For example when spark timing is so advanced or retarded that combustion doesn't happen at all.

To find the correct G_{RBS} to be used for system identification, three preliminary RBS tests are conducted at test condition (A) using the combustion metric θ_{Pmax}. The three G_{RBS} values tested are 2, 4, and 6. The model fit for each test (calculated with the Matlab function "compare") increase with increasing G_{RBS} as shown in Table 5.1. The ARMAX models developed at each G_{RBS} value can be found in section D.1. The equation Matlab uses to calculate model fit is shown in equation 5.2 where y is the validation data output and $\hat{y}$ is the ARMAX model output. The denominator term $||y - \mathrm{mean}(y)||$ is directly related to G_{RBS} because as shown in the previous section, θ_{Pmax} varies directly with spark timing. When G_{RBS} is increased, the denominator $||y - \mathrm{mean}(y)||$ will also increase which will inflate the model fit %, even if the numerator $||y - \hat{y}||$ remains constant. The numerator and denominator values are calculated for each RBS test and shown in Table 5.1. These values can be validated by entering them into equation 5.2 and confirming that the fit % calculated is the same as the Matlab values shown in the table. As predicted, the denominator values increases with G_{RBS}. As shown in the table, the numerator values actually increase as G_{RBS} increases which implies that $G_{\mathrm{RBS}} = 2$ model produces the best model fit.

$$\mathrm{fit} = 100 \left(1 - \frac{||y - \hat{y}||}{||y - \mathrm{mean}(y)||} \right) \tag{5.2}$$

Another issue with using $G_{\mathrm{RBS}} = 6$ is that in order to conduct the test safely, the spark timing as defined in Figure 5.1, must be decreased to prevent extremely advanced spark timing. A spark timing that is too advanced can cause knock which

Table 5.1: Model Fit for G_{RBS} values

G_{RBS}	Matlab Model Fit	$||y - \hat{y}||$	$||y - \text{mean}(y)||$
2	34.93%	38.66	59.43
4	58.02%	42.15	100.41
6	72.97%	47.29	174.79

could possibly damage the engine [Heywood, 1988]. In order to prevent this the base spark timing must be decreased, which means that the system identification test is no longer being conducted at the spark timing the controller will be operated at.

Based on the previous research of Triantos et al. [2003], a minimum variance controller using spark timing will stay within $\pm 1.5\,^{\circ}$ of the mean spark timing when operating at stable conditions. A G_{RBS} value of two would sufficiently cover the controller operating region. Based on this information, $G_{\text{RBS}} = 2$ is chosen for all system identification tests in this study.

The minimum recommended input data length for system identification is 10 times longer than the sum of the time constant and time delay. For this test, 1,000 engine cycles is selected as the input data length which is two orders of magnitude greater than that recommendation.

5.1.3 System Identification Analysis

Since the input and output data contain non-zero means, the data is detrended by subtracting the means from the data before system identification. This is shown for θ_{Pmax} below where $\overline{\theta_{\text{Pmax}}}$ signifies the mean and $\Delta\theta_{\text{Pmax}}$ signifies the detrended data. All model validation plots will use the Δ values as the models were developed with the detrended data. The 1,000 engine cycles of data is partitioned into 750 cycles for model identification and 250 cycles for model validation. This is done so that the performance of the model is evaluated on a fresh data set which was not used to develop the model [Ljung, 1987].

$$\Delta\theta_{\text{Pmax}} = \theta_{\text{Pmax}} - \overline{\theta_{\text{Pmax}}}$$

A discrete time ARMAX model is shown in equation 5.3 with z^{-k} representing a time delay of k engine cycles [Karl J. Astrom, 1970]. A schematic of the input-output structure of the model is shown in Figure 5.2.

$$y(z) = \frac{z^{-k} \cdot B(z)}{A(z)} u(z) + \frac{C(z)}{A(z)} e(z) \tag{5.3}$$

$where$:

$$A(z) = 1 + a_1 z^{-1} + \cdots + a_{n_a} z^{-n_a}$$

$$B(z) = b_1 + b_2 z^{-1} + \cdots + b_{n_b} z^{-(n_b-1)}$$

$$C(z) = 1 + c_1 z^{-1} + \cdots + c_{n_c} z^{-n_c}$$
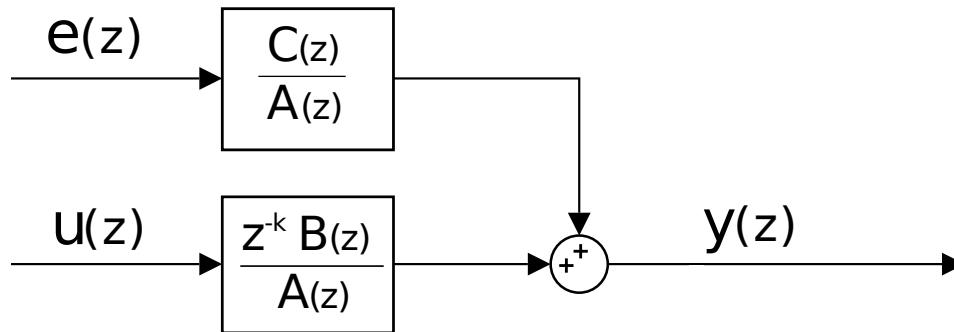
Figure 5.2: ARMAX Model Setup

An example case of the input and output data to be used for the system identification is shown in Figure 5.3. The impulse response shown in Figure 5.4 confirms the prior referenced research that the spark timing has a time delay of 1 in reference

to θ_{Pmax}. This plot is generated with the MATLAB function "impulse".
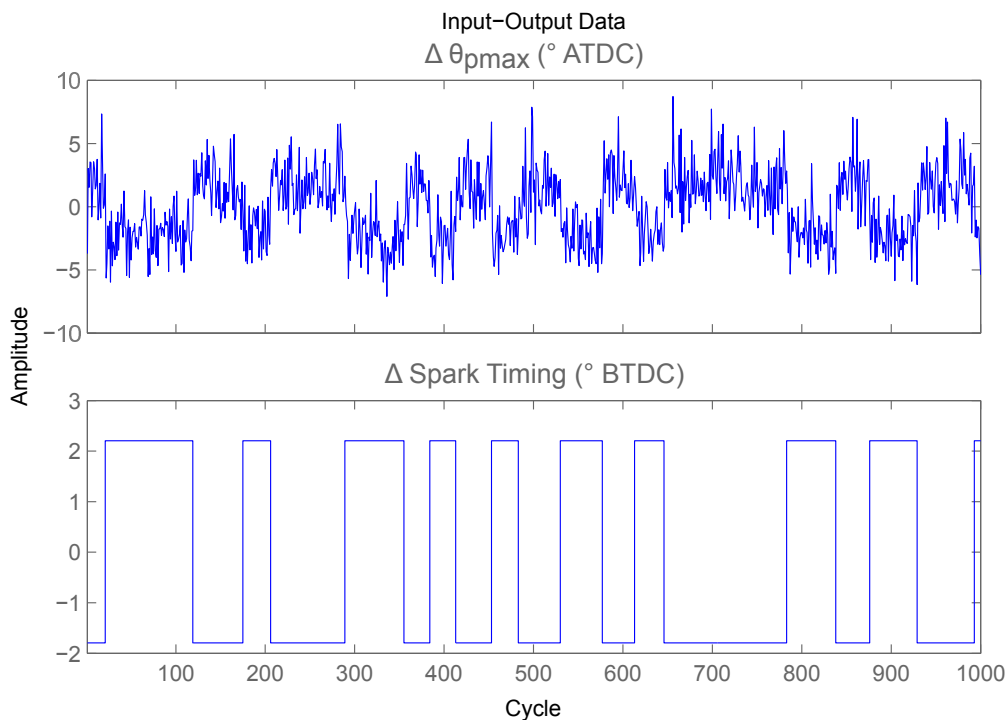
Figure 5.3: Example of Spark Timing RBS Input and θ_{Pmax} Ouput Data at Test Condition (B)

Various model orders are tested to see what effect the model order has on model fit. This is easily done using the MATLAB system identification toolbox. An ARX model is just an ARMAX model with $C(z) = 0$ from equation 5.3. Since an ARX model does not have an error model it can be quickly estimated by a closed-form least squares solution [Huang et al., 2013]. The results of an ARX estimation, where all model orders 1 through 10 are tested for best fit, can be seen in Figure 5.5. It can be seen that increasing the order past 1 for all values, yields almost negligible model improvement. After a certain point, the model fit gets worse as the model is being compared to validation data that was not used to develop the model. If the model was compared to data used to develop the model, the model fit would continue to increase with an increase in model order. While this specific plot is done on the
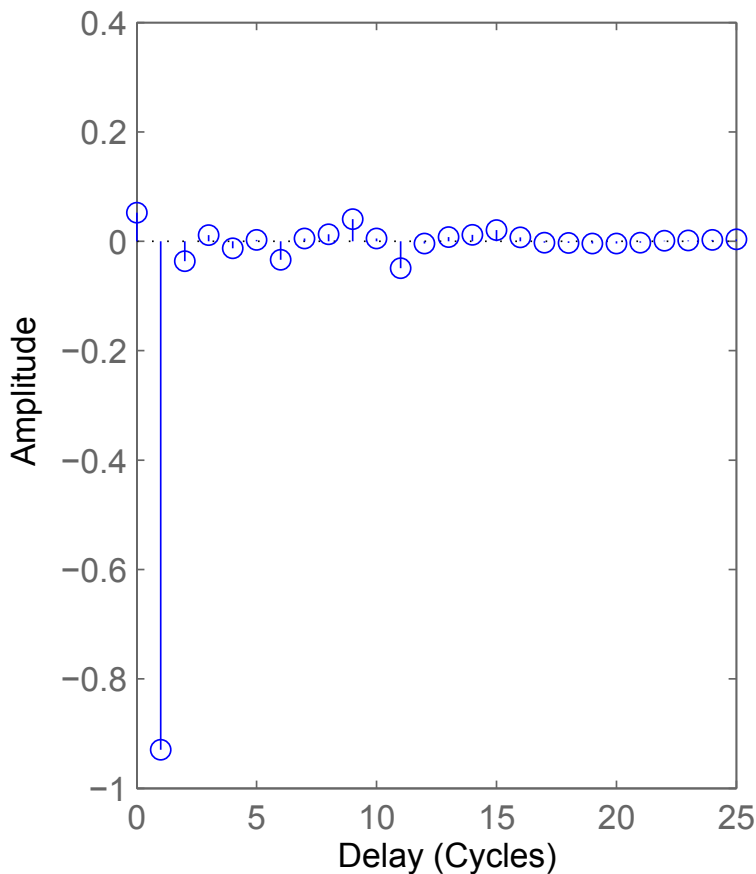
Figure 5.4: Impulse Response between Spark Timing and θ_{Pmax} at Test Condition (B)

θ_{Pmax} combustion metric, the 3 other combustion metrics all yield a similar result to this test. For this reason the lowest order ARMAX model of $n_a = 1$, $n_b = 1$, $n_c = 1, n_k = 1$, which corresponds to the first bar, is chosen.

Using a delay of 1, the ARMAX model is estimated and Figure 5.6 shows the validation for combustion metric θ_{Pmax} at test condition (B). As seen in the figure, the model can accurately predict the mean value of the spark change, but has difficulty following the noise of the system.

The correlation function of residuals determines whether the residuals (the difference between the models predicted output and the validation data output) have any correlation to future residual values [Ljung, 1987]. If the model is developed correctly, there should be no correlation in the residual as the residuals are attributed to white
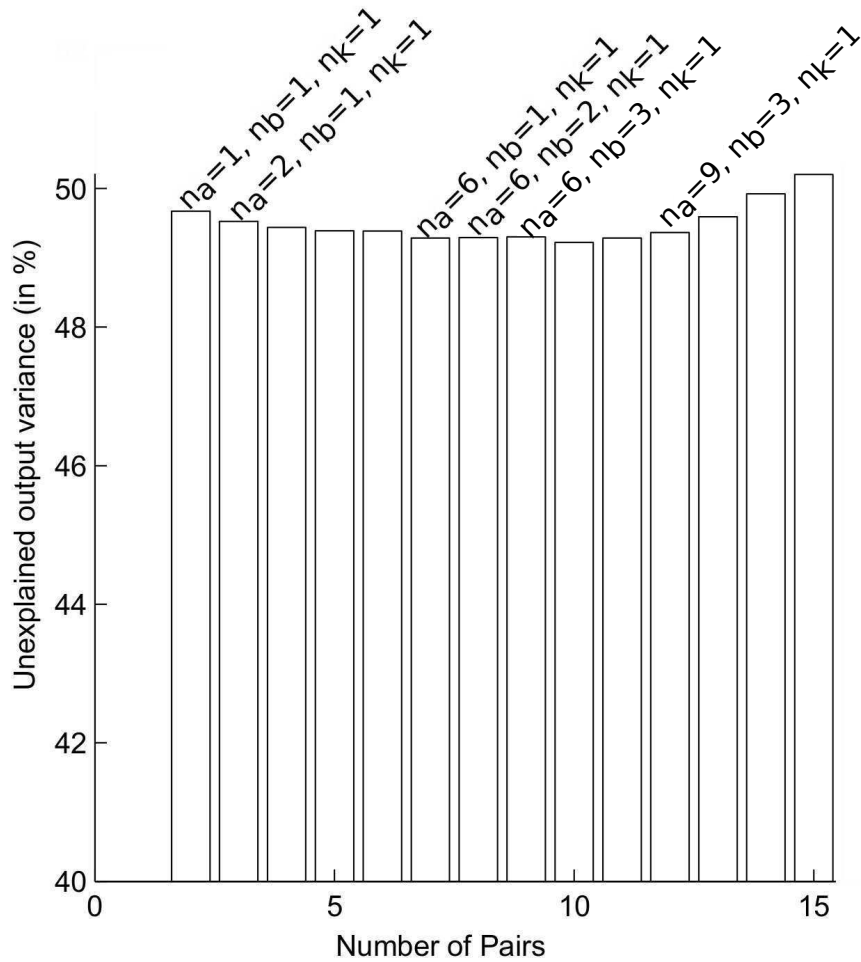
Figure 5.5: ARX Estimation for θ_{Pmax} at Test Condition (A)

noise (which can't be predicted). The correlation function of residuals for θ_{Pmax} concludes that the residuals are attributed to white noise as all points are within the confidence interval as shown in subplot (i) of Figure 5.7.

The cross correlation function determines whether the residuals have any correlation to the inputs. If correlation between the residuals and inputs exist, then the model does not accurately describe the relationship between the input and the output [Ljung, 1987]. If the correlation between the residuals and the input is white noise, then the model accurately describes the input-output relationship. The cross

correlation function between spark timing and the residuals of θ_{Pmax} shows no correlation as shown in subplot (ii) of Figure 5.7. This is shown by all points being within the confidence intervals. The confidence intervals for both correlation tests is 99%. The model validation and correlation tests for the other combustion metrics at the same test condition (B), show that the models that the residuals are attributed to white noise, as seen in Figures 5.7 through 5.13. This confirms that the models for all combustion metrics are admissible. The ARMAX model values for all combustion metrics are shown in Table D.3.
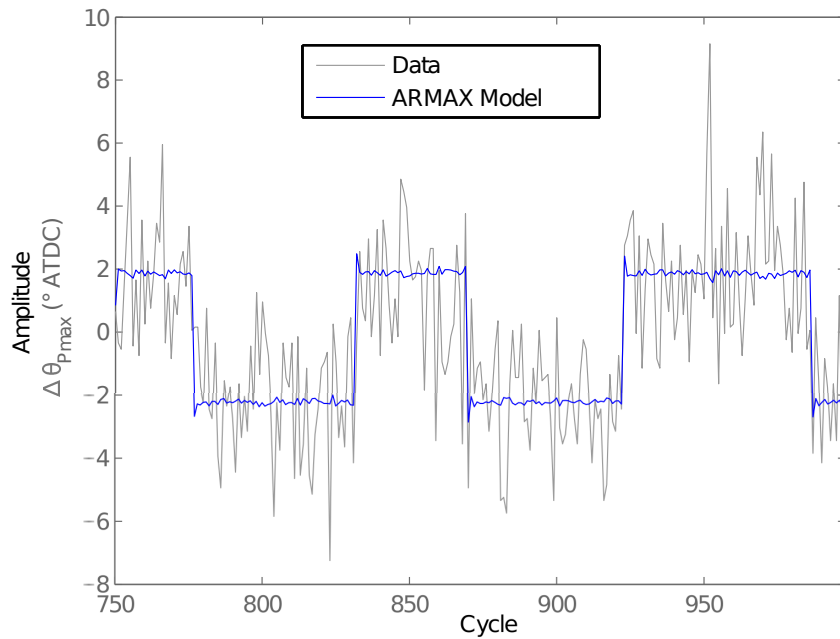
Figure 5.6: Model Validation, θ_{Pmax} at Test Condition (B)
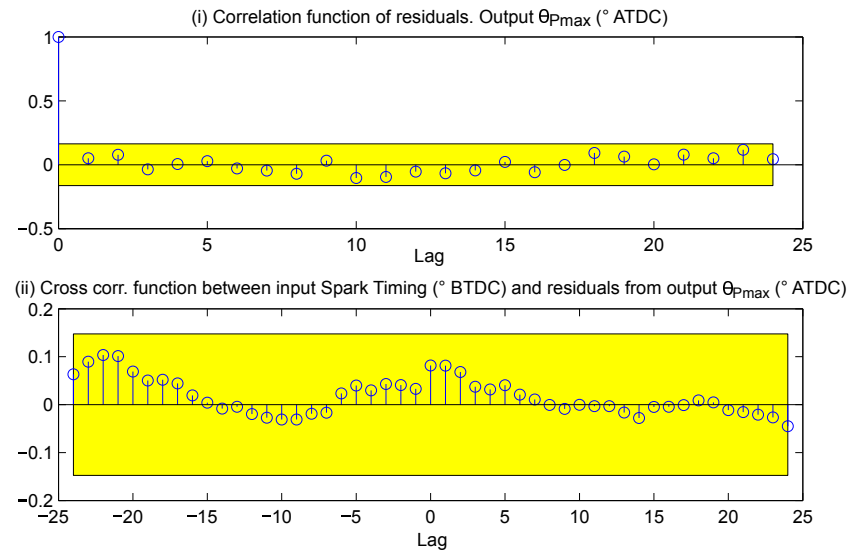
Figure 5.7: Correlation and Cross Correlation of Residuals, θ_{Pmax} at Test Condition (B)

Figure 5.8: Correlation and Cross Correlation of Residuals, Pmax at Test Condition (B)
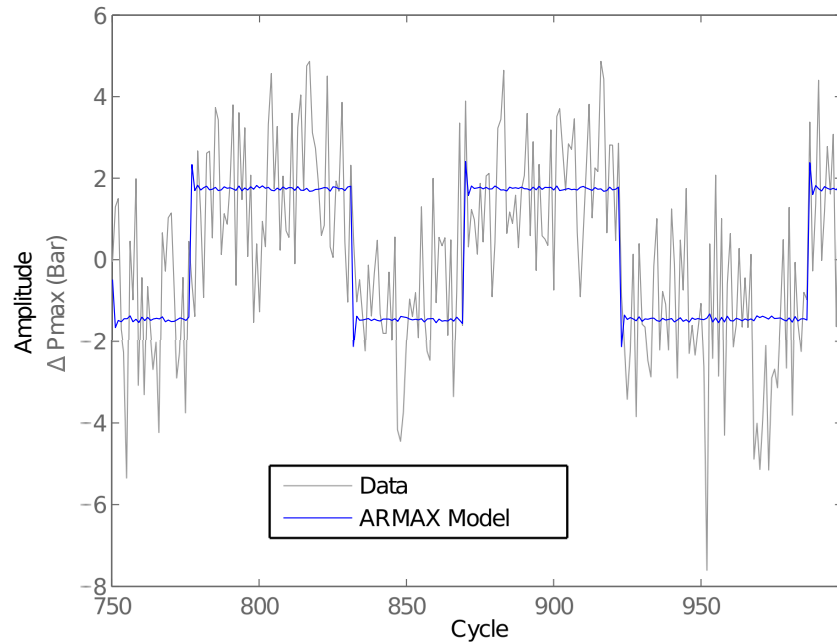
Figure 5.9: Model Validation, Pmax at Test Condition (B)
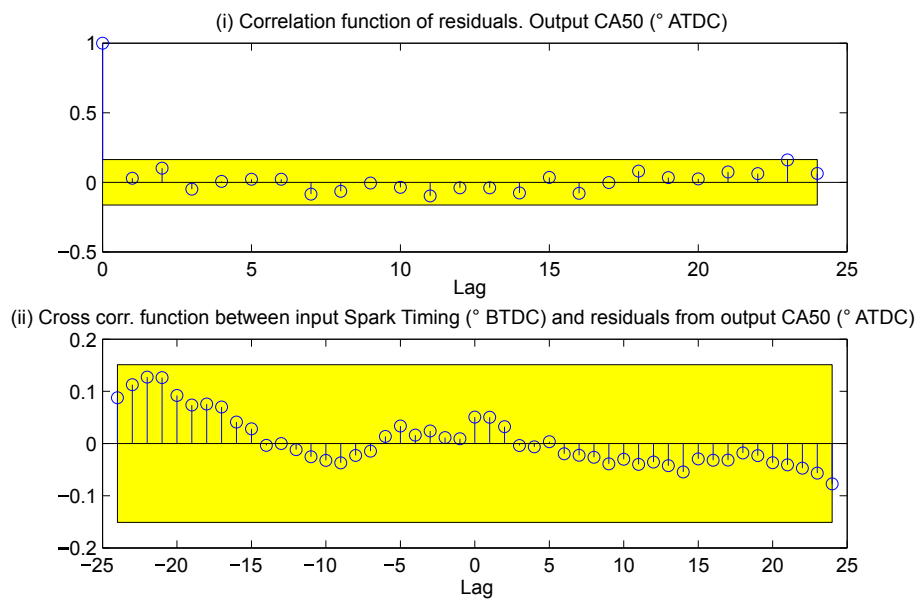
Figure 5.10: Correlation and Cross Correlation of Residuals, CA50 at Test Condition (B)
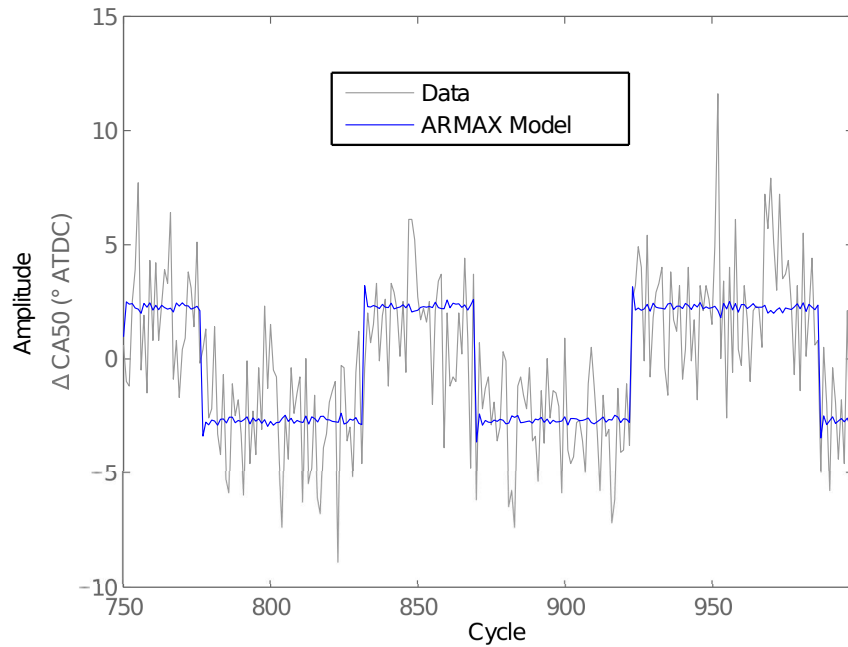
Figure 5.11: Model Validation, CA50 at Test Condition (B)
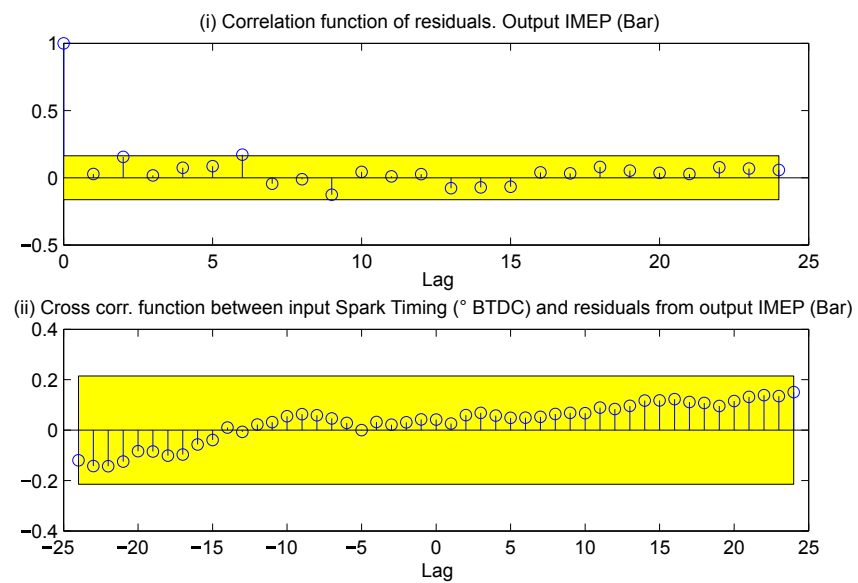
Figure 5.12: Correlation and Cross Correlation of Residuals, IMEP at Test Condition (B)
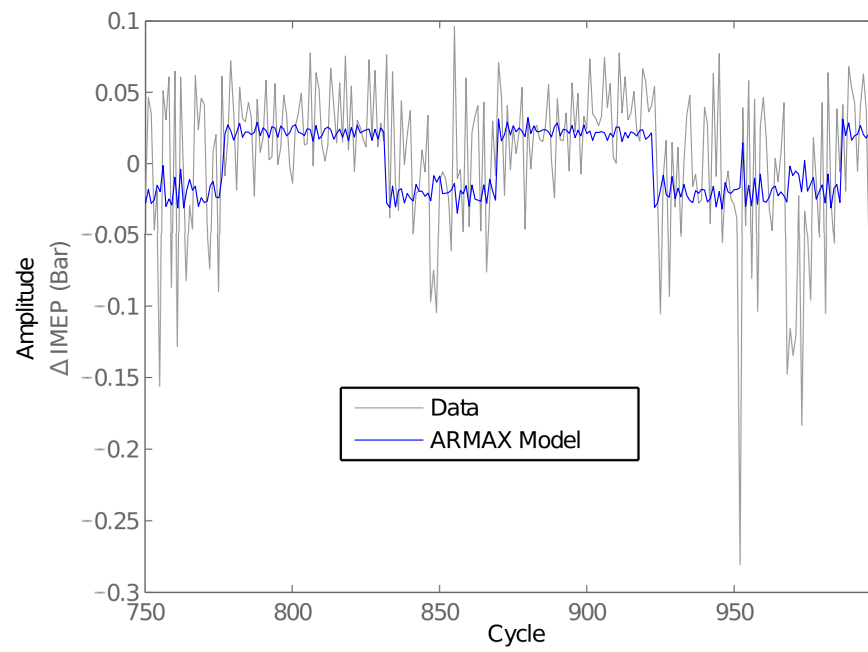
Figure 5.13: Model Validation, IMEP at Test Condition (B)

At the same test condition (B), the intake valve opening is advanced and the exhaust valve closing is retarded 45 CAD in order to generate positive valve overlap. Positive valve overlap causes internal exhaust gas recirculation (iEGR). The same system identification test is performed. The results of the model validation can be seen in Figures 5.14 through 5.17. Table D.4 shows the results of the ARMAX models for the iEGR condition. Tables D.2, D.5 and D.6 show the ARMAX results for test conditions (A), (C), and (D). The model validation plots for these test conditions are shown in Appendix D. This test is performed as the minimum variance controller will be tested with an iEGR disturbance at test condition (B). These system identification results will provide insight into how the controller may react and will be discussed in section 5.1.4.
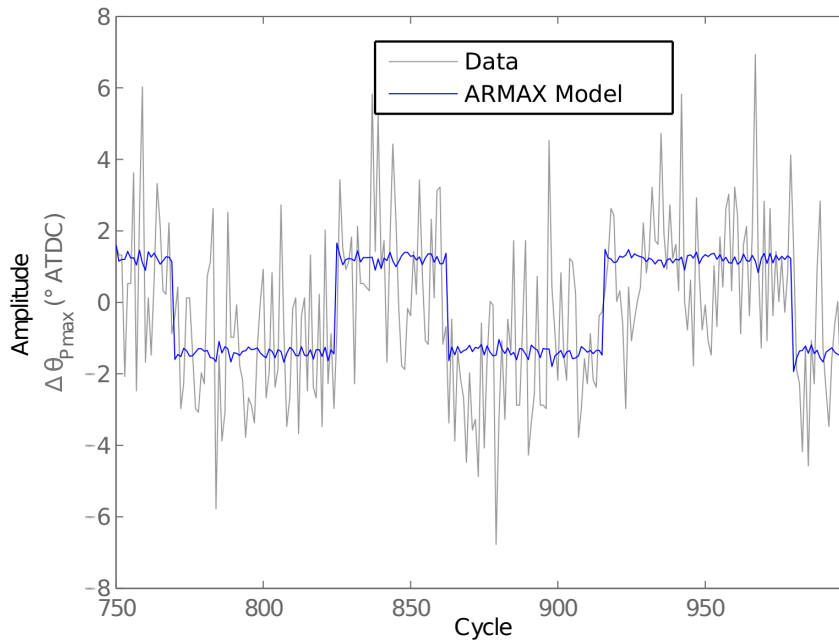
Figure 5.14: Model Validation, θ_{Pmax} at Test Condition (B) with iEGR.
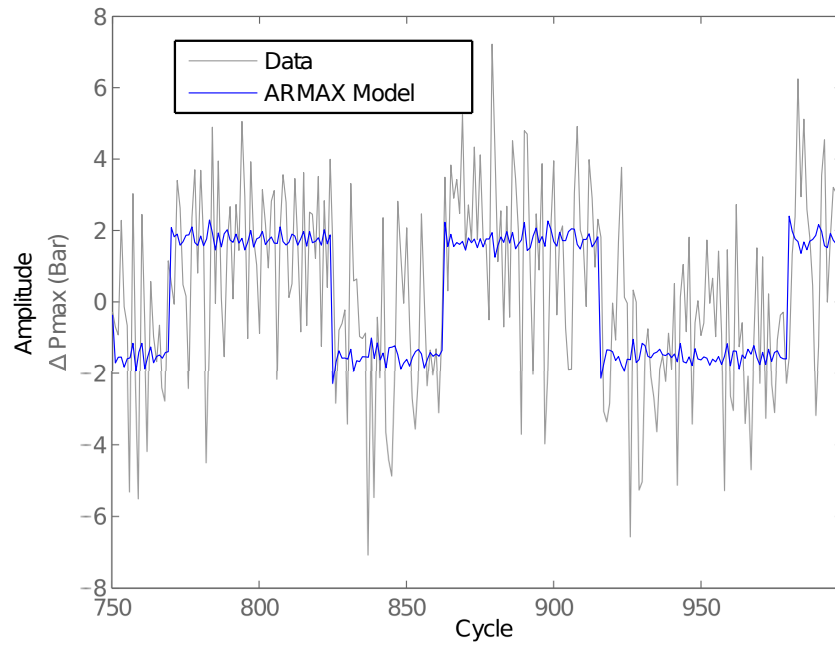
Figure 5.15: Model Validation, Pmax at Test Condition (B) with iEGR.
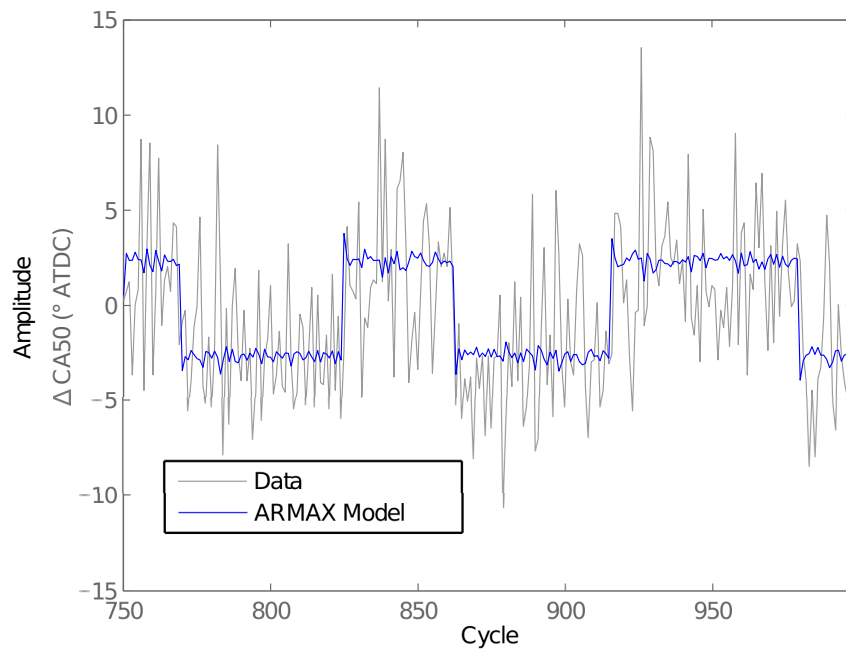
Figure 5.16: Model Validation, CA50 at Test Condition (B) with iEGR.
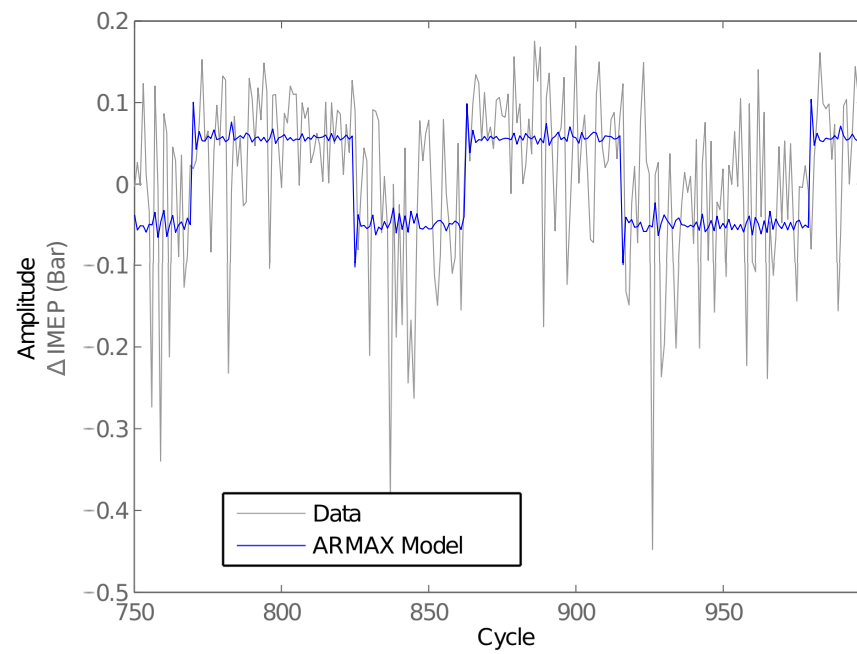
Figure 5.17: Model Validation, IMEP at Test Condition (B) with iEGR.

5.1.4 Discussion

The $B(z)$ term for the ARMAX model is the direct relation between the input and the output as shown in equation 5.3. The prior knowledge presented in section 5.1.1 is validated by the information in Table 5.2 which contains the $B(z)$ value for the ARMAX models developed at all test conditions. The θ_{Pmax} $B(z)$ values of -1.02 and -1.15 confirms that as the spark timing value is advanced (increased value since BTDC), θ_{Pmax} is also advanced (decreased since ATDC). The magnitude is also roughly a degree of θ_{Pmax} change for every degree of spark timing change for test conditions (A) and (B). For the same test conditions, CA50 values of -1.292 and -1.446 confirm that as spark timing is advanced a degree, CA50 is also advanced roughly a degree. Pmax values for the same test conditions show that Pmax increases roughly a 1 bar for every degree of spark advanced. Comparing the $B(z)$ values of θ_{Pmax}, CA50, and Pmax between test conditions (A) and (C) shows that all $B(z)$ values at test condition (C) are smaller compared to test condition (A). This confirms the prior knowledge that the three combustion metrics are effected by a change in spark timing less at test condition (C) than at test condition (A).

Table 5.2: ARMAX Model B(z) for all Test Conditions.

Combustion Metric	(A)	(B)	(B) iEGR	(C)	(D)
θ_{Pmax}	-1.024	-1.154	-0.7373	-0.8603	-0.9734
Pmax	0.8236	0.9615	0.9566	0.6506	0.7378
CA50	-1.292	-1.446	-1.528	-0.9715	-1.159
IMEP	0.0022	0.01285	0.0385	0.00953	0.01451

The $B(z)$ value for θ_{Pmax} for the test condition (B) with iEGR is smaller than the non-iEGR case, as seen in Table 5.2. This is significant if the ARMAX model with no iEGR is used for a tracking controller in conditions with iEGR. This will cause

the controller to undershoot or under perform its designed settling time even though the $B(z)$ term for iEGR is smaller. In equation 5.3 the output is proportional to the $B(z)$ term multiplied by the input $(y(z) \propto B(z) \cdot u(z))$ which means that a smaller $B(z)$ term will require a larger input to move the output the same amount. This is a potential advantage of the CA50 value since the $B(z)$ value for that term is roughly the same for both non-iEGR and iEGR conditions.

Comparing Tables D.3, D.2, D.5, and D.6, each combustion metric produces similar $A(z)$ and $C(z)$ values across all test conditions. All combustion metrics have varying $B(z)$ between the test conditions. The $B(z)$ values for all combustion metrics are all smaller for the gasoline test conditions (C)/(D) than the natural gas test conditions (A)/(B). While this difference isn't as drastic as the non-iEGR to iEGR comparison, this could still cause a controller that is modeled on test conditions (A)/(B) but implemented on test conditions (C)/(D), to slightly under perform its settling time.

The model fit % for all test conditions and combustion metrics is shown in Table 5.3. The calculation for model fit is shown in equation 5.2. The combustion metrics θ_{Pmax}, CA50, and Pmax produce significantly higher model fits than IMEP, based on the models developed at all test conditions. Overall θ_{Pmax} produces the highest model fit followed closely by CA50. θ_{Pmax} and CA50 have an advantage over Pmax because they have a consistent value, regardless of RPM or fuel, which produces the maximum IMEP as shown in the characterization sections 4.3 and 4.4 and the prior referenced research of Zhu et al. [2003]. Either θ_{Pmax} or CA50 can be implemented on the same tracking controller design with the only difference being the specific ARMAX model values and the reference value for the controller to track. The cylinder pressure data acquisition system has a limited time to calculate and output the combustion metric as described in section 3.7.4. Since θ_{Pmax} has a slightly higher model fit than CA50 for all test conditions, and the calculation for θ_{Pmax} is

less computationally intensive than CA50, θ_{Pmax} is the combustion metric that will be used in the closed loop control experiments.

Table 5.3: ARMAX Model Fit % for all Test Conditions.

Combustion Metric	(A)	(B)	(B) iEGR	(C)	(D)
θ_{Pmax}	33.25	28.91	15.44	33.68	22.6
Pmax	28.89	25.42	14.26	28.72	22.14
CA50	32.11	28.16	13.35	32.66	22.59
IMEP	2.25	9.464	8.74	2.368	10.08

5.2 Minimum Variance Control

This section will outline the theory behind minimum variance control design. First the theory behind minimum variance control will be outlined. Next an extension of minimum variance control, which allows set-point tracking, will be detailed. This section will conclude with the description of a detuned minimum variance tracking controller.

Set-point tracking is beneficial to engine efficiency because different cylinders of the same engine will produce different θ_{Pmax} values even with the exact same spark timing, as shown in Table 5.4. In this study, the minimum variance tracking control is only applied to one cylinder because of the technical challenges related to the limited computation window of the cylinder pressure system. However if the technical challenges are overcome, the controller designed in this chapter could be implemented on all four cylinders.

Table 5.4: Average θ_{Pmax} of 1,000 Engine Cycles for all Cylinders at Test Condition (A).

Cylinder	Spark Timing	θ_{Pmax}
1	20° BTDC	15.1° ATDC
2	20° BTDC	15.8° ATDC
3	20° BTDC	14.7° ATDC
4	20° BTDC	16.2° ATDC

5.2.1 Minimum Variance Control Background

An ARMAX model with a minimum variance controller (MVC) is shown in Figure 5.18. The dotted section is the plant model that is being identified and is modeled in the discrete time equation 5.3.
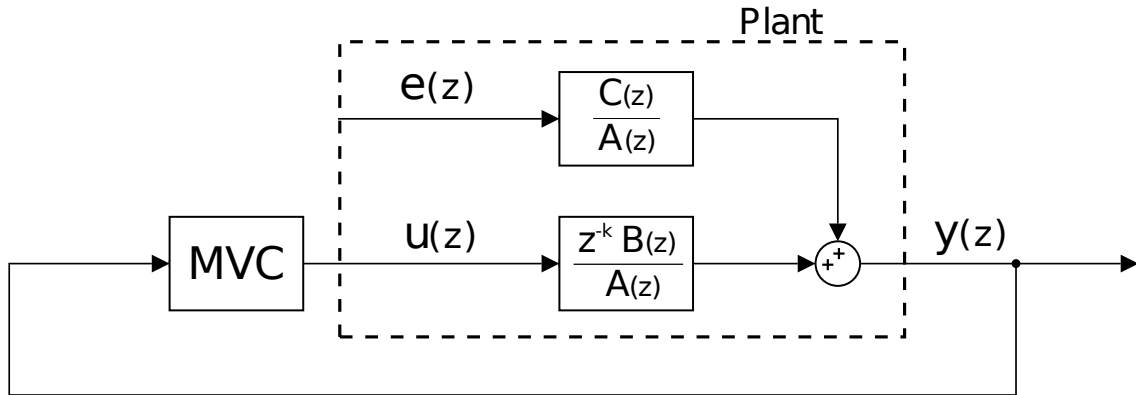
Figure 5.18: ARMAX Model with MVC

The controller is designed to minimize the variance of the plant output.

$$\min \quad \sigma_{y(z)}^2 = E[y^2(z^k)] \tag{5.4}$$

F and G, seen in equation 5.5, are polynomials with orders relating to the time delay, k, and the highest order between the $C(z)$ and $A(z)$ ARMAX terms, $n = max(n_a - 1, n_c - k)$. Since a spark will affect the next engine cycles output, as

reported in section 5.1.3, $k = 1$. Li et al. [2009], Kaleli et al. [2015], and Zhu et al. [2003] all found $k = 1$. Although Triantos et al. [2003] reported $k = 2$ this doesn't conform to the impulse response data presented or the prior research.

$$F(z) = 1 + f_1 z^{-(1)} + \cdots + f_{k-1} z^{-(k-1)}$$
$$G(z) = g_0 + g_1 z^{-(1)} + \cdots + g_{n-1} z^{-(n)}$$
(5.5)

The k-step ahead predictor which minimizes the variance of the prediction error, is given by Karl J. Astrom [1970]:

$$C(z) = A(z)F(z) + z^{-k}G(z) \tag{5.6}$$

using F and G defined in equation 5.5.

Since the time delay $k = 1$, and with $n_a = 1$, $n_b = 1$, $n_c = 1$, $F(z) = 1$, equation 5.6 becomes:

$$(1 + c_1 z^{-1}) = (1 + a_1 z^{-1})(1) + g_0 z^{-1} \tag{5.7}$$

Solving for g_0, the minimum variance plant input can be designed by substituting the values into:

$$u(z) = -\frac{G(z)}{B(z)F(z)} y(z) \tag{5.8}$$

5.2.2 MVC Tracking

Figure 5.19 shows an ARMAX model with an MVC as in Figure 5.18 but now the model is augmented with an integrator and the feedback has a reference input to allow for set-point tracking. A discrete time backwards integrator is used [Wellstead and Zarrop, 1991].

The addition the integrator allows for set-point tracking however, the plant output variance is no longer the minimum variance because of the difference between the controller output produced by the MVC, $\Delta u(z)$, and the plant's input, $u(z)$ [Wellstead and Zarrop, 1991]. With the addition of the integrator, a trade off has been made between the magnitude of the plant output variance and the ability of the controller to track a set-point [Wellstead and Zarrop, 1991].
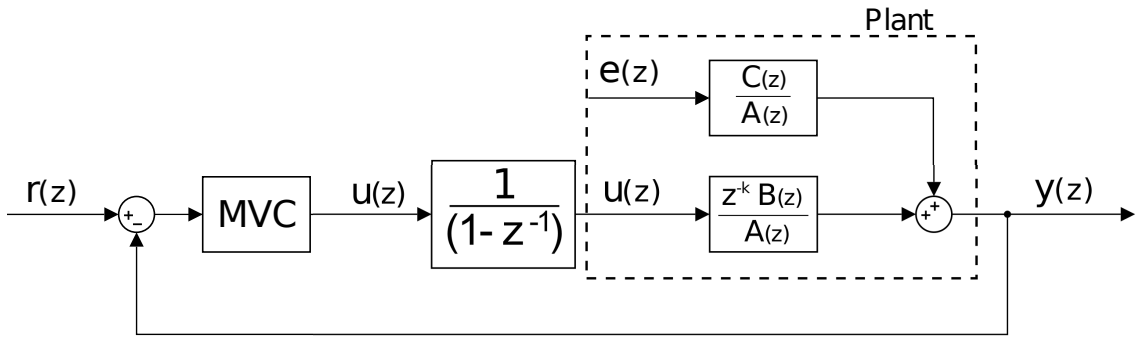
Figure 5.19: ARMAX Model with MVC Tracking

The backwards integrator denominator, $(1 - z^{-1})$ is multiplied by the $A(z)$ term. This causes the order of the $A(z)$ term to increase. Since the order of $G(z)$ is defined by $n = \max(n_a - 1, n_c - k)$, $G(z)$ order is also increased and equation 5.6 becomes:

$$C(z) = (1 - z^{-1})A(z)F(z) + z^{-k}G(z) \tag{5.9}$$

Increasing the order of $G(z)$, as defined by equation 5.5, $G(z) = g_0 z^{-1} + g_1 z^{-2}$. Substituting $A(z)$, $C(z)$, $F(z)$, and $G(z)$, equation 5.9 is:

$$(1 + c1z^{-1}) = (1 - z^{-1})(1 + a_1 z^{-1})(1) + (g_0 z^{-1} + g_1 z^{-2}) \tag{5.10}$$

Solving for both g_0 and g_1, the minimum variance plant input, $\Delta u(z)$, is designed

by solving for the equation:

$$\Delta u(z) = \frac{G(z)}{B(z)F(z)}(r(z) - y(z)) \tag{5.11}$$

5.2.3 MVC Detuned Tracking

The MVC tracking controller can be detuned so that the trade off between the increase in output variance, and the ability to track a set-point discussed in section 5.2.2, can be selected. Without this detuning, this trade off is determined by the model's $A(z)$, $B(z)$, and $C(z)$ values as opposed to the controller designer. In some cases, this can lead to large control input variations which greatly increase the output variance of the system [Wellstead and Zarrop, 1991].

MVC detuned tracking modifies the original cost function, so that the equation 5.4 becomes:

$$\min \ \sigma^2_{y(z)} = E[T(z) \cdot y^2(z^k)] \tag{5.12}$$

where $T(z) = 1 - t_1 z^{-1}$ [Wellstead and Zarrop, 1991]. The coefficient t_1 is the detuning parameter that determines the controllers trade off between increase in output variance, and ability to track a set-point. Choosing a t_1 value approaching but not equalling 0 will yield a faster settling time but will cause greater increase in output variability. Choosing a t_1 value approaching but not equalling 1 will cause a reduced settling time for the controlled output but will also have the benefit of decreasing output variability.

With the addition of the $T(z)$ term, equation 5.9 becomes:

$$C(z)T(z) = (1 - z^{-1})A(z)F(z) + z^{-k}G(z) \tag{5.13}$$

with $A(z)$, $B(z)$, and $C(z)$ terms from the system identification ARMAX models. All values are substituted into equation 5.13 then rearranged to solve for g_0 and g_1 as:

$$(1 + c_1 z^{-1})(1 - t_1 z^{-1}) = (1 - z^{-1})(1 + a_1 z^{-1})(1) + (g_0 z^{-1} + g_1 z^{-2})$$

$$(1 + c_1 z^{-1} - t_1 z^{-1} + c_1 \cdot t_1 z^{-2}) = (1 - z^{-1} + a_1 z^{-1} - a_1 z^{-2}) + (g_0 z^{-1} + g_1 z^{-2})$$

$$(5.14)$$

resulting in:

$$g_0 = c_1 - t_1 - a_1 + 1 \tag{5.15}$$

$$g_1 = a_1 - c_1 \cdot t_1 \tag{5.16}$$

The final control output is solved by putting these values in equation 5.11.

$$\Delta u(z) = \frac{g_0 + g_1 z^{-1}}{b_1}(r(z) - y(z)) \tag{5.17}$$

5.3   Controller Implementation

A minimum variance controller and a detuned minimum variance tracking controller are tested experimentally in this section. The minimum variance controllers ability to reduce the cyclic variability (standard deviation of the combustion metric θ_{Pmax}) is tested. The detuned minimum variance tracking controller ability to track a set-point and resulting increase in cyclic variability is also tested.

Before the detuned minimum variance controller is implemented, the parameter t_1, is selected based on results from simulation and experimental data. For the t_1

parameter selected, controllers are designed for each of the test conditions from Table 4.1 and the results are compared. As discussed in section 5.1.4, all controllers are designed using the θ_{Pmax} combustion metric. Finally, the controller is implemented on the engine for 15,000 cycles to see the controllers performance at tracking a set-point. The results of the controller are also compared to simulation.

5.3.1 MVC without tracking

The MVC controller (without tracking) is tested on the engine at test condition (A) using the combustion metric θ_{Pmax} as the closed loop controller input. For the experiment 4 baselines and 4 controller data sets are recorded. Each data set is 2,000 engine cycles with 300 cycles between each set which is used to save the data.

The MVC is designed using a system identification model developed with data that is taken just prior to the controller operation to provide a model that minimizes long term drift. Without turning the engine off, this data is then used to develop a system identification model and the controller is designed based off of this model in an offline process that takes 1-2 minutes. Then the minimum variance controller values are entered into the engine controller and the test is run. The controller used for this experiment can be seen in equation 5.18. With the low order of the ARMAX model used, this controller structure is identical to a discrete proportional integral controller using a backwards integration.

$$u(z) = \frac{0.03696}{-1.022} y(z) \tag{5.18}$$

The combined baseline and controller standard deviations of θ_{Pmax} are calculated using the pooled variance method [Killeen, 2005]. The difference between the two combined standard deviations indicates that the controller decreases the standard deviation of θ_{Pmax} by 1.4% shown in Table 5.5. This was calculated using the equation

below where a negative value indicates the controller decreases the cyclic variability
(standard deviation of combustion metric).

$$\% \text{ Difference} = \frac{\sigma_{\text{Controller}} - \sigma_{\text{Baseline}}}{(\sigma_{\text{Controller}} + \sigma_{\text{Baseline}})/2} \cdot 100\% \qquad (5.19)$$

Table 5.5: MVC with θ_{Pmax} at Test Condition (A)

	STD of θ_{Pmax} (°)
Baseline	2.0180
Controller	1.9825
Baseline	1.9746
Controller	1.9572
Baseline	2.0053
Controller	1.9436
Baseline	1.9717
Controller	1.9755
Combined Baseline	1.9925
Combined Controller	1.9648
% Difference	-1.4%

5.3.2 Detuned MVC Tracking

Detuned MVC tracking includes a new parameter t_1 that is adjusted based on the
desired trade off controller between the controllers ability to track a set-point, and
increase in output variability [Wellstead and Zarrop, 1991]. A detuned MVC with
tracking will produce a higher output variability than a MVC with no tracking, re-
gardless of the t_1 value selected [Wellstead and Zarrop, 1991]. This result is reported
experimentally in Triantos et al. [2003]. However, even though tracking may increase
the cyclic variability at its current operating point, it is still beneficial overall given a
properly selected t_1 value since tracking is able to keep the combustion metric at its
optimal position. Without tracking, disturbances could move the combustion met-

ric to a position with greater cyclic variability and possibly to a position away from maximum brake torque.

To find an initial value of t_1, preliminary simulations are performed using the ARMAX model for test condition (A) from Table 4.1. This initial simulation found that $t_1 < 0.6$ will produce large spark timing inputs which would require saturation to prevent possible engine damage. For this reason only $t_1 > 0.6$ are tested in this section.

The low signal to noise ratio of the system makes it difficult to consistently measure the settling time to a step input experimentally. Since consistent settling time calculation is needed for proper tuning of the t_1 parameter, the ARMAX model simulation with $e(z) = 0$, from Figure 5.2, is used as the plant. This models the deterministic input and output relationship without noise. The ARMAX model for test condition (A) with a $t_1 = 0.9$ detuned controller response to a step input with noise and without noise is shown in Figure 5.20. The controller converges in both cases. The settling time is easily obtained from the no-noise step test by finding how many cycles the controller takes to reach $\pm 2\%$ of the step input. The controller used in both step tests is shown in equation 5.20.

$$t_1 = 0.9, \quad \Delta u(z) = \frac{0.0983 - 0.0009z^{-1}}{-1.22}(r(z) - y(z)) \tag{5.20}$$

The no-noise, $e(z) = 0$ simulation step test is compared to engine experimental data using the same controller in Figure 5.21. Despite the significant noise in the system, the simulation and experimental data seem to fit. Since the simulation matches the experimental data, the ARMAX model simulations are useful in determining consistent settling times which are used to find the tuning parameter.

Another method of determining the step time response for noise experimental data is to use an ensemble average of 50 steps of $r(z)$. An ensemble average of 50 simulation
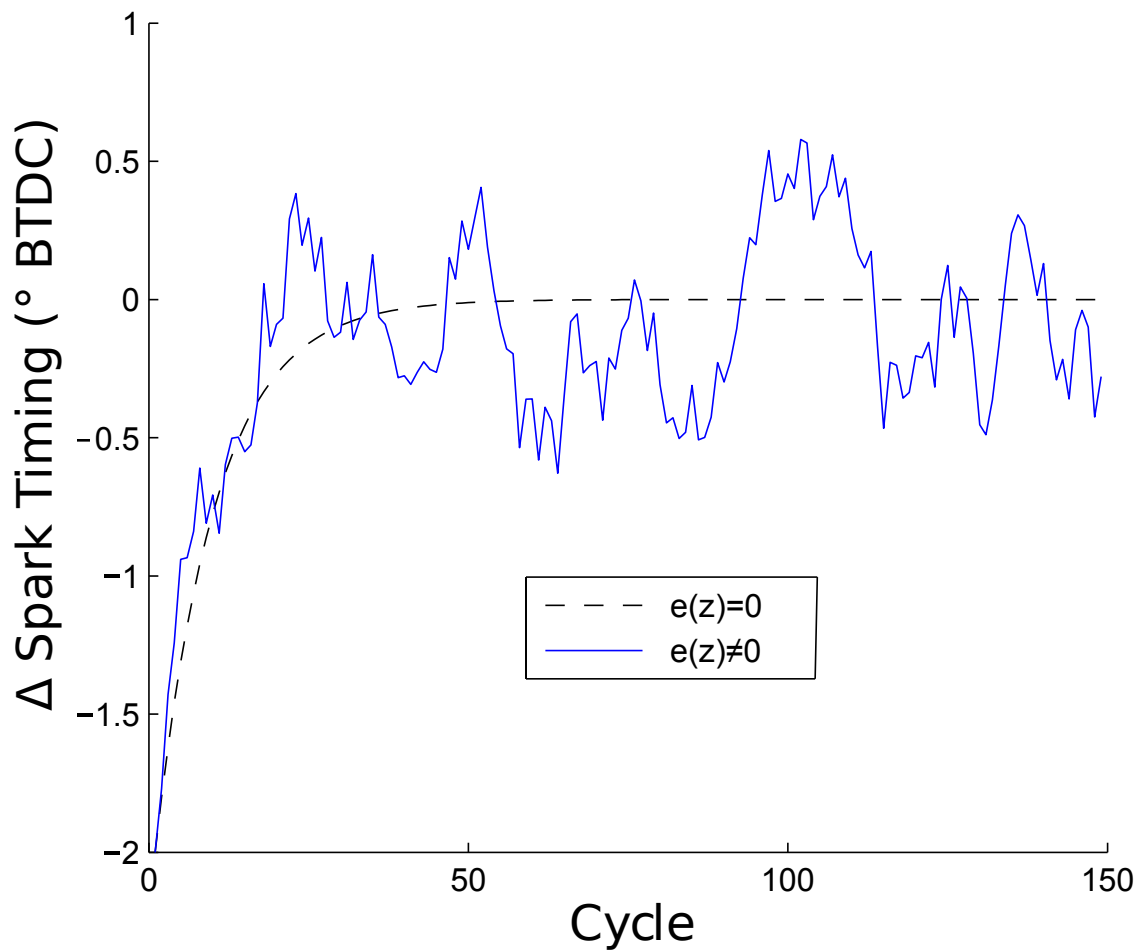
Figure 5.20: t_1=0.9 Simulation Step Test

step tests are compared with no-noise simulation in Figure 5.22. The results from the 50 ensemble step tests also match with the no-noise simulation quite well.

How different t_1 values will yield different settling times is listed in Table 5.6. The different t_1 controllers values are tested on the same no-noise ARMAX plant used previously. Smaller t_1 values produce shorter settling times as shown in Figure 5.23 where the solid line represents t_1=0.9. The controllers designed for the varying t_1 values can be seen in equations 5.21 through 5.25.
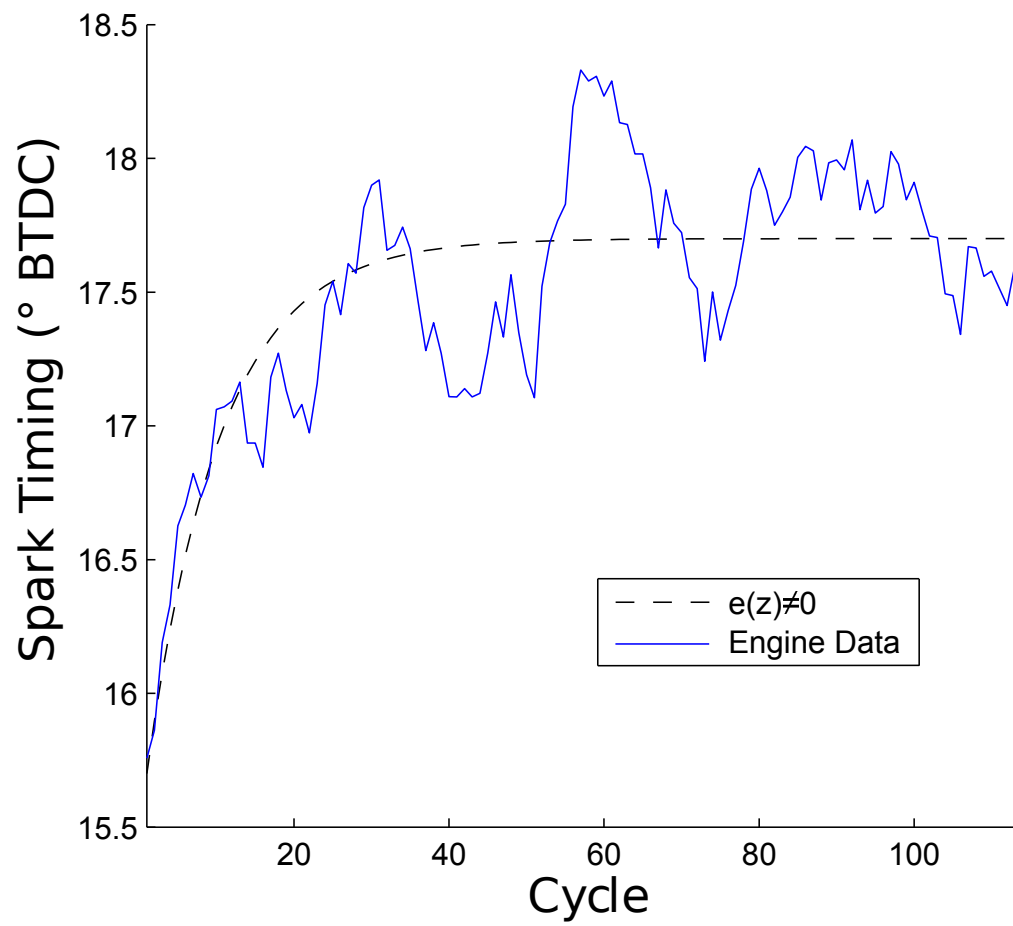
Figure 5.21: t_1=0.9 Comparing Simulation Step Test and Engine Step Test Data at Test Condition A

Table 5.6: t_1 Simulation Tuning

t_1 Value	Settling Time (Cycles)
0.6	8.7
0.7	12
0.8	18.56
0.9	38.14
0.95	76.8

Figure 5.22: Simulation Noise vs 50 Simulation Ensemble Average

Figure 5.23: t_1 Value Settling Time Comparison

$$t_1 = 0.6, \quad \Delta u(z) = \frac{0.3983 - 0.0015z^{-1}}{-1.22}(r(z) - y(z)) \tag{5.21}$$

$$t_1 = 0.7, \quad \Delta u(z) = \frac{0.2983 - 0.0007z^{-1}}{-1.22}(r(z) - y(z)) \tag{5.22}$$

$$t_1 = 0.8, \quad \Delta u(z) = \frac{0.1983 + 0.0001z^{-1}}{-1.22}(r(z) - y(z)) \tag{5.23}$$

$$t_1 = 0.9, \quad \Delta u(z) = \frac{0.0983 + 0.0009z^{-1}}{-1.22}(r(z) - y(z)) \tag{5.24}$$

$$t_1 = 0.95, \quad \Delta u(z) = \frac{0.0483 + 0.0013z^{-1}}{-1.22}(r(z) - y(z)) \tag{5.25}$$
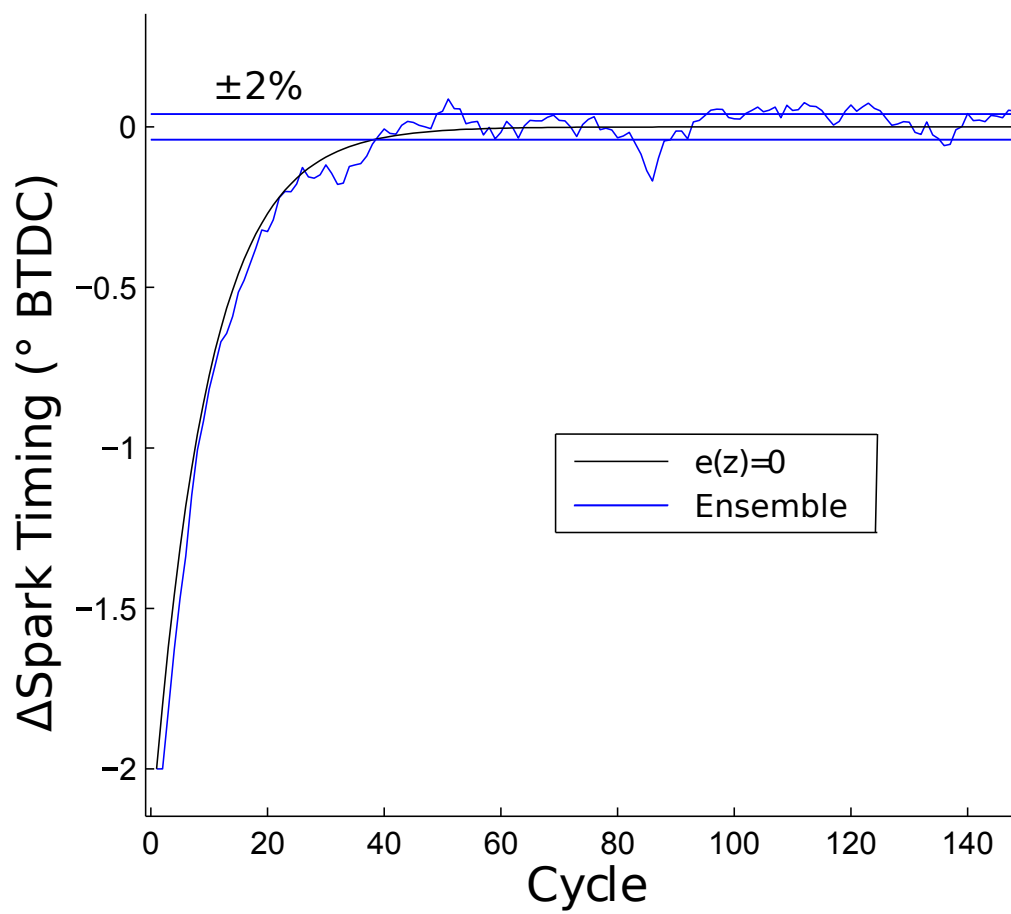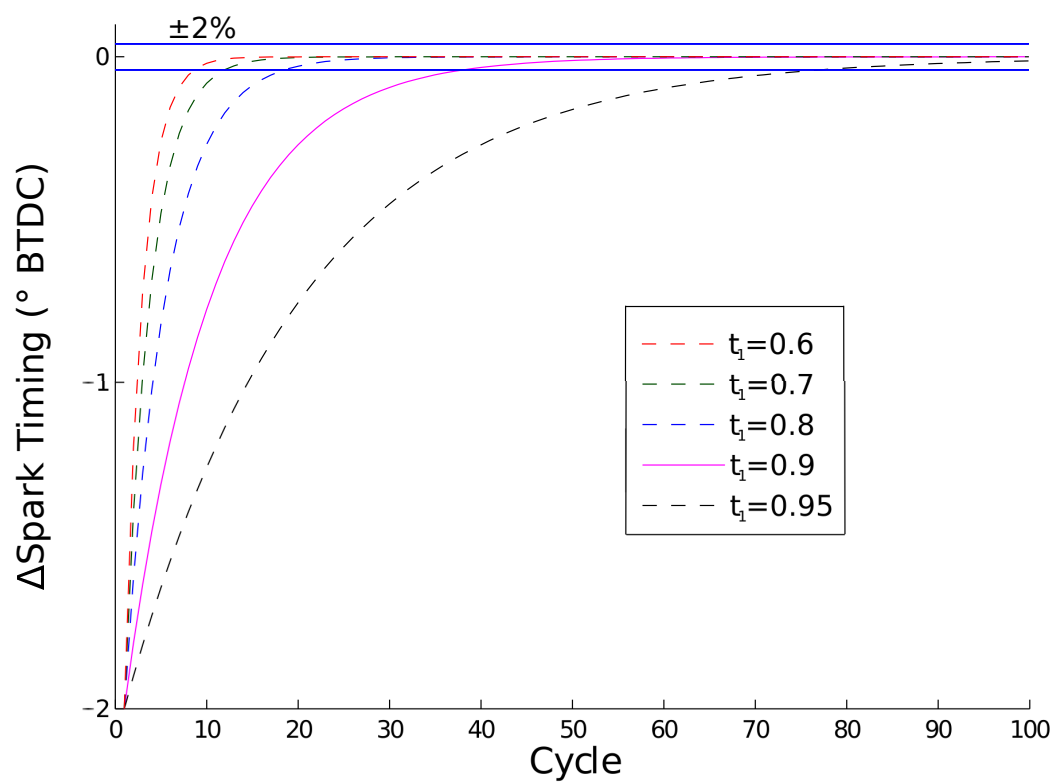
Table 5.7 shows the trade off between t_1 value and effect on cyclic variability. The % change of cyclic variability is calculated using equation 5.19. The results were simulated by alternating between flat spark input and controller input every 200 cycles for 20,000 cycles. This produced 50 flat spark sets of 200 cycles, and 50 controller sets of 200 cycles, the combined standard deviations of which, is used to calculate the results shown in Table 5.7. It should be noted that even though on average the cyclic variability was increased, there is still cases where because of the noise, the baseline would have a higher cyclic variability than the following controller data set. This is why, as used earlier, a combined average over a number of alternating data sets must be done to draw a more accurate conclusion of the controllers effect on cyclic variability.

The k_p and k_i values seen in Table 5.7 are from Zhu et al. [2003]. That paper presented that a PI controller is able to track an input as well as reduce the cyclic variability. These results are not replicated in simulation. They also only took baseline data, then controller data. For the reasons listed in the previous paragraph it could have happened for one specific test but isn't necessarily representative of the controllers overall effect.

Based on the results presented, $t_1 = 0.9$ is determined to have the best trade off

between settling time and increase of cyclic variability when using the θ_{Pmax} combustion metric.

Table 5.7: 50 cycle Simulation of Different Controllers Effect on Cyclic Variability (Standard Deviation) using Combustion Metric θ_{Pmax}

	% Difference Between Flat Spark and Controller σ (+ indicates Controller increase)
$k_p = k_i = 0.2$	+11.87 %
t_1=0.6	+11.64 %
t_1=0.7	+8.60 %
t_1=0.8	+5.80 %
t_1=0.9	+2.65 %
t_1=0.95	+1.41 %
T=0 Pure MVC	-0.53 %

5.3.3 MVC Detuned Controller Design Comparison

The system identification results in section 5.1 are calculated through offline filtering and calculation of the in cylinder pressure traces from cylinder 1. The offline pressure trace analysis differs from the online closed loop control process described in sections 3.7.4 and 3.8.7 as the offline data is able to compare 4 combustion metrics from the same data set. Online, with the closed loop dSPACE recording, only one combustion metric at a time is calculated. This subsection will take new input and output data directly from the dSPACE controller to find controller values that can be used in the experiments. The combustion metric θ_{Pmax} is used based on the analysis done in section 5.1.4. The dSPACE controller data is collected over 2,000 engine cycles. Based on the data presented in section 5.3.2 all controller designs for θ_{Pmax} are done with a MVC detuned parameter of $t_1 = 0.9$.

Table 5.8 shows the results of the $t_1 = 0.1$ detuned MVC design using data recorded directly from the dSPACE controller. The ARMAX models used to calculate each controller can be seen in Appendix D. The method to calculate the controller values for a given ARMAX model is outlined in section 5.2.3. The results show that

all controllers produced at the four main test conditions (A)-(D) produce very similar numerator results. This is expected since the results in the system identification analysis in section 5.1.4 showed very little difference in $A(z)$ and $C(z)$ terms. As with the system identification results from section 5.1, the largest difference is between the controllers is the $B(z)$ values which can be seen by comparing the denominators of the natural gas test conditions (A)/(B) with the gasoline test conditions (C)/(D).

Table 5.8: θ_{Pmax} Detuned $t_1 = 0.9$ MVC Designed for Test Conditions from Table 4.1 based on System Identification Results Recorded on dSPACE Controller

Test Condition	MVC Detuned $t_1 = 0.9$
(A)	$\Delta u(z) = \dfrac{0.0930 - 0.0028z^{-1}}{-0.9820}(r(z) - y(z))$
(B)	$\Delta u(z) = \dfrac{0.1023 - 0.0044z^{-1}}{-0.996}(r(z) - y(z))$
(C)	$\Delta u(z) = \dfrac{0.0831 + 0.0157z^{-1}}{-0.9143}(r(z) - y(z))$
(D)	$\Delta u(z) = \dfrac{0.1169 + 0.0148z^{-1}}{-0.9275}(r(z) - y(z))$

5.3.4   Detuned MVC Tracking for 15,000 Consecutive cycles

To test the ability of a detuned MVC ability to track θ_{Pmax}, a 15,000 cycle test is conducted. The amount of cyclic variability increase from the tracking control inputs is also tested and will be compared to the simulated value from Table 5.7. For cases with large disturbances, detuned MVC will decrease the cyclic variability compared to a constant spark input. However for this experiment, all engine variables are kept within the ranges specified in Table B.1 and a detuned MVC is expected from simulation to increase the cyclic variability slightly.

Before the controller is activated, 15,000 consecutive cycles of θ_{Pmax} data is taken for a constant spark input at test condition (B). The MVC detuned tracking controller for test condition (B), shown in equation 5.26), is then activated and θ_{Pmax} is recorded for 15,000 consecutive cycles by the dSPACE controller. The mean of θ_{Pmax} for the

flat spark input data of 15.652° ATDC is set as the control reference for the MVC with detuned tracking controller to ensure that cyclic variability isn't being tested at a different operating point.

$$t_1 = 0.9, \quad \Delta u(z) = \frac{0.1023 - 0.0044z^{-1}}{-0.996}(r(z) - y(z)) \tag{5.26}$$

The mean θ_{Pmax} for the 15,000 engine cycles with the controller activated is 15.649° ATDC. This determines that the controller is able to track θ_{Pmax} effectively. The controller increased cyclic variability by 3.1 % which is calculated using equation 5.19. This increase is higher than the simulated increase of 2.65 % shown in Table 5.7. However this experiment is performed at test condition (B) where as the simulations are done at test condition (A). Characterization section 4.4 measured higher cyclic variability in test condition (B) compared to condition (A) which could account for this slightly higher than simulated cyclic variability increase.

The simulation results presented by Triantos et al. [2003], predicted an increase in cyclic variability by 3.7 % when using a detuned minimum variance tracking controller. The experimental results reported a decrease in cyclic variability of 0.5 % however, only a single set of 1,500 engine cycles of baseline data were compared to 1,500 engine cycles of controller data. Based on the information provided in section 5.3.2, alternating data sets, or longer data sets should be taken to accurately measure the controllers impact on cyclic variability.

A low frequency disturbance is characterized in this study as a disturbance which affects the combustion metric for 50 consecutive cycles or more. Figure 5.24 shows the controllers spark timing in °BTDC, the baseline data with 50 cycle moving average, and the controller data with a 50 cycle moving average with a -2° offset applied so that the two sets of data can be better distinguished. Without largely increasing the cyclic variability, Figure 5.24 shows that the detuned minimum variance tracking

controller is able to reduce the impact of any lower frequency disturbances and force θ_{Pmax} to the reference value. This is a best case scenario since outside of a lab there would be many factors disturbing the engine operating conditions such as changing engine coolant temperature. These factors could have an impact on θ_{Pmax} and could move it out of the optimal position for maximum IMEP.
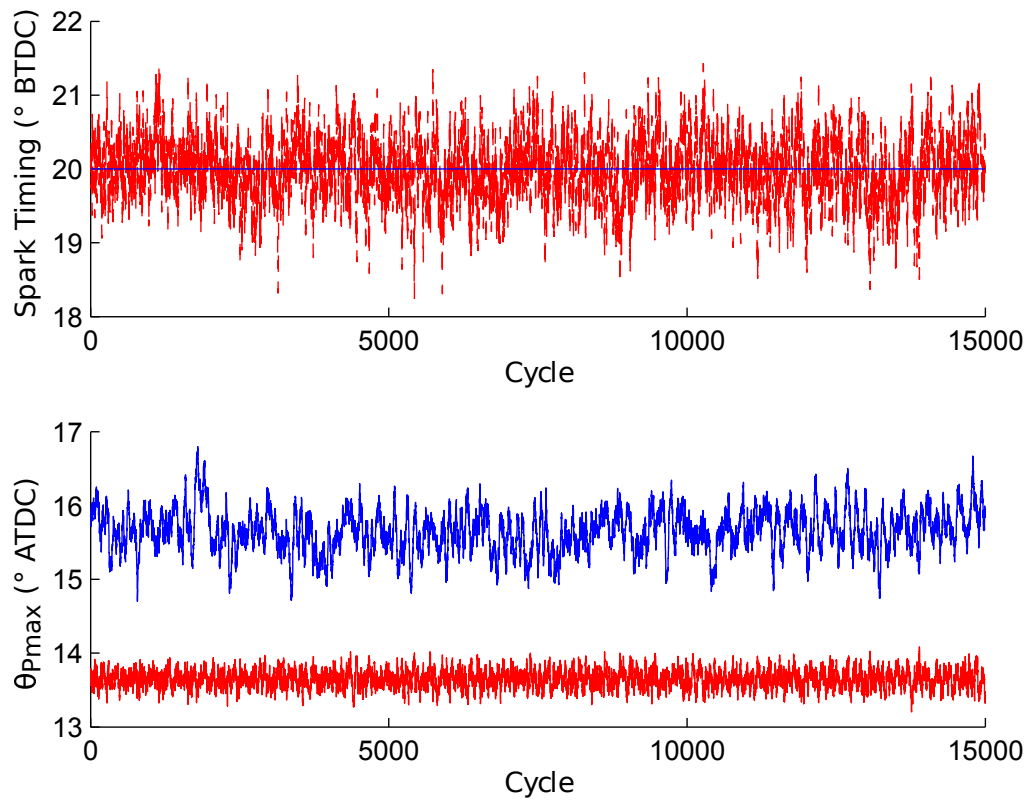
Figure 5.24: θ_{Pmax} for MVC Detuned Controller and Flat Spark Input at Test Condition B Spark Timing and θ_{Pmax} with 50 cycle moving average and -2° Offset

The NI data acquisition card is not able to measure cylinder pressure for 15,000 consecutive cycles. For this reason, 1,000 cycles of cylinder pressure data is recorded and saved for every 2,000 cycles of the experiment resulting in eight groups of 1,000 cycles for each of the flat spark input and detuned MVC tests as shown in Figure 5.25.

Figure 5.26 shows the average values for cylinder 1, the cylinder in closed loop

Figure 5.25: Timing for dSPACE Recording and Cylinder Pressure Recording

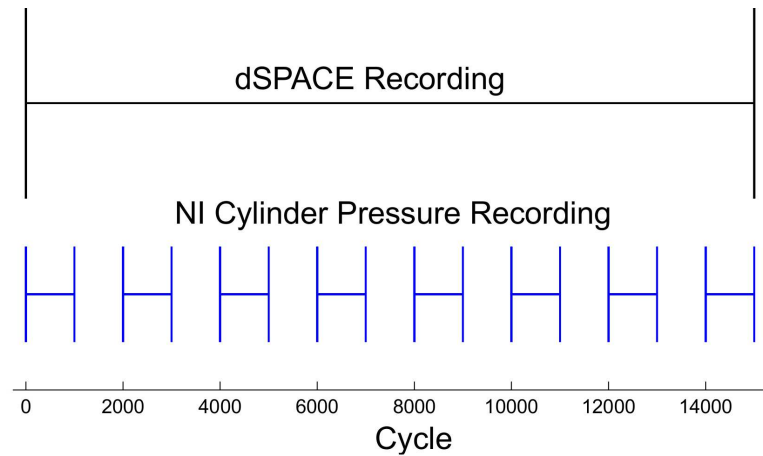control, for each of the 4 combustion metrics throughout the test. Average value of θ Pmax for each 1,000 cycle data set is very consistent as seen in subplot (i) of Figure 5.26. CA50 value is also more consistent with the controller activated even though it is not being directly calculated and controlled as seen in subplot (ii) in Figure 5.26. Average Pmax and IMEP are also increased for the controller case. The standard deviations for each combustion metric show no discernible difference between the controller and flat spark input tests, as seen in Figure 5.27.

The average values and standard deviations combined for cylinders 2, 3, and 4 can be seen in Figures 5.28 and 5.29. As with cylinder 1, no significance difference in standard deviations can be seen between flat spark input and the controller in Figure 5.29. The average values for all parameters, except for IMEP, seem consistent for both cases. IMEP for cylinders 2, 3, and 4 show a similar but not as large of an increase as cylinder 1 as seen in subplot (iv) in Figure 5.28.

Figure 5.26: Cylinder 1 Average Values for 1,000 cycles, Error Bars Signify Standard Error, at Test Condition B where BASE signifies Flat Spark Input.

Figure 5.27: Cylinder 1 Standard Deviations for 1,000 cycles at Test Condition (B) where BASE signifies Flat Spark Input.
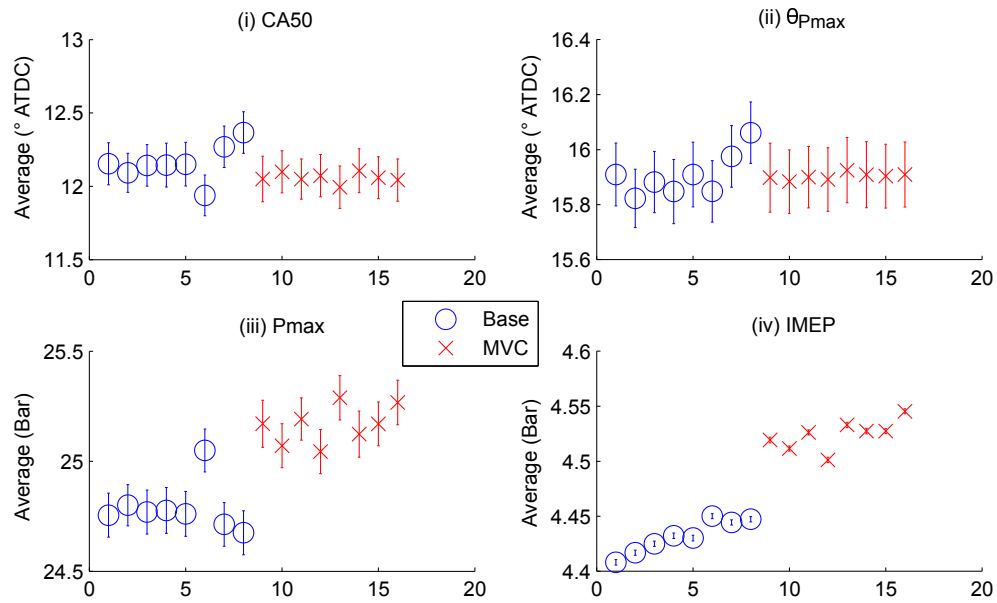
Figure 5.28: An average value for Cylinders 2, 3, and 4 Averages for 1,000 cycles, Error Bars Signify Standard Error, at Test Condition B where BASE signifies Flat Spark Input.
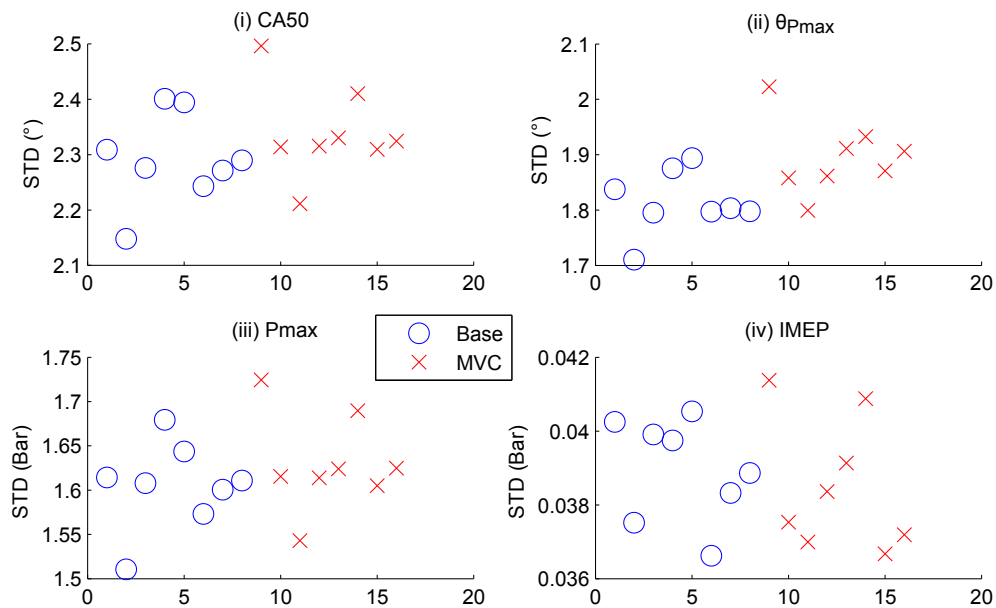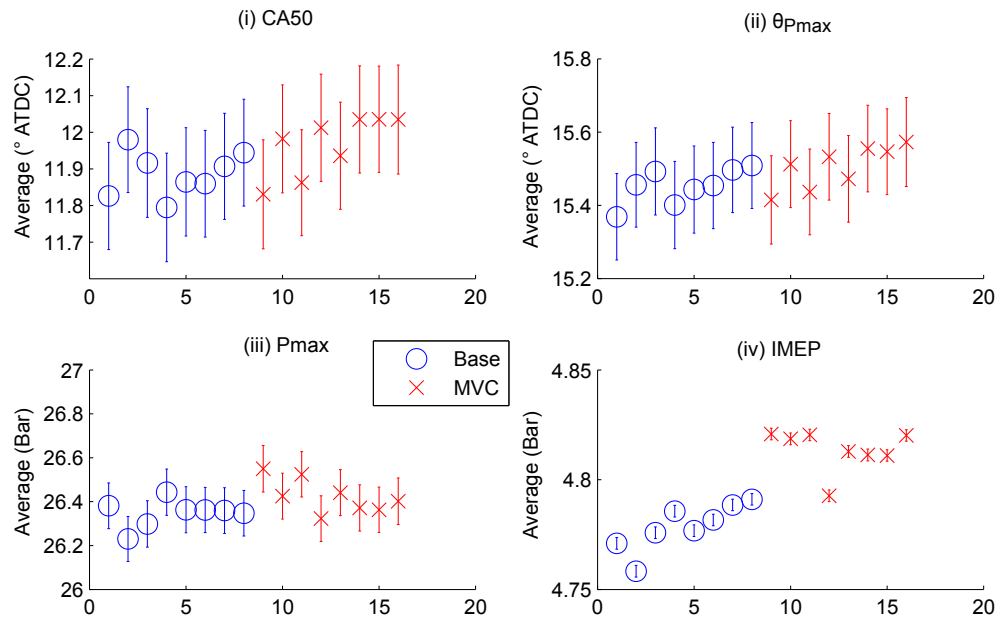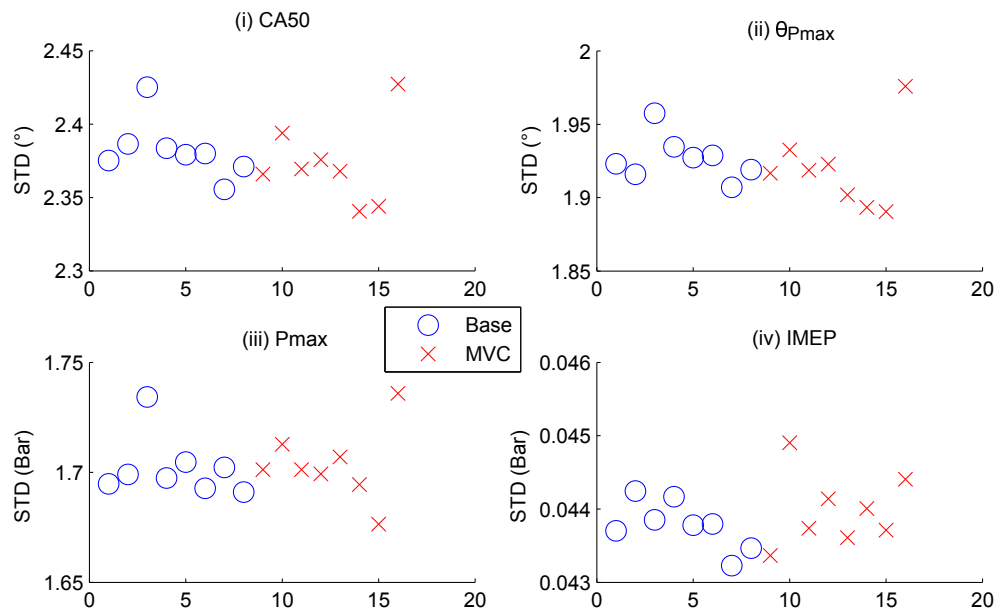

Figure 5.29: Cylinders 2, 3, 4 Pooled Standard Deviations for 1,000 cycles at Test Condition (B) where BASE signifies Flat Spark Input

5.4 Rejecting Disturbances

The ability of a detuned MVC to track a reference with almost negligible increase in cyclic variability was tested in section 5.3.4. This test was done with all engine inputs and variables being held within the ranges specified in Table B.1. In real operation disturbances are present so in this section, disturbances are introduced and the results from the uncontrolled flat spark input and a detuned MVC controller are compared.

5.4.1 iEGR Disturbance

An iEGR disturbance is generated by moving both intake and exhaust valves 35 CAD to increase the positive valve overlap as described in section 5.1.3. The test is done at operating condition (B). No RBS test is done for system identification as the controller is programmed with the same values used in section 5.3.4. Figure 5.30 shows the iEGR disturbance with a flat spark input. Over the entire test the Pmax value has a standard deviation of 2.51 degrees for the flat spark input. Figure 5.31 shows the same disturbance happening with the controller on. The θ_{Pmax} value has a standard deviation of 2.10 degrees with the controller operating.

Figure 5.32 shows the effect the iEGR disturbance has on each individual cylinders IMEP with the disturbance starting at cycle 200. The initial large spike in IMEP after the disturbance is caused by the initial increase of manifold air pressure and hot exhaust gases introduced into the cylinder. Cylinder 1 is the only cylinder operating under detuned minimum variance tracking control. The figure shows not only the variance of the IMEP being reduced compared to the other cylinders, but the average IMEP also increases with the disturbance. It should be noted that the difference between the cylinders initial IMEP before the disturbance is not a product of the controller but is inherent in the engine. For example before the disturbance, Figure 5.32 shows the initial IMEP values for each cylinder as: cylinder 1 $\approx$ 4.4 Bar,
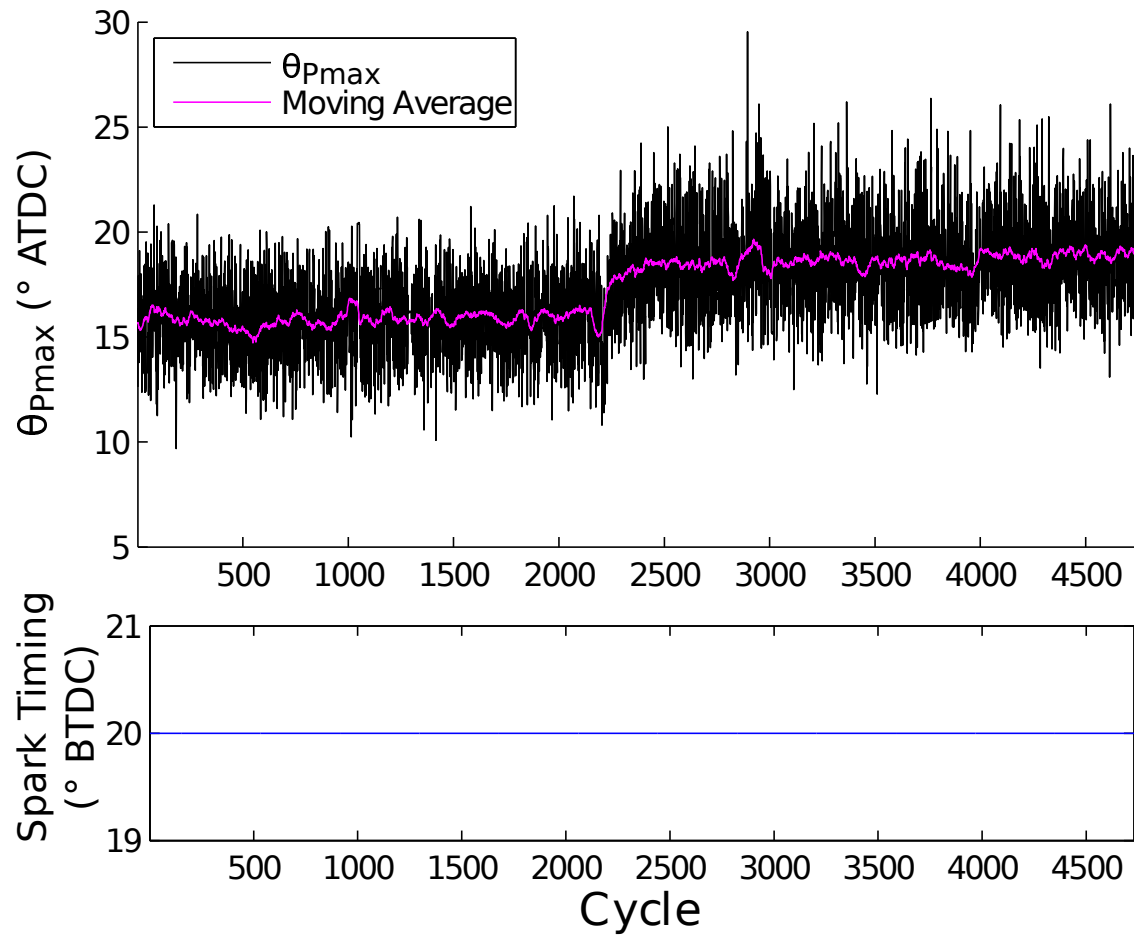
Figure 5.30: Disturbance of iEGR for θ_{Pmax} at Test Condition B, Flat Spark Input

cylinder 2 $\approx$ 4.8 Bar, cylinder 3 $\approx$ 4.7 Bar, cylinder 4 $\approx$ 4.7 Bar. This same offset appears even when the controller is not operating.

As discussed in section 5.3.2 a minimum variance controller with detuned tracking will for this specific implementation will on average increase the cyclic variability by a small amount where as a straight minimum variance controller will slightly decrease the cyclic variability. However, the benefit of the detuned tracking addition is that it can reduce the impact that disturbances or changes in the engine operating conditions have on the cyclic variability. It can also keep the engine operating in the maximum brake torque spark timing.
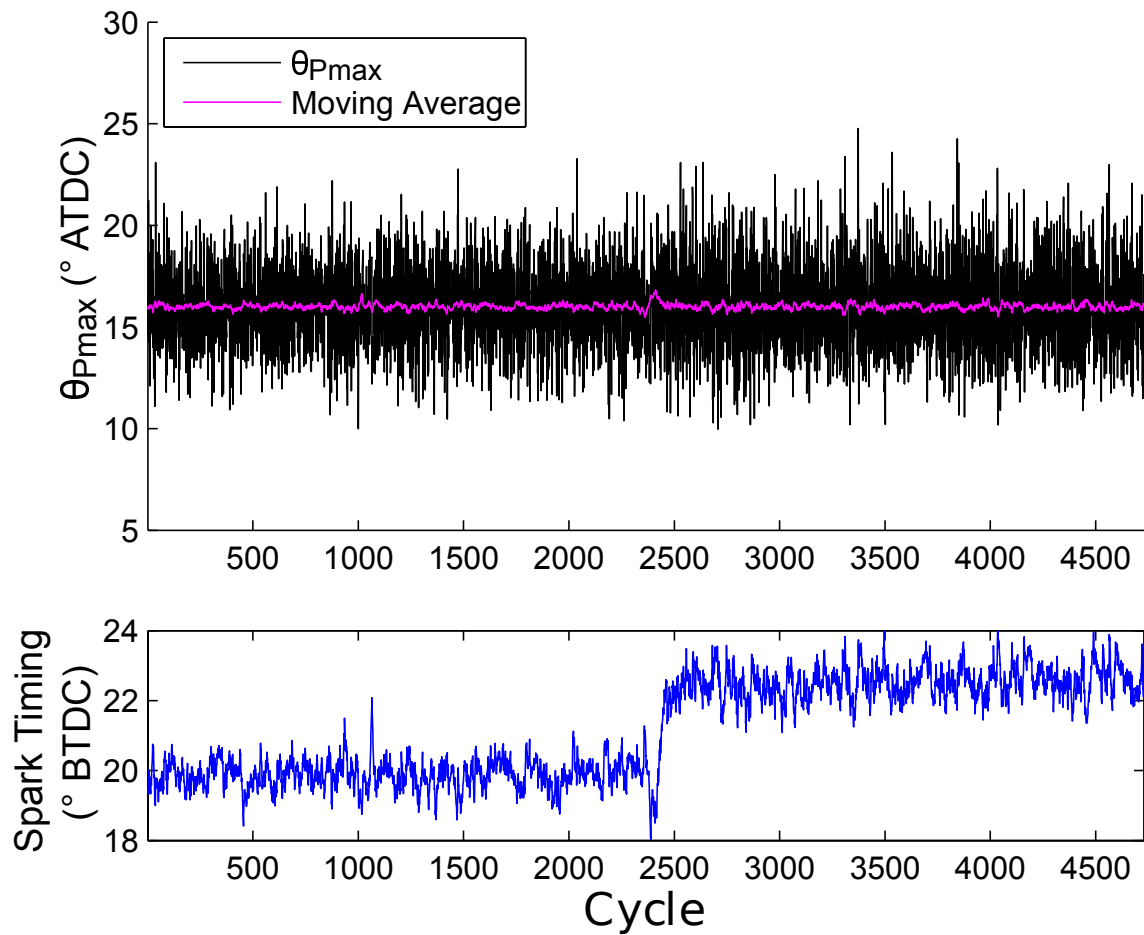
Figure 5.31: Disturbance of iEGR for θ_{Pmax} at Test Condition B,MVC Detuned Controller On

Table 5.9 shows the standard deviation for the iEGR disturbance done with both flat spark input and the minimum variance detuned tracking spark input. All of the data is from cylinder 1. Each data set is 1,000 cycles with 1,000 cycles taken before the step input, during the step input, and after the step input. The data labeled step, is the same data seen in Figure 5.32 with the iEGR disturbance starting at cycle 200. As seen in the table, there is no discernible increase in cyclic variability either before or after the step input when using the controller. However a reduction in the cyclic variability of the parameters can be seen for the data set that includes the step input.

Table 5.9: iEGR Disturbance Results at Test Condition B.

CA50	Flat Spark STD	MVC Detuned STD
1–Pre-Step	2.32 °	2.31 °
2–Step	3.36 °	2.78 °
3–Post-Step	2.81 °	2.79 °

θ_{Pmax}		
1–Pre-Step	1.87 °	1.89 °
2–Step	2.46 °	2.18 °
3–Post-Step	2.18 °	2.16 °

Pmax		
1–Pre-Step	1.64 Bar	1.63 Bar
2–Step	2.02 Bar	2.02 Bar
3–Post-Step	1.95 Bar	1.99 Bar

IMEP		
1–Pre-Step	0.035 Bar	0.039 Bar
2–Step	0.074 Bar	0.072 Bar
3–Post-Step	0.062 Bar	0.042 Bar

Figure 5.33 shows the average values for the same data sets from cylinder 1 shown in Table 5.9. The numbers on the X axis correspond to the same numbers in Table 5.9. As seen in the figure, θ_{Pmax} is held to 16 ° for the entire test since the controller is operating. With the disturbance of iEGR, the controller is better able to increase average IMEP of the system since θ_{Pmax} remains in the optimal position of 16 ° ATDC.

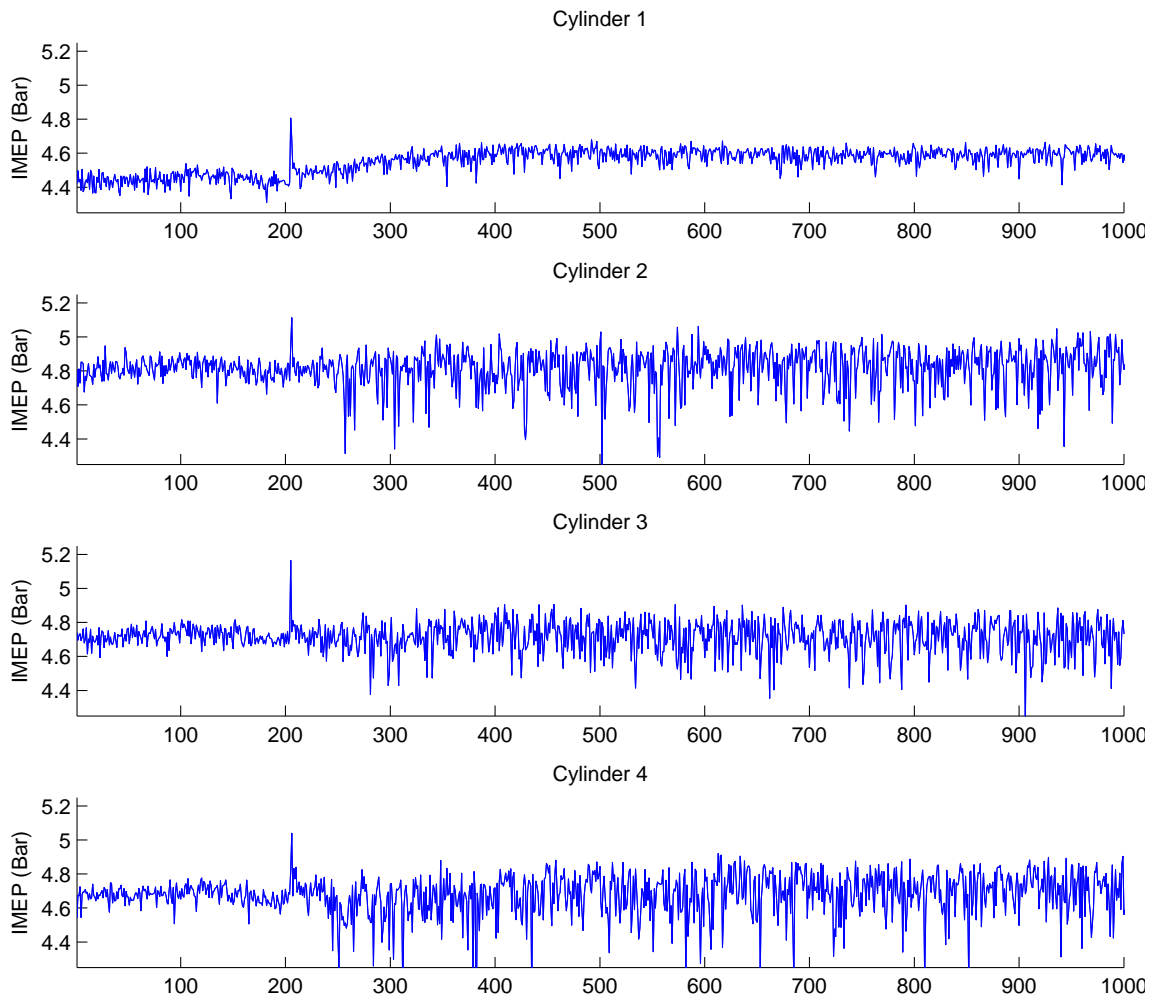Figure 5.32: Disturbance of iEGR for IMEP at Test Condition B, MVC Detuned Controller for Cylinder 1, Cylinders 2, 3, and 4 have Flat Spark Input.
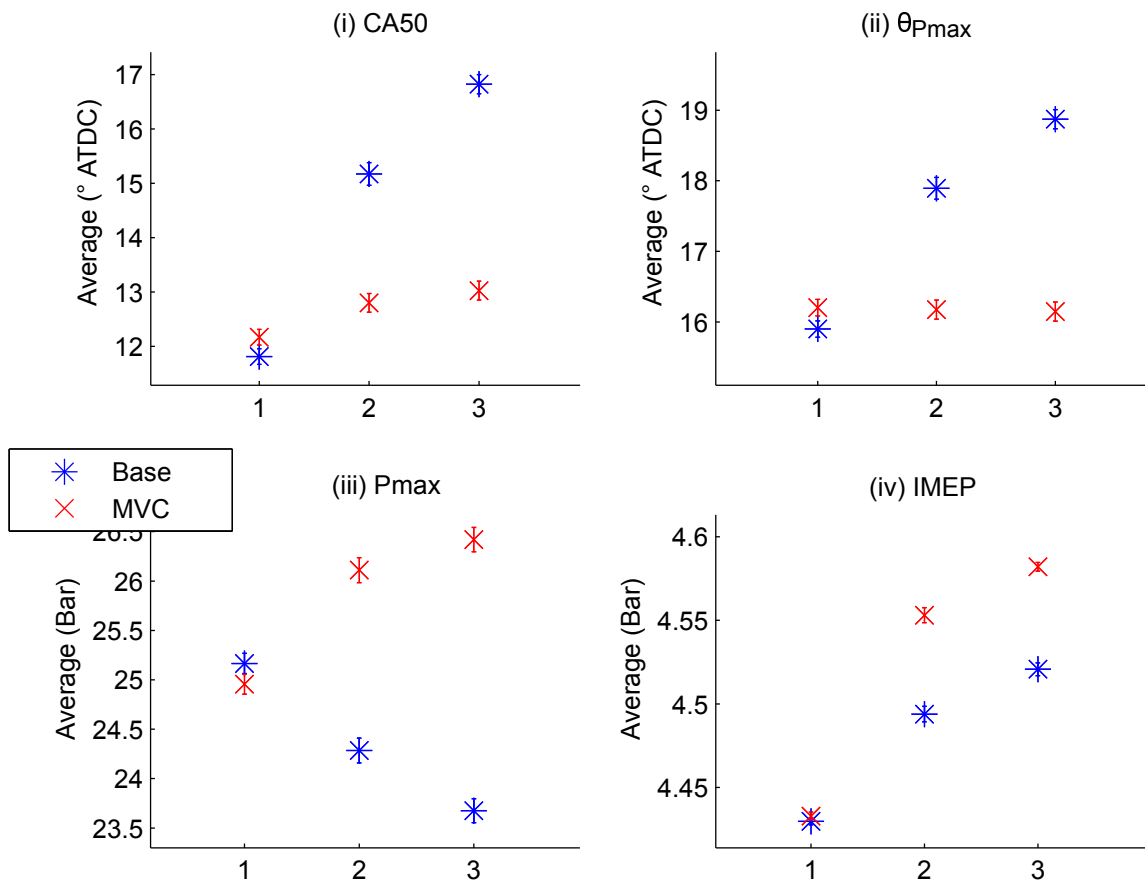
Figure 5.33: Cylinder 1 Average Values for 1,000 cycles, Error Bars Signify Standard Error, at Test Condition B where Base signifies Flat Spark Input and Controller signifies Detuned MVC, X axis label 1 signifies pre-step, 2 step input, and 3 post step data sets.

5.4.2   Natural Gas to Gasoline Fuel Disturbance

The controllers performance at rejecting a disturbance of fuel is tested between test conditions (A) and (C). The fuel disturbance is introduced by changing the injector pulse widths as seen in Table 5.10. These pulse widths are determined based off the information in Appendix E.1.

Table 5.10: Injector Pulse Width Step for Fuel Disturbance between test conditions (A) and (C).

	Pre-Step Pulse Width	Post-Step Pulse Width
Natural Gas	9.1 ms	2.8 ms
Gasoline	0.3 ms	2.0 ms

The response of fixed spark input to the fuel disturbance can be seen in Figure 5.34. A change in the average θ_{Pmax} value happens immediately with the fuel step. An increase (retard) of θ_{Pmax} when replacing natural gas with gasoline at the same spark timing is consistent with the results presented in section 4.3. The same controller from section 5.4.1 is used for this test and the controller is able to successfully reject the gasoline disturbance of θ_{Pmax} as seen in Figure 5.35.
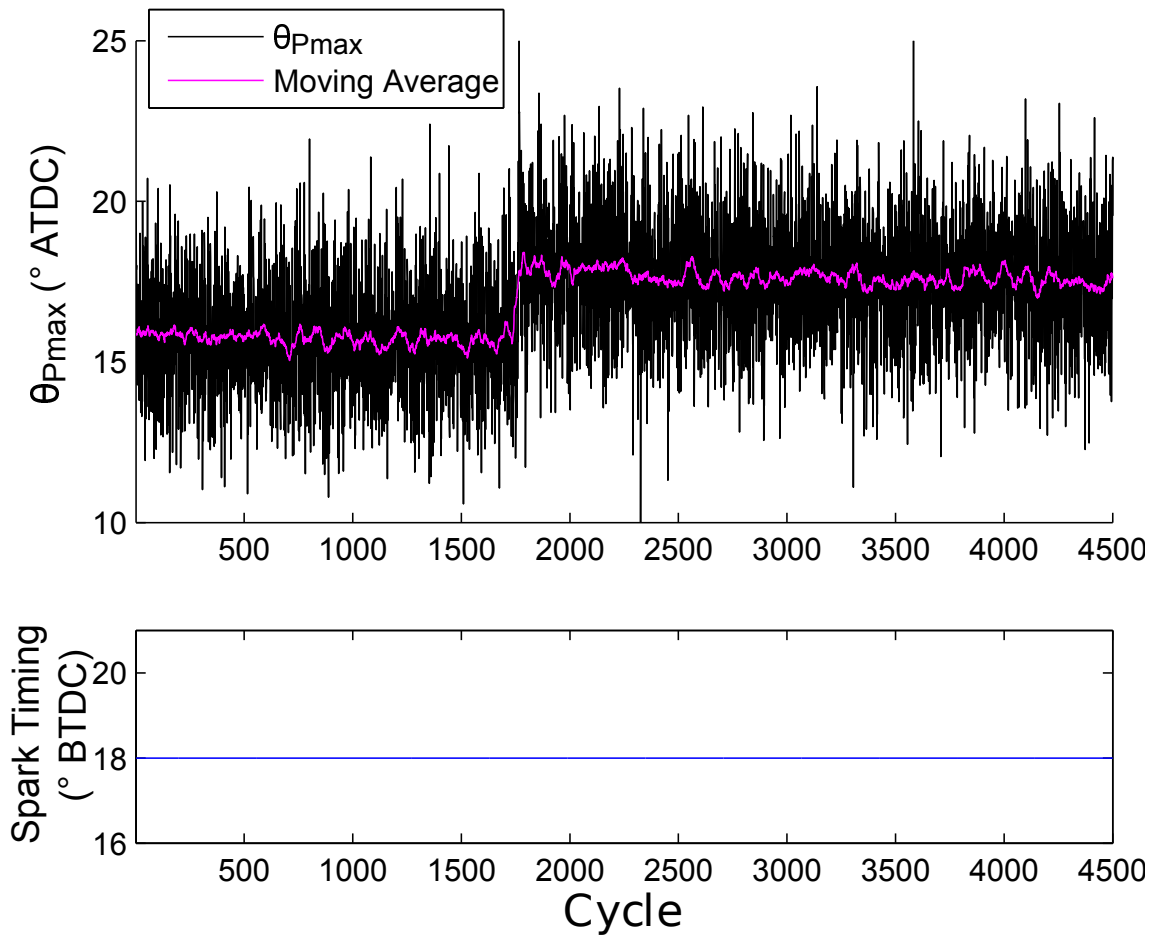
Figure 5.34: Combustion Metric θ_{Pmax} for Disturbance of Fuel, Flat Spark.
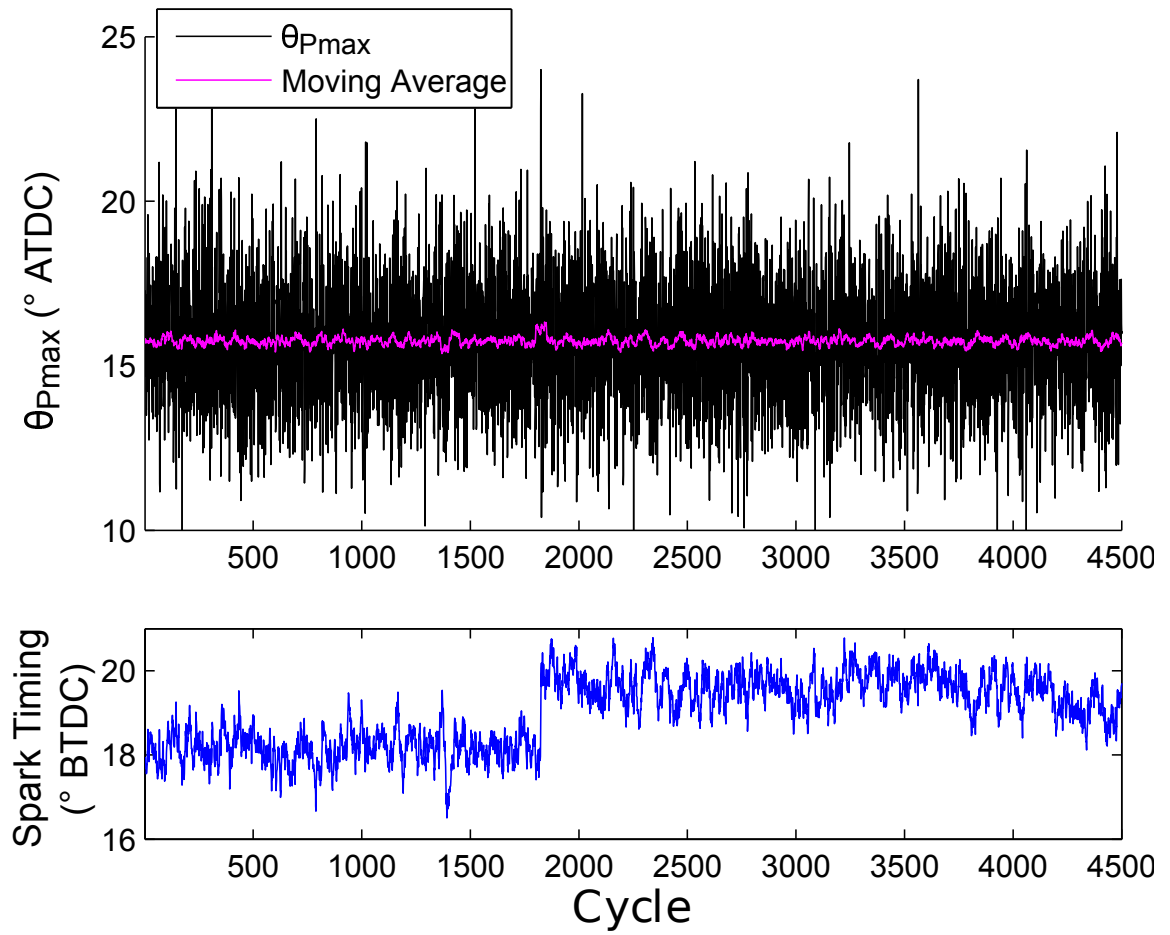
Figure 5.35: Combustion Metric θ_{Pmax} for Disturbance of Fuel, Controller On.

5.4.3   Cold Start Tracking

To test the controllers reaction to a disturbance of engine coolant temperature, the engine is started and immediately set to run at test condition (A). As the engine warms up, the change in engine coolant temperature causes θ_{Pmax} to shift. When operated at a fixed spark timing, as seen in Figure 5.36, the average value of θ_{Pmax} will not remain at the same value as it depends on engine coolant temperature. The characterization data in figure 4.4 shows that for the engine coolant temperature for this study of $90\,^{\circ}\mathrm{C}$, the average θ_{Pmax} for a spark timing of $18\,^{\circ}$ BTDC should be equal to $15.4\,^{\circ}$. From the figure it can be seen that the average θ_{Pmax} is above $16\,^{\circ}$ while the engine is heating up.

The response of the controller to this change in engine coolant temperature can be seen in Figure 5.37. The spark timing output shifts to compensate for the change of θ_{Pmax} because of the engine coolant temperature. The controller is able to keep θ_{Pmax} at its reference set point of $16\,^{\circ}$ despite this disturbance. The controller can be seen consistently outputting a spark timing $\approx 17\,^{\circ}$ BTDC from cycles 4,000 to 5,000. This is not an artifact of the minimum variance controller. Comparing the results in Figure 5.37 to the results previously discussed in Figure 5.24, it can be seen that at stable operating conditions, the spark timing output will only move a degree from its midpoint for around 10 cycles over the entire 15,000 cycle test. While for the cold start case presented, the spark timing stays moves from $18\,^{\circ}$ to an average value of $17\,^{\circ}$, and stays there for 1,000 cycles between cycle 4,000 and 5,000. This is the controller responding to the changing engine coolant temperature and doesn't happen with constant engine coolant temperature.

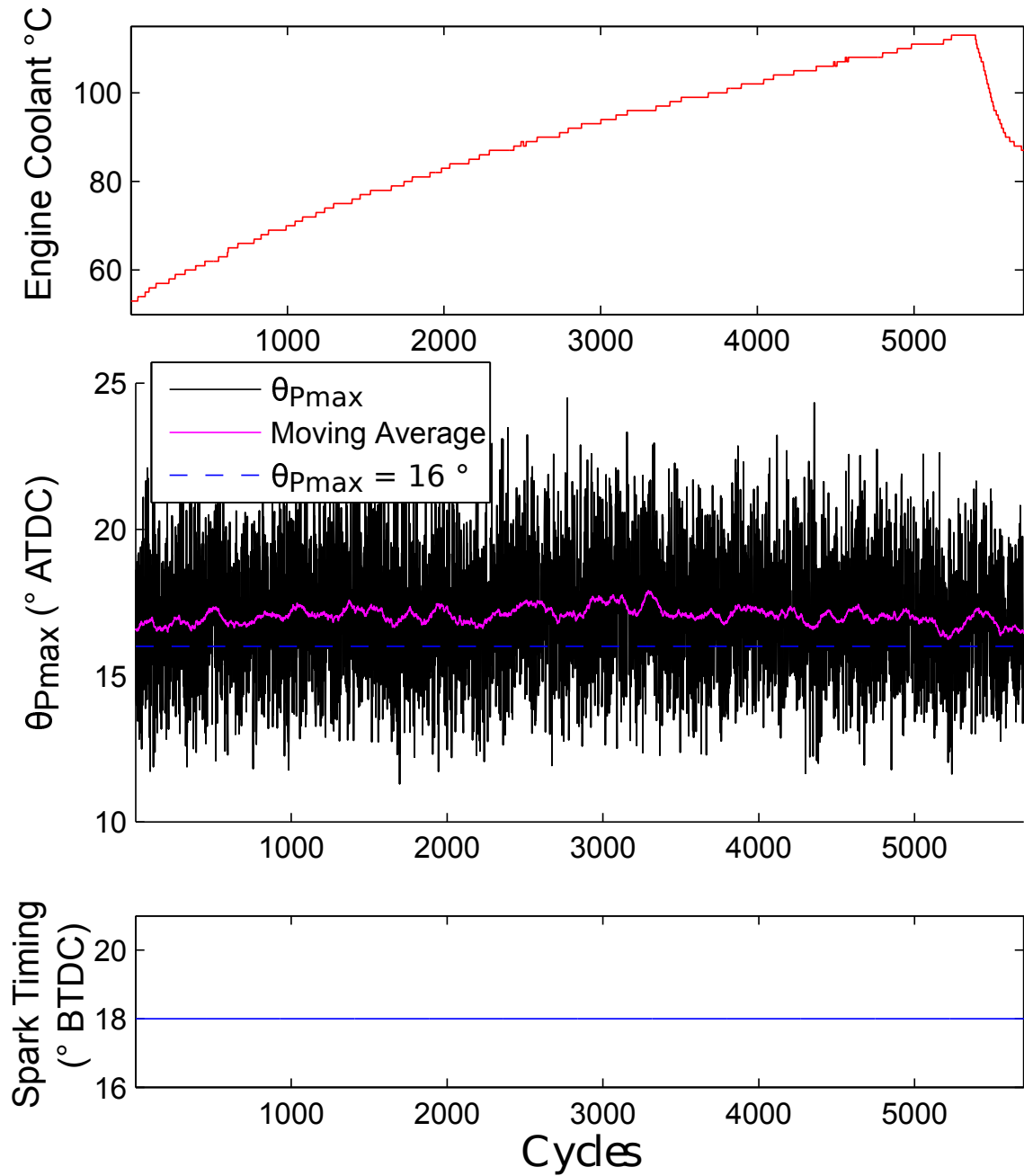Figure 5.36: Combustion Metric θ_{Pmax} for Cold Start with Fixed Spark Timing at Test Condition (A) from Table 4.1
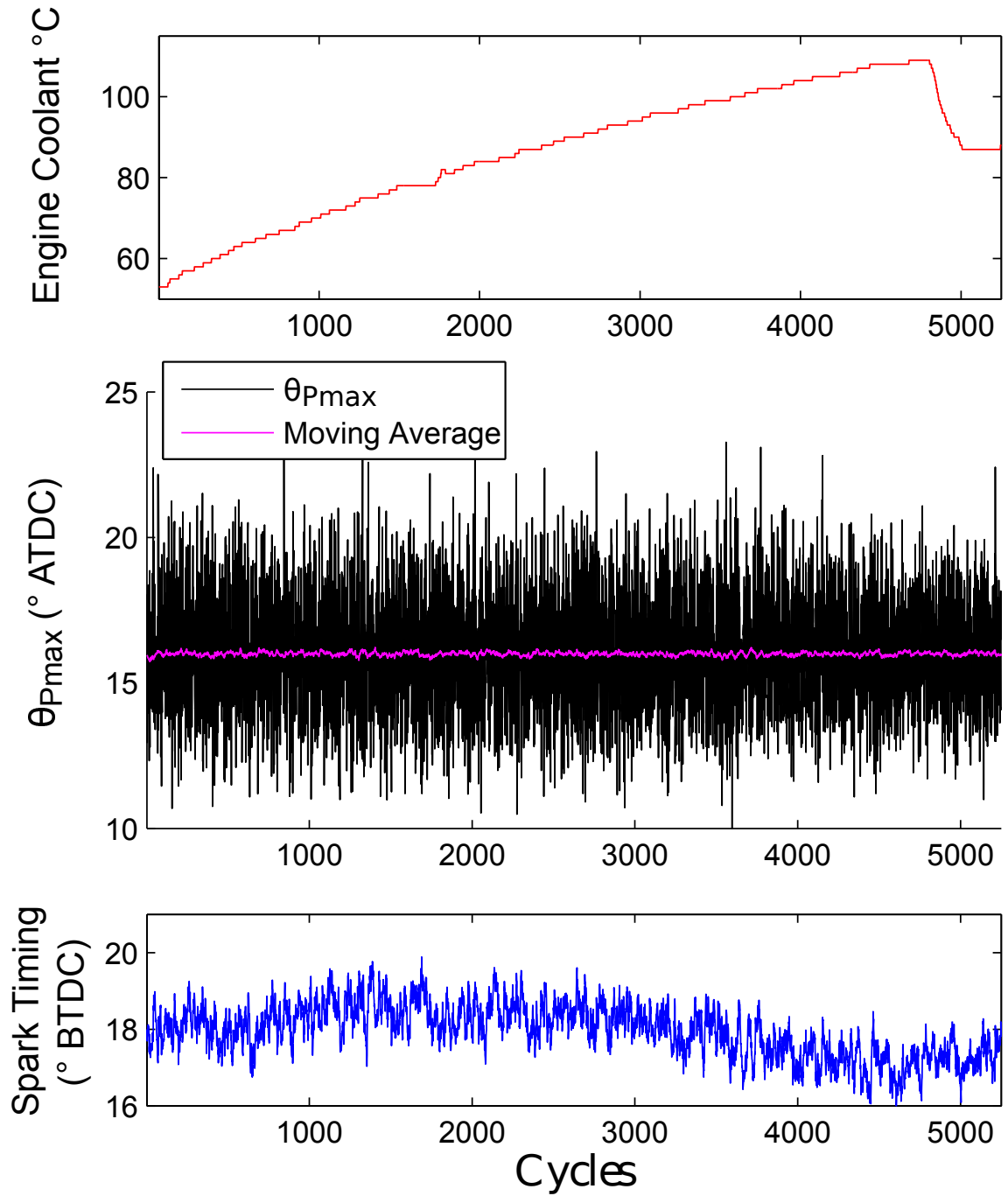
Figure 5.37: Combustion Metric θ_{Pmax} for Cold Start with Controller On at Test Condition (A) from Table 4.1

5.5 Summary

Four combustion metrics, θ_{Pmax}, Pmax, CA50, and IMEP, are used as outputs for a system identification test. The model fit of each combustion metric determines which metric can be best predicted when using spark timing as an input. θ_{Pmax} is determined to have the highest model fit and best ability to be predicted using the developed system identification model. A minimum variance controller is then designed for θ_{Pmax} and the amount of cyclic variability in the system is reduced by 1.4%. A detuned minimum variance tracking controller is designed which slightly increases the cyclic variability but is able to track a specific θ_{Pmax} value. In chapter 4, $\theta_{\text{Pmax}} = 16$ was found to produce peak IMEP at all test conditions used in this study. The controller is able to reject disturbances such as changes to, internal exhaust gas recirculation, fuel type, and engine coolant temperature, by manipulating spark timing so $\theta_{\text{Pmax}} = 16^{\circ}$ after top dead center despite of the change in operating conditions. The impact of the set-point tracking is a cyclic variability increase of 3.1%.

CHAPTER 6

CONCLUSION

6.1   Major Results and Conclusions

In this study a 4 cylinder General Motors direct injection engine is modified into a state of the art test facility. The features of this facility are:

- Operation of both a production vehicle engine controller and a flexible dSPACE controller capable of manipulating engine inputs, such as spark timing and fuel pulse width, while the engine is running.

- Dual injection allowing the operation of in cylinder direct injection and port injection at the same time.

- Ability to run either liquid fuels, such as gasoline or biofuels, or gaseous fuels, such as natural gas, through the port injectors.

- Recording the engines cylinder pressure every $0.1\,^{\circ}$ of crank angle for all 4 cylinders with cylinder head donated by General Motors.

- Online cylinder pressure feedback to the engine controller allowing for closed loop control.

The cyclic variability of the engine is characterized by manipulating the spark timing, type of fuel, and engine speed and recording how the standard deviation of four

combustion metrics, θ_{Pmax}, Pmax, CA50, and IMEP are affected. The major results from characterization are:

- Advancing spark timing reduces the standard deviation of all combustion metrics except for IMEP, which varies non linearly with spark timing.

- Gasoline produces a higher standard deviation for all combustion metrics, except for Pmax, compared to natural gas.

- Increasing engine speed increases the standard deviation of all combustion metrics except for IMEP.

The four combustion metrics are modeled using system identification and the metric with the highest model fit, θ_{Pmax}, is selected for use in a minimum variance controller. Using spark timing as controller output and θ_{Pmax} as a controller input in a minimum variance controller, the standard deviation of θ_{Pmax} is reduced 1.4% compared to a unchanging spark input. A detuned minimum variance tracking controller is designed which allows for closed loop tracking on a reference θ_{Pmax} value by slightly increasing the cyclic variability. The controllers ability to reject disturbances is tested by introducing internal exhaust gas recirculation, changing fuel from natural gas to gasoline, and changing engine coolant temperature. The controller is able to reject all disturbances and keep the engine operating at the reference θ_{Pmax} value. The controllers impact is an increase in the standard deviation of θ_{Pmax} by 3.1% under constant operating conditions.

6.2 Future Work

Possible areas of future research are:

- In this study, only single input single output models and controllers are investigated. It is possible that increasing the model inputs could lead to higher

model fits and improved next cycle predictability.

- Implementation of similar system identification modeling and minimum variance controller development on less stable operating conditions such as lean burn or higher efficiency engine modes such as homogeneous charge compression ignition.

- Only one cylinders θ_{Pmax} value is used as a controller input, and only that cylinders spark timing is changed as the controller output. The minimum variance controller designed in this study can track the reference θ_{Pmax} of all four cylinders separately allowing for all cylinders to be operating at optimal conditions. However, the technical challenge arising from the limited computation window must be solved.

- Increase the engines compression ratio by installing custom pistons to allow for experimenting with advanced low temperature combustion techniques in the test facility.

Bibliography

An, F. and Sauer, a. (2004). Comparison of passenger vehicle fuel economy and greenhouse gas emission standards around the world. *Pew Center on Global Climate Change.*

Audet, A. D. (2008). Closed loop control of HCCI using camshaft phasing and dual fuels.

Chanchaona, S. (1990). *Cyclic variability in a natural gas fuelled spark ignition engine.* PhD thesis, ResearchSpace@ Auckland.

Clerk, D. (1921). Cylinder Actions in Gas and Gasoline Engines. Technical report, SAE Technical Paper.

Dai, W., Trigui, N., and Lu, Y. (2000). Modeling of Cyclic Variations in Spark-Ignition Engines. *SAE Technical Paper*, (724).

Daw, C. S. (2002). Controlling Cyclic Combustion Variations in Lean-Fueled Spark-Ignition Engines. *AIP Conference Proceedings*, 2001(724):265–277.

EPA (2012). EPA and NHTSA Set Standards to Reduce Greenhouse Gases and Improve Fuel Economy for Model Years 2017-2025 Cars and Light Trucks. (August 2012).

Finney, C. E., Kaul, B. C., Daw, C. S., Wagner, R. M., Edwards, K. D., and Green,

J. B. (2015). A review of deterministic effects in cyclic variability of internal combustion engines. *International Journal of Engine Research*, 16(3):366–378.

Heywood, J. B. (1988). *Internal Combustion Engine Fundamentals*. Automotive technology series. McGraw-Hill.

Huang, B., Qi, Y., and Murshed, A. K. M. M. (2013). *Dynamic modeling and predictive control in solid oxide fuel cells: first principle and data-based approaches*. John Wiley & Sons.

Kaleli, A., Ceviz, M. A., and Erenturk, K. (2015). Controlling spark timing for consecutive cycles to reduce the cyclic variations of SI engines. *Applied Thermal Engineering*, 87:624–632.

Karl J. Astrom (1970). Introduction to Stochastic Control Theory. pages 166–180.

Killeen, P. R. (2005). An alternative to null-hypothesis significance tests. *Psychological science*, 16(5):345–353.

Li, P., Shen, T., Kako, J., and Liu, K. (2009). Cyclic moving average control approach to cylinder pressure and its experimental validation. *Journal of Control Theory and Applications*, 7(4):345–351.

Ljung, L. (1987). System Identification: Theory for the user. *PTR Prentice Hall Information and System Sciences Series*, 198.

Ozdor, N., Dulger, M., and Sher, E. (1996). An experimental study of the cyclic variability in spark ignition engines. Technical report, SAE Technical Paper.

Petrovic, S. (1982). Cycle by Cycle Variations of Flame Propagation in a Spark Ignition Engine. Technical report, SAE Technical Paper.

Reyes, M., Tinaut, F., Giménez, B., and Pérez, a. (2015). Characterization of cycle-to-cycle variations in a natural gas spark ignition engine. *Fuel*, 140:752–761.

Stone, R. (2012). *Introduction to internal combustion engines*. Palgrave Macmillan.

Swords, M. D., Kalghatgi, G. T., and Watts, A. J. (1982). An experimental study of ignition and flame development in a spark ignited engine. Technical report, SAE Technical Paper.

Triantos, G., Shenton, A. T., and Carroll, S. D. (2003). Minimum Variance Control of Cylinder Peak Pressure Position. In *Proceedings of IFAC Symposium on Advances in Automative Control*, pages 143–148.

Wellstead, P. E. and Zarrop, M. B. (1991). Self-Tuning Systems: Control and Signal Processing. *Chichester: Johon Wiley & Sons Ltd*.

Zhang, H. G., Han, X. J., Yao, B. F., and Li, G. X. (2013). Study on the effect of engine operation parameters on cyclic combustion variations and correlation coefficient between the pressure-related parameters of a CNG engine. *Applied Energy*, 104:992–1002.

Zhu, G., Daniels, C., and Winkelman, J. (2003). MBT timing detection and its closed-loop control using in-cylinder pressure signal. *Proc. of the Society of Automotive Engineering World Congress*, c(724):3266.

Appendix A
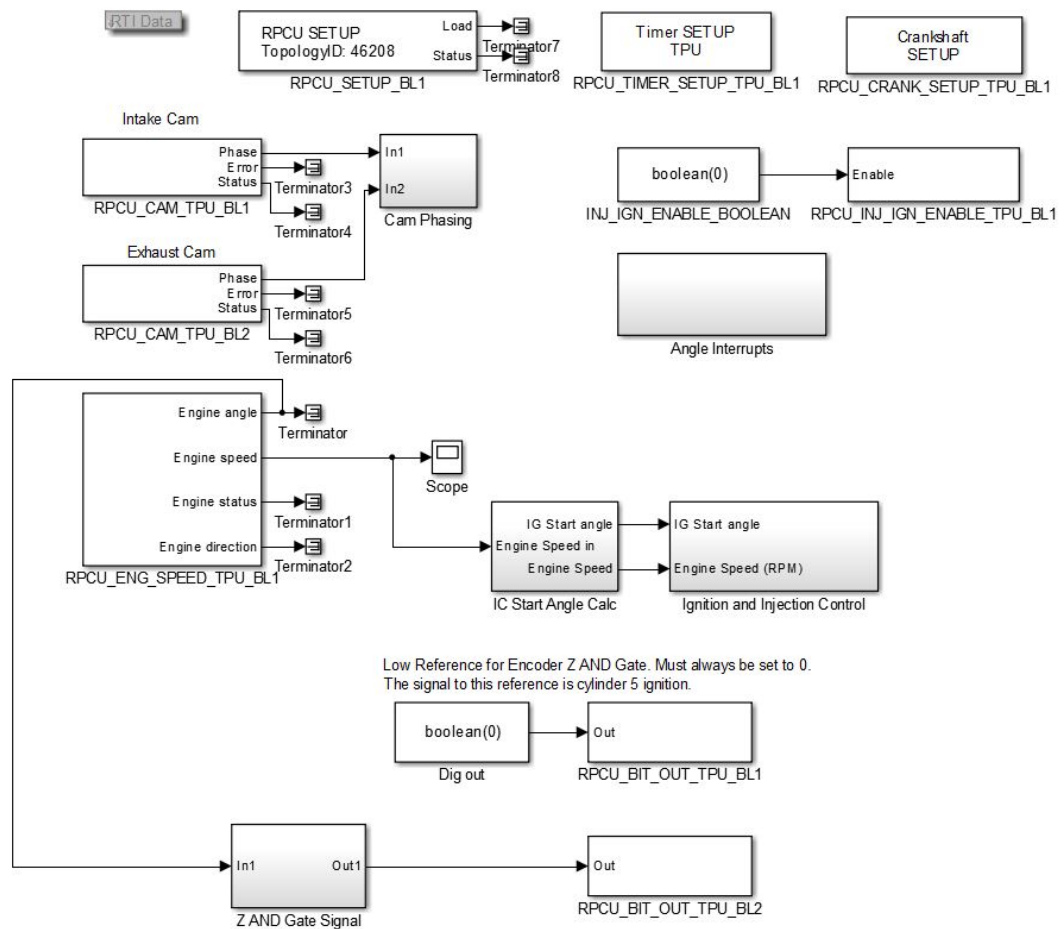
Experimental Setup Supporting Figures
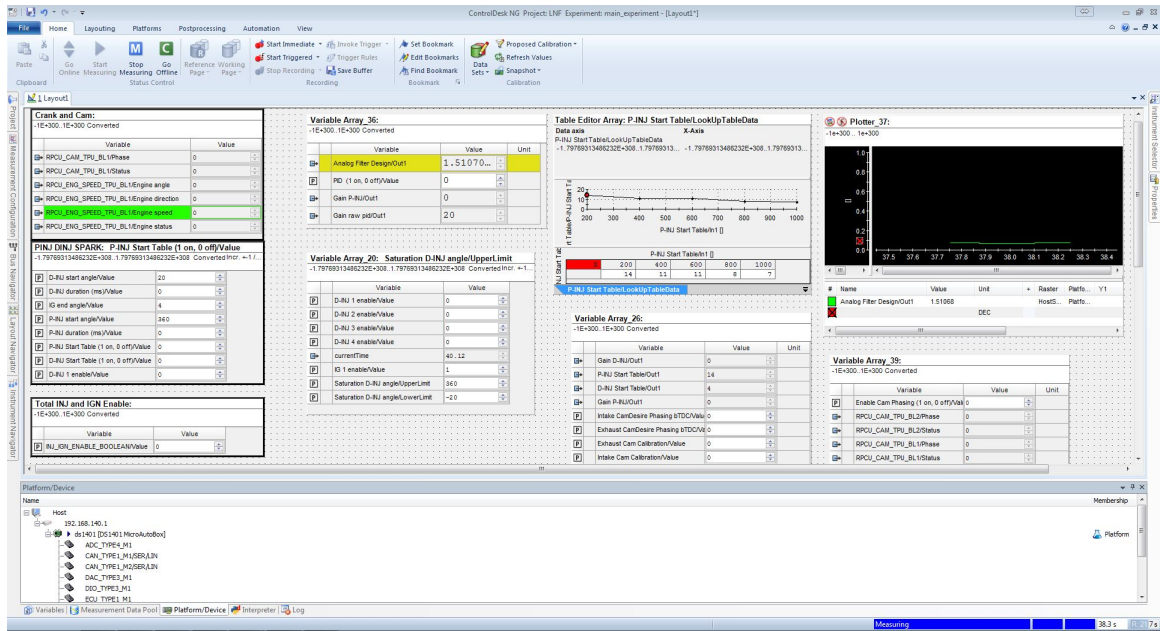

Figure A.1: Simulink Block Diagram
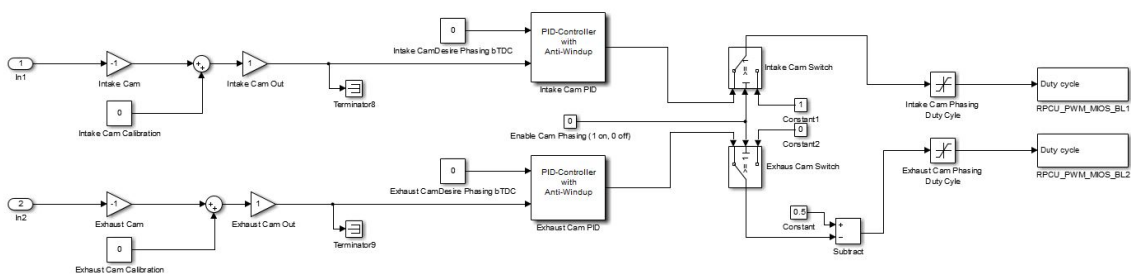
Figure A.2: ControlDesk Interface

Figure A.3: Cam Phasing Block Diagram

Figure A.4: Cam Phasing PID Gains

Appendix B

Engine Inputs and Engine Variables for Test Conditions

The terms used in the table are listed below along with their units.

- Spark Timing - ($^\circ$ BTDC).

- P-INJ PW- Port Injection Pulse Width (ms).

- P-INJ $^\circ$ - Port Injection Start Angle ($^\circ$ BTDC).

- D-INJ PW - Direct Injection Pulse Width (ms).

- D-INJ $^\circ$ - Direct Injection Start Angle ($^\circ$ BTDC).

- Dyno Torque - (Nm).

- Dyno RPM - (RPM)

- MAP - Manifold Air Pressure (kPa).

- MAF - Mass Air Flow (g/sec).

- λ - Airfuel equivalence ratio, $\lambda > 1$ lean (more air than stoich), $lambda < 1$ rich (more fuel than stoich).

- FRP - Direct Injection Fuel Rail Pressure (MPa)

- IAT - Intake Air Temperature ($^\circ$ C)

- TPS - Throttle Position Sensor (%)

- ECT- Engine Coolant Temperature ($^\circ$ C).

Table B.1: Engine Inputs and Engine Variables for Test Conditions

Test Condition	Spark Timing	P-INJ PW	P-INJ °	D-INJ PW	D-INJ °	Dyno Torque	Dyno RPM
(A)	18	10.05	360	0	0	62	1250
(B)	20.5	10.25	360	0	0	64	1750
(C)	23.5	0	0	2.55	310	63	1250
(D)	24.5	0	0	2.55	310	64	1750
Max Variation	-	-	-	-	-	±1	±1

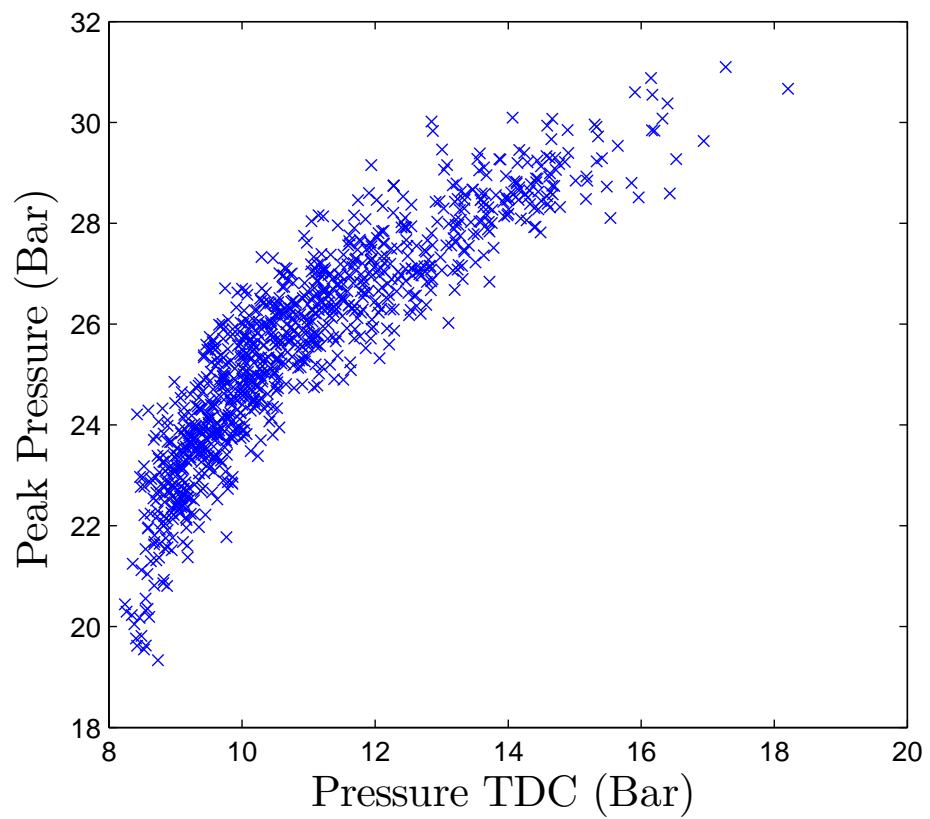| Test Condition	MAP	MAF	λ	FRP	IAT	TPS	ECT
(A)	65	9.75	1	-	24	31	90
(B)	65	14.25	1	-	23	34	90
(C)	65	9.9	1	2	24	31	90
(D)	63	14.2	1	2	24	34	91
Max Variation	±1	±0.4	±.05	±0.1	±1	±1	±2

Appendix C

Replication Supporting Figures

Figure C.1: Correlation Between Pmax and Pressure TDC

APPENDIX D

SYSTEM IDENTIFICATION ARMAX MODELS

D.1 ARMAX Models for G_{RBS} Comparison

Table D.1: θ_{Pmax} ARMAX Models for G_{RBS} Recorded on the dSPACE Controller

G_{RBS}	ARMAX Model	Model Fit (%)
± 2	$A(z) = 1 - 0.03566z^{-1}$ $B(z) = -0.982$ $C(z) = 1 - 0.0427z^{-1}$	31.69
± 4	$A(z) = 1 + 0.003851z^{-1}$ $B(z) = -1.001z^{-1}$ $C(z) = 1 - 0.02342z^{-1}$	58.02
± 6	$A(z) = 1 - 0.04367z^{-1}$ $B(z) = -1.227z^{-1}$ $C(z) = 1 + 0.02106z^{-1}$	72.97

D.2 ARMAX Model for Test Condition (A)

Table D.2: ARMAX Model for Condition (A)

Combustion Metric	ARMAX Model	Model Fit (%)
θ_{Pmax}	$A(z) = -0.01796z^{-1}$ $B(z) = -1.024$ $C(z) = 1 + 0.02797z^{-1}$	33.25
Pmax	$A(z) = 1 - 0.09109z^{-1}$ $B(z) = 0.8236$ $C(z) = 1 - 0.1322z^{-1}$	28.89
CA50	$A(z) = 1 + 0.09482z^{-1}$ $B(z) = -1.292$ $C(z) = 1 + 0.1184z^{-1}$	32.11
IMEP	$A(z) = 1 - 0.5875z^{-1}$ $B(z) = 0.0022$ $C(z) = 1 - 0.5659z^{-1}$	2.25
P_{TDC}	$A(z) = 1 + 0.1376^{-1}$ $B(z) = 0.7819$ $C(z) = 1 + 0.1564z^{-1}$	32.76
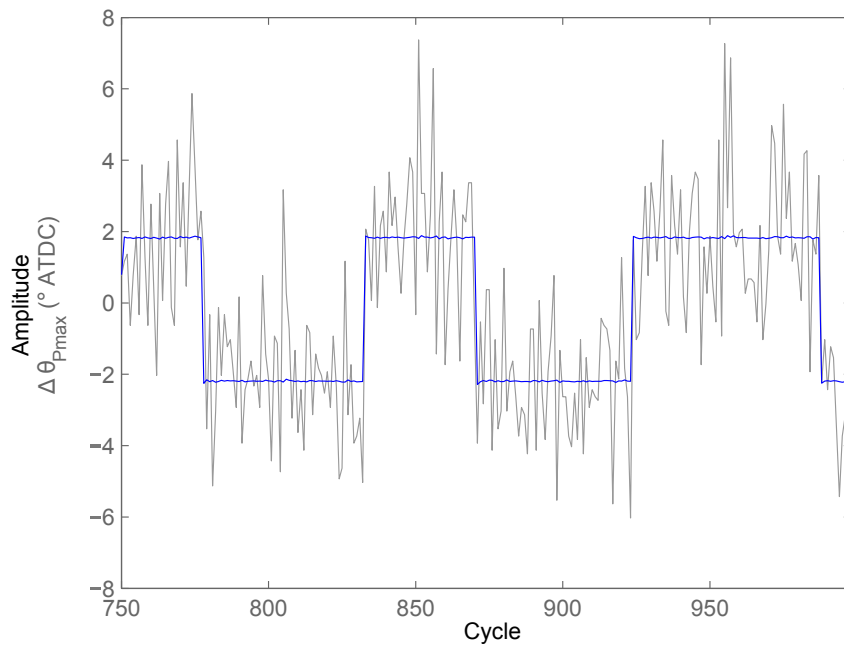
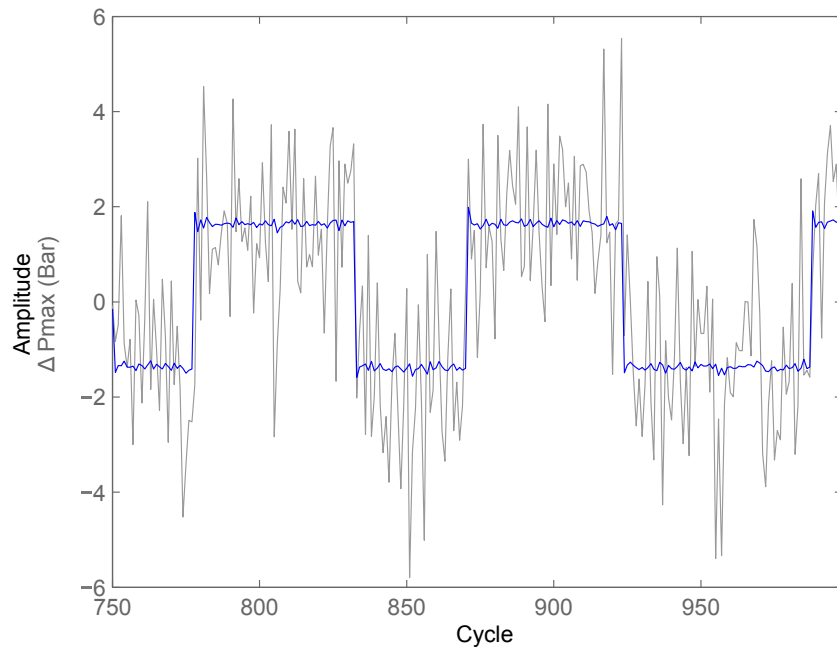Figure D.1: Model Validation, θ_{Pmax} at Test Condition (A)

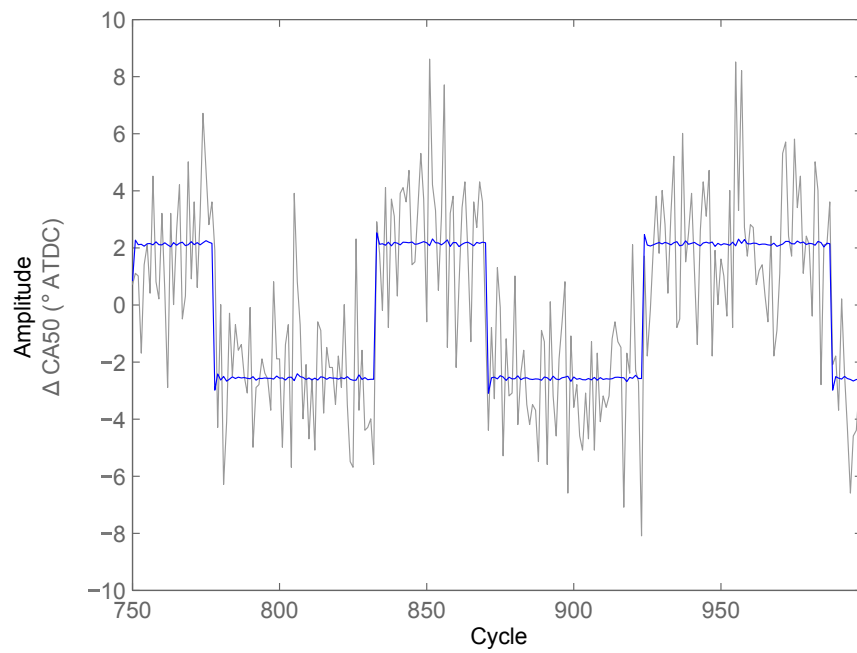Figure D.2: Model Validation, Pmax at Test Condition (A)

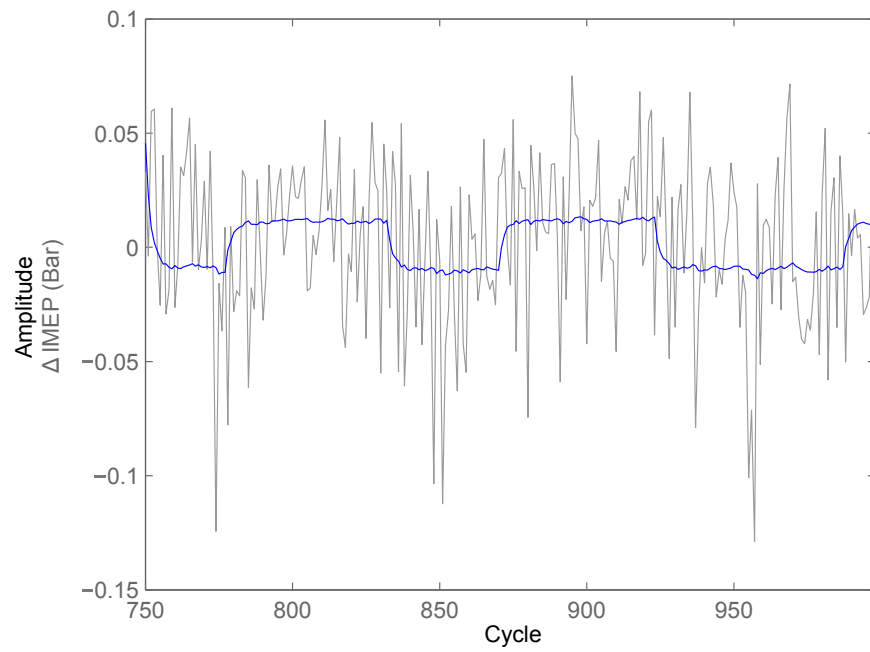Figure D.3: Model Validation, CA50 at Test Condition (A)

Figure D.4: Model Validation, IMEP at Test Condition (A)
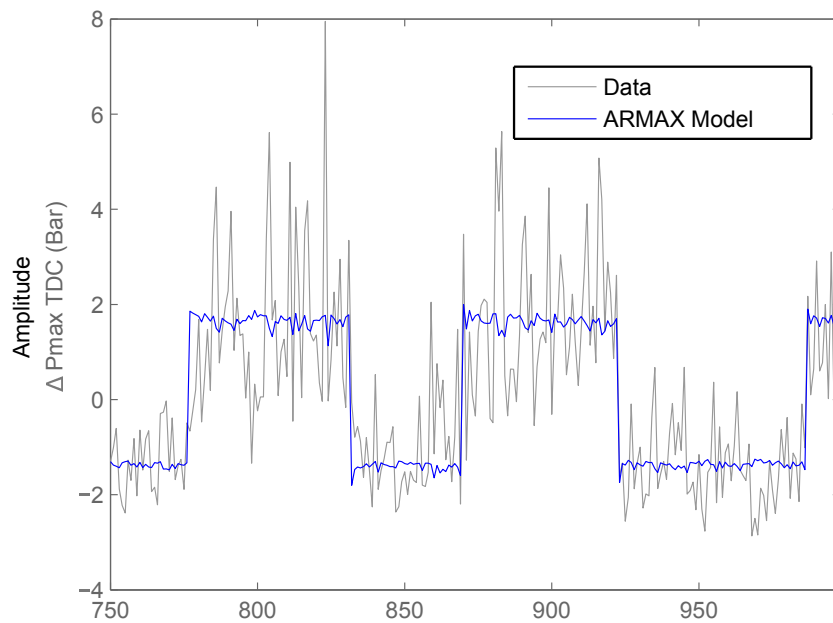
D.3 ARMAX Model for Test Condition (B)

Figure D.5: Model Validation, Pmax TDC at Test Condition (B)

Table D.3: ARMAX Models for Condition (B)

Combustion Metric	ARMAX Model	Model Fit (%)
θ_{Pmax}	$A(z) = 1 + 0.1314z^{-1}$ $B(z) = -1.154$ $C(z) = 1 + 0.0893z^{-1}$	28.91
Pmax	$A(z) = 1 + 0.1995z^{-1}$ $B(z) = 0.9615$ $C(z) = 1 + 0.1768z^{-1}$	25.42
CA50	$A(z) = 1 + 0.0.1667z^{-1}$ $B(z) = -1.446$ $C(z) = 1 + 0.1162z^{-1}$	28.16
IMEP	$A(z) = 1 + 0.2215z^{-1}$ $B(z) = 0.01285$ $C(z) = 1 + 0.09148z^{-1}$	9.464

D.4   ARMAX Model for Test Condition (B) with iEGR

Table D.4: ARMAX Model for Condition (B) with iEGR

Combustion Metric	ARMAX Model	Model Fit (%)
θ_{Pmax}	$A(z) = 1 + 0.1307z^{-1}$ $B(z) = -0.7373$ $C(z) = 1 + 0.0648z^{-1}$	15.44
Pmax	$A(z) = 1 + 0.1768z^{-1}$ $B(z) = 0.9566$ $C(z) = 1 + 0.08931z^{-1}$	14.26
CA50	$A(z) = 1 + 0.2355z^{-1}$ $B(z) = -1.528$ $C(z) = 1 + 0.1485z^{-1}$	13.35
IMEP	$A(z) = 1 + 0.4495z^{-1}$ $B(z) = 0.0385$ $C(z) = 1 + 0.3869z^{-1}$	8.74

D.5 ARMAX Model for Test Condition (C)

Table D.5: ARMAX Model for Condition (C)

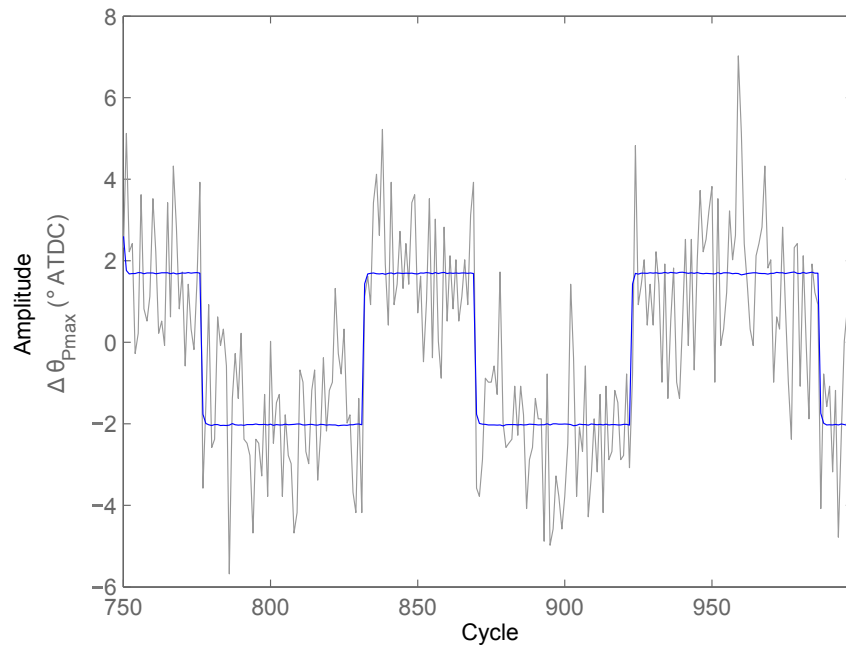| Combustion Metric	ARMAX Model	Model Fit (%)
θ_{Pmax}	$A(z) = -0.07358z^{-1}$ $B(z) = -0.8603$ $C(z) = 1 + 0.08069z^{-1}$	33.68
Pmax	$A(z) = 1 - 0.0807z^{-1}$ $B(z) = 0.6506$ $C(z) = 1 - 0.1039z^{-1}$	28.72
CA50	$A(z) = 1 - 0.08463z^{-1}$ $B(z) = -0.9715$ $C(z) = 1 - 0.1052z^{-1}$	32.66
IMEP	$A(z) = 1 + 0.1781z^{-1}$ $B(z) = 0.00953$ $C(z) = 1 + 0.1325z^{-1}$	2.368

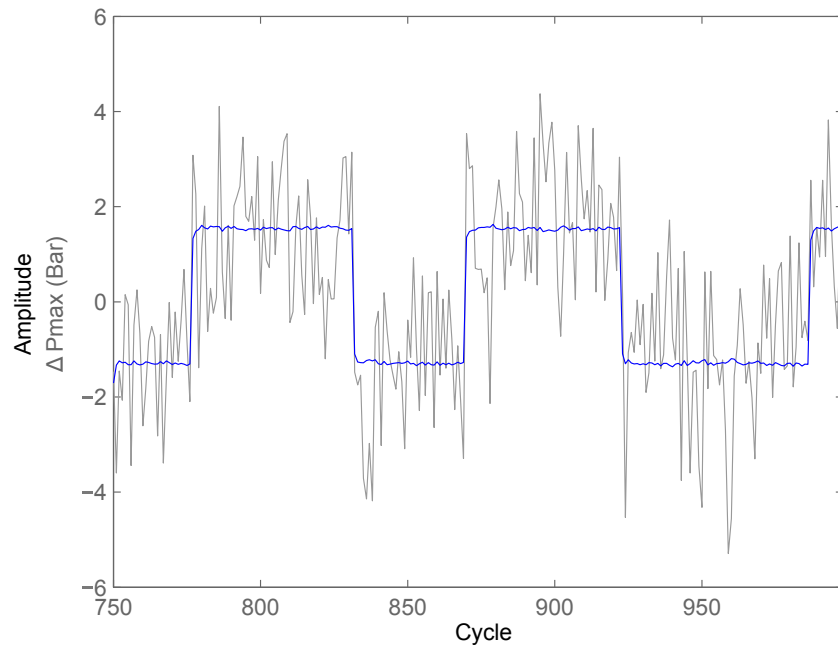Figure D.6: Model Validation, θ_{Pmax} at Test Condition (C)

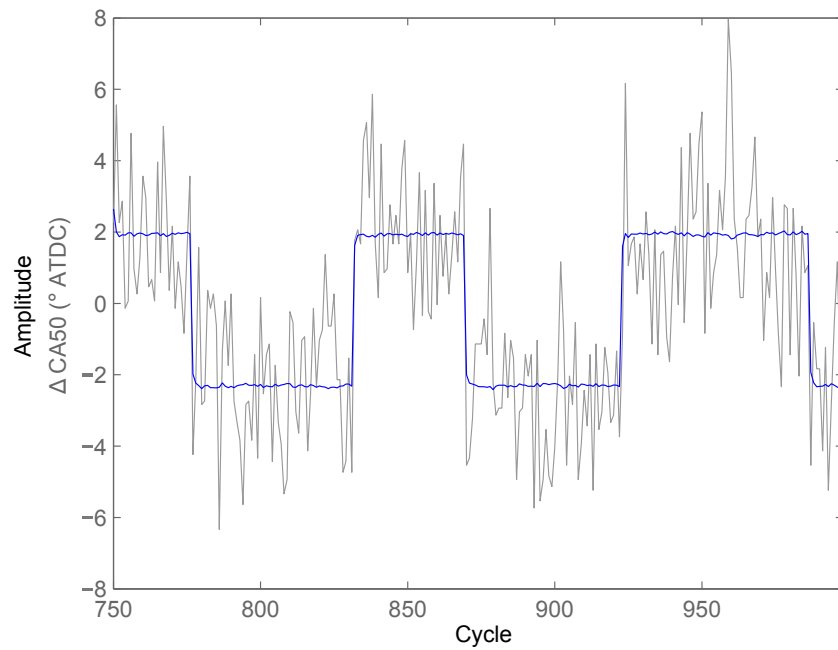Figure D.7: Model Validation, Pmax at Test Condition (C)

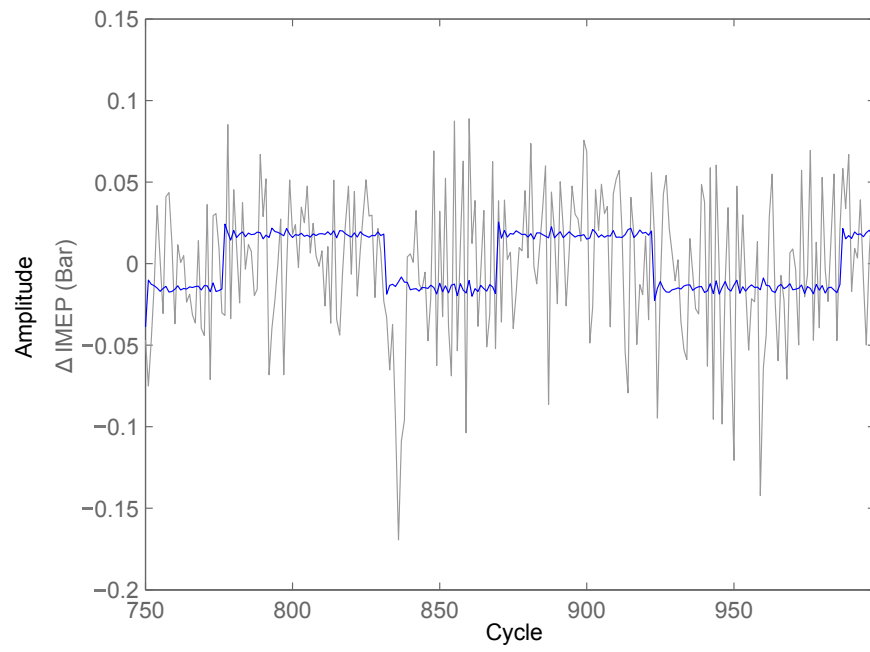Figure D.8: Model Validation, CA50 at Test Condition (C)

Figure D.9: Model Validation, IMEP at Test Condition (C)

D.6 ARMAX Model for Test Condition (D)

Table D.6: ARMAX Model for Condition (D)

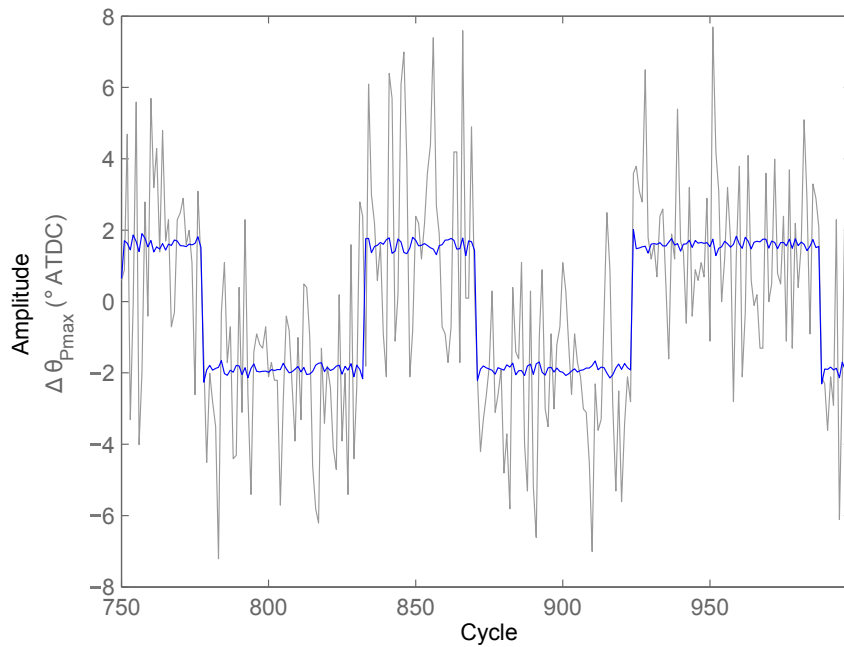| Combustion Metric	ARMAX Model	Model Fit (%)
θ_{Pmax}	$A(z) = 0.1043z^{-1}$ $B(z) = -0.9734$ $C(z) = 1 + 0.05331z^{-1}$	22.6
Pmax	$A(z) = 1 + 0.09874z^{-1}$ $B(z) = 0.7378$ $C(z) = 1 + 0.03288z^{-1}$	22.14
CA50	$A(z) = 1 + 0.1256z^{-1}$ $B(z) = -1.159$ $C(z) = 1 - 0.1052z^{-1}$	22.59
IMEP	$A(z) = 1 - 0.03813z^{-1}$ $B(z) = 0.01451$ $C(z) = 1 - 0.1337z^{-1}$	10.08

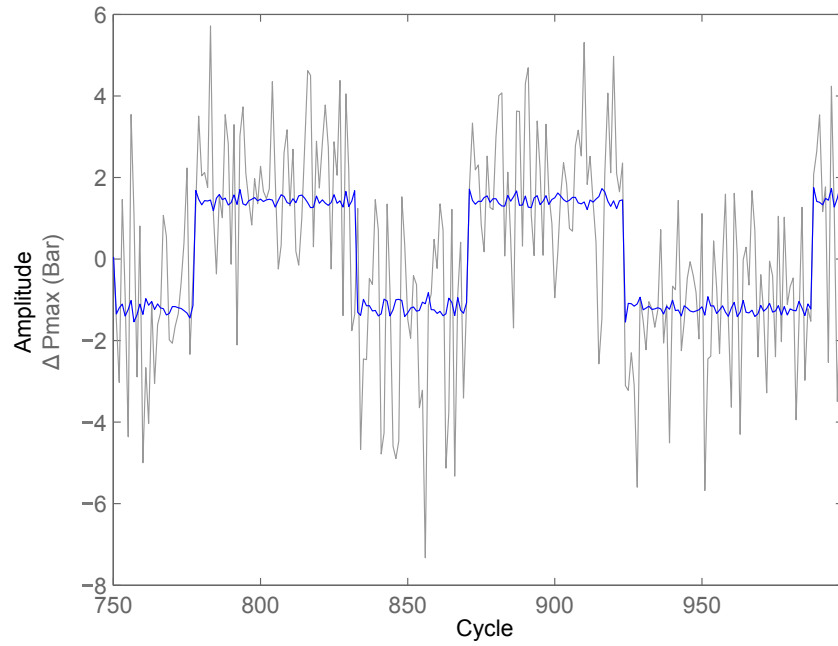Figure D.10: Model Validation, θ_{Pmax} at Test Condition (D)

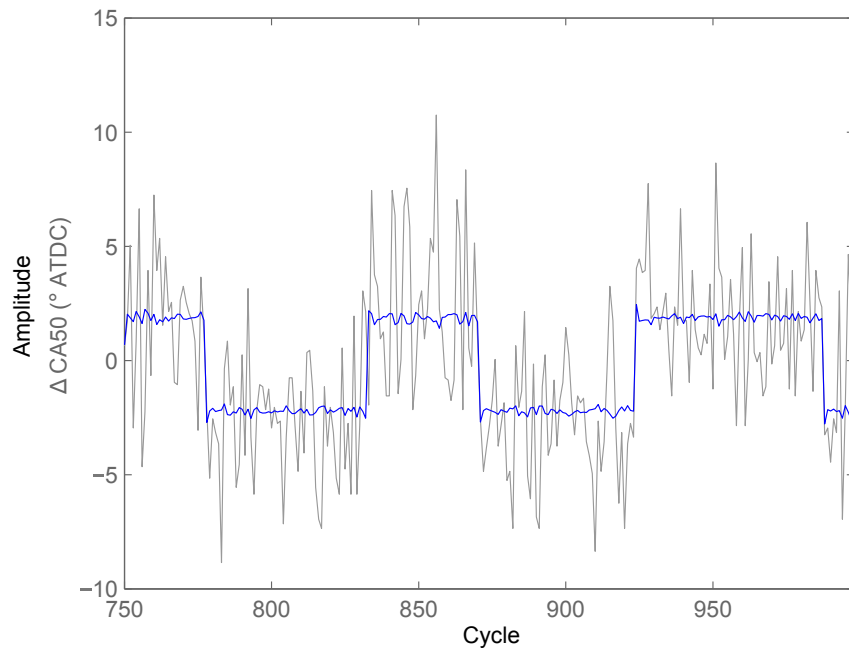Figure D.11: Model Validation, Pmax at Test Condition (D)

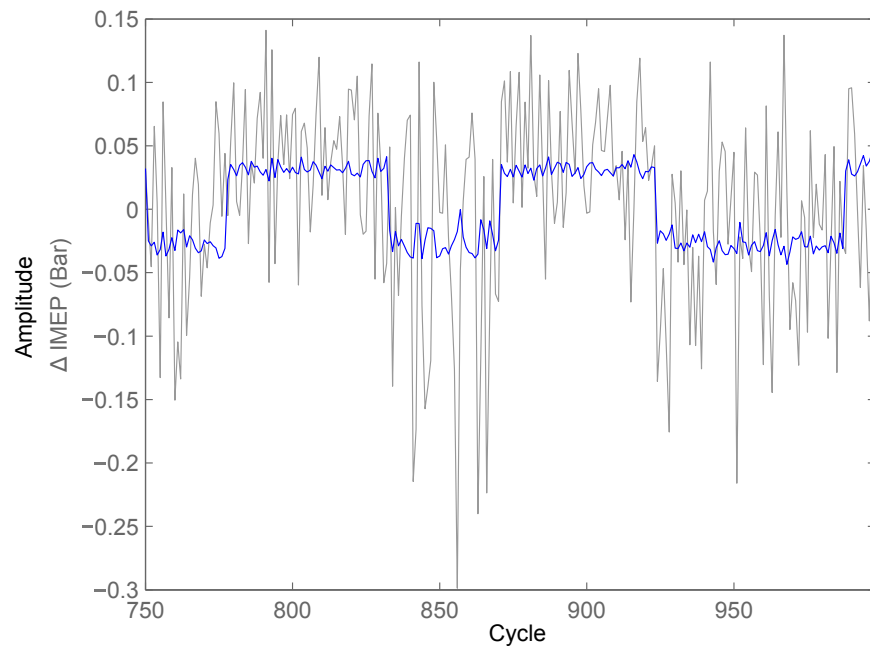

Figure D.12: Model Validation, CA50 at Test Condition (D)

Figure D.13: Model Validation, IMEP at Test Condition (D)

Appendix E

Minimum Variance Control Supporting Data

E.1 Injector Pulse Width Selection

It is not possible to do a full step from the 100% natural gas of condition (A) to 100% gasoline of condition (C) without engine misfires occurring. These misfires happen because the high pressure pump which supplies the direct injectors with fuel, as described in section 3.2, is not capable of responding fast enough to such a large change in demand. The largest step of fuel injector pulse widths that yields no misfires is used for this determined to be:

Table E.1: Max Injector Pulse Width Step

	Pre-Step Pulse Width	Post-Step Pulse Width
Natural Gas	9.1 ms	2.8 ms
Gasoline	0.3 ms	2.0 ms

Appendix F

Standard Operating Procedure

1. Turn on the power supply

   - The power supply should be out putting 13.5 V.

2. Connect Labview to Dyno. Test to make sure throttle moves with input.

   - Make sure that you change all variables then set them (Ex. Position) as the system only sends when there is a change. Thus when the system is first started, the variables displayed are not correct until changed.

   - If the system won't connect, reset the system by flipping the breaker switch until the green light inside of the Dyne Systems I/O box turns off.

3. Switch the ignition on.

   - The ignition is labeled power, and is located on the desk.

4. Start VCM Scanner.

   - Once started click the lighting bolt in the top left corner of VCM scanner and click scan in the top right corner of MEFI to connect to the ECU's. Check to ensure all sensors are checking in and reading reasonable values.

5. Turn on HE water if needed.

- The red tap on the bottom of the HE will control the water. Keep off until the engine coolant temperature is done oscillating and the thermostat remains open.

6. Load simulink and CRTL+B to load it to the MAB.

   - Ensure matlab is in the correct folder to generate the SDF file. If its not ControlDesk will load an old SDF file and any changes won't be processed.

7. Turn on ControlDesk and load main-experiment.

8. Flip red switch on dyno to turn on dyno water.

   - The switch is located on top of the dyno control box. You should hear water start running through the dyno if it is on. If this switch is not engaged, when the dyno is attempts to control engine speed, the dyno will disengage and the engine will be able to run free.

9. Turn on Room natural gas and open valve to allow NG to fill port injector rail.

10. Turn on fuel pumps and check that the pressure gauges read 70 psi.

11. Turn on all room fans.

12. Set INJ-IGN-ENABLE-BOOLEAN to 1 to enable all injectors and spark.

13. Set P-INJ Start Table to 1 and P-INJ duration to 7 if starting on natural gas. Leave both 0 if starting with stock controller.

14. Ensure relay is in correct position depending on if you are starting with natural gas, or gasoline.

15. Turn on cylinder pressure charge amplifier. Hit button to change into operate mode. Calibration should be 33 pC/MU and 10 MU/Volt, Time constant set to Short and in Operate mode.

16. Check Dyno clearance with other diesel engine.

17. Hold the starter toggle switch until the engine fires.

18. Set Dyno to engage at 1250 RPM if running on Natural gas and add engine power until the dyno is engaged. Once engaged. Ensure that P-INJ start table is 0, and engage the PI controller. If operating gasoline on the stock controller, engine is free to idle.

    • Do not idle on natural gas as the engine runs extremely rich. NEVER activate the PI controller if the engine is not engaged by the dyno. The PI controller will cause the engines speed to oscillate as it was not designed for the extra degree of freedom.

    • Once at 1250 RPM on natural gas, allow the engine to warm up. To increase engine speed, increase the torque output so that the dyno will always engage the engine regardless of RPM. Slowly step the RPM of the engine up in 150 - 200 RPM increments.

    • If using gasoline on the stock controller, feel free to accelerate the engine to the appropriate speed without engaging the dyno. Once the correct speed is reached, engage the dyno and apply throttle until the required torque is reached.

Appendix G

Major Files Summary

This chapter contains a summary of all the major files used in this thesis.

Table G.1: Major Files used for Research

File Name	Purpose
datacomb_v04.m	Filter, peg, and align all four cylinder pressures using NI and MAP Data.
character_v01.m	Using filtered and properly aligned cylinder pressure generated from datacomb, calculate CA50, Pmax, θ_{Pmax}, and IMEP for individual cycles and organize. Change comments at the bottom to save different values.
checkvar.m	Take ControlDesk Data (MAB/RP) that is sampled by time and change it so its sampled by cycle. Also calculate closed loop feedback standard deviation.
sysid_onfly.m	Do on fly ARMAX Modeling and check model fit of spark timing and combustion metric.
sysid_onfly otherparam.m	ARMAX Model for all four combustion metrics at the same time with same engine cylinder pressure.
sim_onfly_v02.m	Simulate ARMAX model under minimum variance control.
calculate mvcvalues.m	Calculate g_0 and g_1 for MVC based on ARMAX Model.
analysis_v05.m	Used for characterization plots of character.m data.
LNF_v23.slx	Simulink model for entire dSPACE controller operation.
lnfcylpress_v06.c	NI Cylinder Pressure and MAP viewing and recording into CSV file.
dyno-write3TC.vi	View dyno data (speed, torque), move throttle position, and record dyno and thermocouples.
stock start ecm .hpt+dyno dtc +max torque +6000rpm-lim +FRPlower.hpt	Stock ECU Calibration file with removed VATS Remove DTC codes not needed allow max torque limit to 6,000 RPM Set Fuel rail pressure to max of 2 MPa.